PNC TN941 77－39Tr

Out-of-Pile Experiments of Fission Gas Release in LMFBR Subassemblies-2

Gas Release in a Normal Pin Bundle

Jan., 1978

POWER REACTOR AND NUCLEAR FUEL DEVELOPMENT CORPORATION

動力炉・核燃料開発事業団 (Power Reactor and Nuclear Fuel Development Corporation)

PNC TN941 77－39Tr

Jan., 1978

Out-of-Pile Experiments of Fission Gas Release in LMFBR Subassemblies-2

Gas Release in a Normal Pin Bundle

Kazuo HAGA*
Yoshimichi DAIGO*
Tadashi OKOUCHI*
Takashi KOMABA*
Yoshihiro KIKUCHI*
Masao HORI*

Abstract

Out-of-Pile experiments were conducted to evaluate the thermal and hydrodynamic effects due to gas release into sodium flowing in a 37-pin bundle, which consisted of a central gas-injector pin, seven electrically heated pins and other dummy pins. Each pin, except the gas-injector pin, was wrapped with a spacer wire.

Argon was released transiently or continuously through a nozzle (0.3, 0.5, 0.8mm in diameter) on the gas-injector pin into flowing sodium. The experimental conditions were as follows.

Transient release experiments;

Gas plenum pressure : 29.6 - 75.9 bar

Gas plenum volume : 70, 1,240 cm^3

---

* Fast Reactor Safety Section, O-arai Engineering Center, PNC.

Inlet sodium velocity : 1.95, 4.79 - 5.03m/s

Heat flux : 36.4, 77.3 - 91.6W/cm^2

Inlet sodium temperature: 228 - 276°C

Continuous release experiments;

Gas plenum pressure : 6 - 64 bar

Inlet sodium velocity : 0.45 - 5.07m/s

Heat flux : 8.0 - 92.3W/cm^2

Inlet sodium temperature: 238 - 290°C

Pin surface temperatures increased by gas release. In the transient release experiments, the highest temperature rise was observed in the gas impingement area. Analyses of measured temperature rises by the transient heat transfer computer code SURFACE showed that the two-phase heat transfer coefficient after inception of gas release decreased to 1/20 - 3/20 of the sodium single-phase flow heat transfer coefficient. This two-phase heat transfer coefficient was similar to that obtained in the continuous release experiments. If the experimental results are extrapolated to reactor conditions, in which the heat flux is 200W/cm^2, the flow velocity is 5m/s, the temperature rise due to gas release is estimated to be less than 240°C.

The measured pressure pulses were less than 1/5 of initial gas plenum pressure in the transient release experiments. Neither damage nor deformation was observed in the pin bundle after the present experiments (total 14 transient experiments), and then the mechanical effect of FP gas release will be negligible.

In the transient release experiments the higher the gas plenum pressure was, the more rapid the increase of outlet velocity was. But the initial acceleration of downstream liquid from the gas injection plane was extremely lower than the analytical results by the one-dimensional slug-ejection model.

The outlet velocity fluctuation and the acoustic noise increased with the increase in gas release rate.

CONTENTS

Introduction

As the fuel burns in the liquid metal fast breeder reactor (LMFBR), the fission gas is accumulated in the fuel pins and thus built up pressure is said to be nearly 60 bars at the time of refueling. Such being the case, if pinholes or cracks develop in a fuel pin cladding tube due to material defects, thermal stresses or corrosion, high-pressure fission gas will be released through such openings into the sodium to impinge on the surrounding fuel pins. The fission gas release is considered to have thermal and mechanical effects on the surrounding fuel pins. If the impinged pin surface is blanketed and raised in temperature until it leads to the pin failure or if the pin failure is caused by the mechanical stresses arising from the impingement of the gas jet which is considered to have the velocity of sound (630m/s at 800°C for xenon, a principle component of fission gas), the fission gas injection from a single fuel pin can trigger a chain of similar failure, propagating from one fuel pin to another, giving rise to a serious problem from a viewpoint of reactor safety.

Outside Japan, fission gas injection experiments have been carried out in Britain[1] and the United States.[2],[3],[4],[5] Honglund et al[2] used a 431.8mm long test section with a flow channel of 14.68mm x 0.64mm rectangular cross-section in a water loop to release gas from the orifices (0.41, 0.76 and 1.20mm in diameter) in the longer wall against the opposite wall which was a heat transfer surface (water velocity: 0.25 - 0.76m/s,

gas pressure: 34.5 - 69.0 bars). The measured impinged surface temperature dropped due to the gas release. As the causes of this phenomenon, (1) an extremely violent spray pattern was observed on the impinged surface by means of high-speed photography and (2) the temperature rose higher than in the case of water single-phase flow when the orifice diameter was so large that the water flew back and consequently the gas contained almost no liquid drops. From such findings, Hoglund et al considered that the spray cooling would be dominant on the gas impinged surface. Wilson et al[5] released gas (gas pressure: 5 - 57 bars) through the needles (0.33, 0.58 and 0.84mm in inside diameter) at a distance of - 1.42mm against one of the three heater pins in a sodium flow (1.1m/s - 5.3m/s in velocity) and obtained such results that the pin surface temperature rose higher than in the case of sodium single-phase flow due to the gas release and the maximum temperature rise of the gas impinged surface was - 240°C at 250W/cm^2, which was contrary to the result in the case of water.

In Japan, similar experiments were conducted by the Power Reactor and Nuclear Fuel Development Corporation when it was called the Atomic Fuel Corporation. According to the experiments, when a pin located in the center of a 60-pin simulant fuel assembly was caused to fail by the pressure of nitrogen gas (82 - 166 bars), the released nitrogen gas had only a negligible effect of mechanical stresses on the surrounding pins[6] and it was found that the surface temperature of the heater pin downstream from the position of the gas release rose due to blanketing but the

transient temperature rise on the pin surface was not important as far as a normal flow rate was maintained.[7] The surface of the pin downstream from the failure where the fission gas-sodium two-phase flow passes is considered to have a heat transfer mechanism different from that for the gas impinged surface. In this connection, liquid metal-gas two-phase flow heat transfer experiments were performed by Mizushina et al[8] with mercury-nitrogen system and Ochiai et al[9] sodium-argon system, both using the circular flow channel. Both groups of researchers reported that the heat transfer coefficient decreased due to the mixture of gas into the flow.

These experiments are not sufficient to estimate the condition in the actual reactor core in which the bundle is large and gas is released transiently into the sodium. For this reason, since November 1974 the Fast Reactor Safety Section of O-arai Engineering Center of the PNC, has carried out experiments, using the fuel failure heat transfer test facility, in which argon gas simulating the fission gas was released transiently and continuously from one of the 37 pins in a bundle in order to make investigations on the thermal effect of the gas release on the surrounding pins. Of those experiments, the results of the two transient and continuous gas release tests (gas release rate (Note 1): 0.08 - 0.74g/s, Quality (Note 2): 1.8×10^{-5} - 1.1×10^{-3}) using 0.2mm and 0.3mm diameter gas injector nozzles were described in the preceding report.[10] In the tests, the maximum pin surface temperature rise measured in the 4.9m/s continuous release test, when extrapolated to the Extrapolation of experimental data showed that the temperature rise

in the conditions of 4.9m/s and 400w/cm is less than 70°C. In the following year of 1975 we performed the tests in which the gas injection nozzle diameters were increased (0.3, 0.5, 0.8mm) and the gas pressure during the transient release was also increased (29.3 - 75.9 bars) so that the gas release rate was so much higher. Since the volume of released gas in the previous transient release tests was 1240cm^3, very large as compared with the actual fuel pin (20 - 30cm^3), the test facility was partially modified in the midst of these series of tests so that the gas volume (gas plenum volume) would be reduced to 70cm^3. In the previously reported tests, the spacer wire was located just between the gas injector nozzle and the pin to be impinged by the gas, thus making it impossible to make evaluation for the direct impingement of gas jet on the pin. So, in the present tests, the position of the gas injector nozzle was shifted so that the gas jet would directly impinge on the pin. After each transient release test was conducted, constant pressure continuous gas release tests (Gas release rate: 0.06 - 3.44g/s, Quality: 1.5×10^{-5} - 3.8×10^{-3}) were performed. Apart from those

---

(Note 1) In the tests, argon (1.783 g/ℓ (STP)) was used to simulate the actual fission gas consisting mainly of xenon (5.851 g/ℓ (STP)), and therefore in the case of xenon when the gas release rate (which is, strictly speaking, the gas weight release rate although referred to simply as "gas release rate" in this report) is the same as in the tests, the gas volume release rate is 0.305 times (1.783/5.851) that in the tests. "STP" above means the standard condition of 0°C and 1 atm.

(Note 2) Quality $X = Wg/(W\ell + Wg)$
where Wg: weight flow rate of gas phase
Wℓ: weight flow rate of liquid phase

tests, we also performed the homogeneous sodium-gas two-phase flow heat transfer tests by mixing argon into the sodium flow upstream from the starting point of heated section of heater pin for the purpose of evaluating the surface temperature downstream from the position of gas release.

This report deals with the temperature, flow rate, pressure, acoustic noise, etc. which were measured in these tests and also discusses the fuel pin surface temperature rise in the event of fission gas release in the actual fuel assembly.

Chapter 1. Test Facility and Test Section

1-1 Test facility

The tests were performed by the use of the sodium boiling and fuel failure propagation test loops (SIENA) at Fast Reactor Safety Section of O-arai Engineering Center of PNC. The SIENA facilities will be described only briefly because the details thereof were discussed in the preceding report.

Fig. 1 shows a schematic diagram of SIENA. The 37-pin bundle was set in the T-3 test section in the FPL loop on the right-hand side in Fig. 1. The FPL loop has the main circulation line comprising the flow of main pump T-3 test section → expansion tank → separator → main cooler → main pump.

The gas releasing system supplies the simulant fission gas to the gas-injector pin from above the T-3 test section. The gas is heated by the gas heater after having been reduced in pressure to required level by means of the pressure regulator. The argon, a simulant fission gas, which was mixed into sodium in the T-3 test section is separated into the cover gas in the expansion tank and separator. As a result the cover gas pressure continues to rise during the gas release test but when it exceeds 0.5 - 0.6kg/cm^{2}g the vent valve located in the vapor trap will be opened to release the gas to the air.

1-2 Test section

Fig. 2 shows a simplified representation of the test section and the positions in which the measuring sensors were mounted. The test section vessel is regular hexagonal in shape and 10mm in wall thickness and 50.4mm in the distance between the opposite sides, in which are inserted the 36-pin bundle heater from below and the gas-injector pin from above. Fig. 2 shows that the six of the bundled pins are the electrically heated sheathed heater pins and the remaining 30 are dummy pins. The sodium flows into the plenum and thereafter flows upward through the bundle. Both heater and dummy pins are 6.5mm in diameter and 1515mm in length. In the heater pin, the middle section 450mm in length is the effecting heating section which is heated uniformly throughout its length. A spacer wire 1.3mm in outside diameter is wound around each pin clockwise as viewed from the upstream side with a pitch of 264.8mm. The pins are triangularly arranged with a pitch of 7.9mm. The gas-injector pin, which is not wrapped with the spacer wire, has a diameter of 6.5mm and is positioned in the center of the bundle and its end is inserted in the guide hole provided in the lower flange of the test section. On the surface of the gas-injector pin is a gas injector nozzle with a prescribed diameter, through which the gas is injected in the direction indicated by an arrow in Fig. 2 onto the heater pin. The axial position of the gas releasing hole is 185mm downstream from the point of inception of heating in this figure. It is 225mm downstream in other tests. In the two-phase flow heat transfer test, gas is mixed

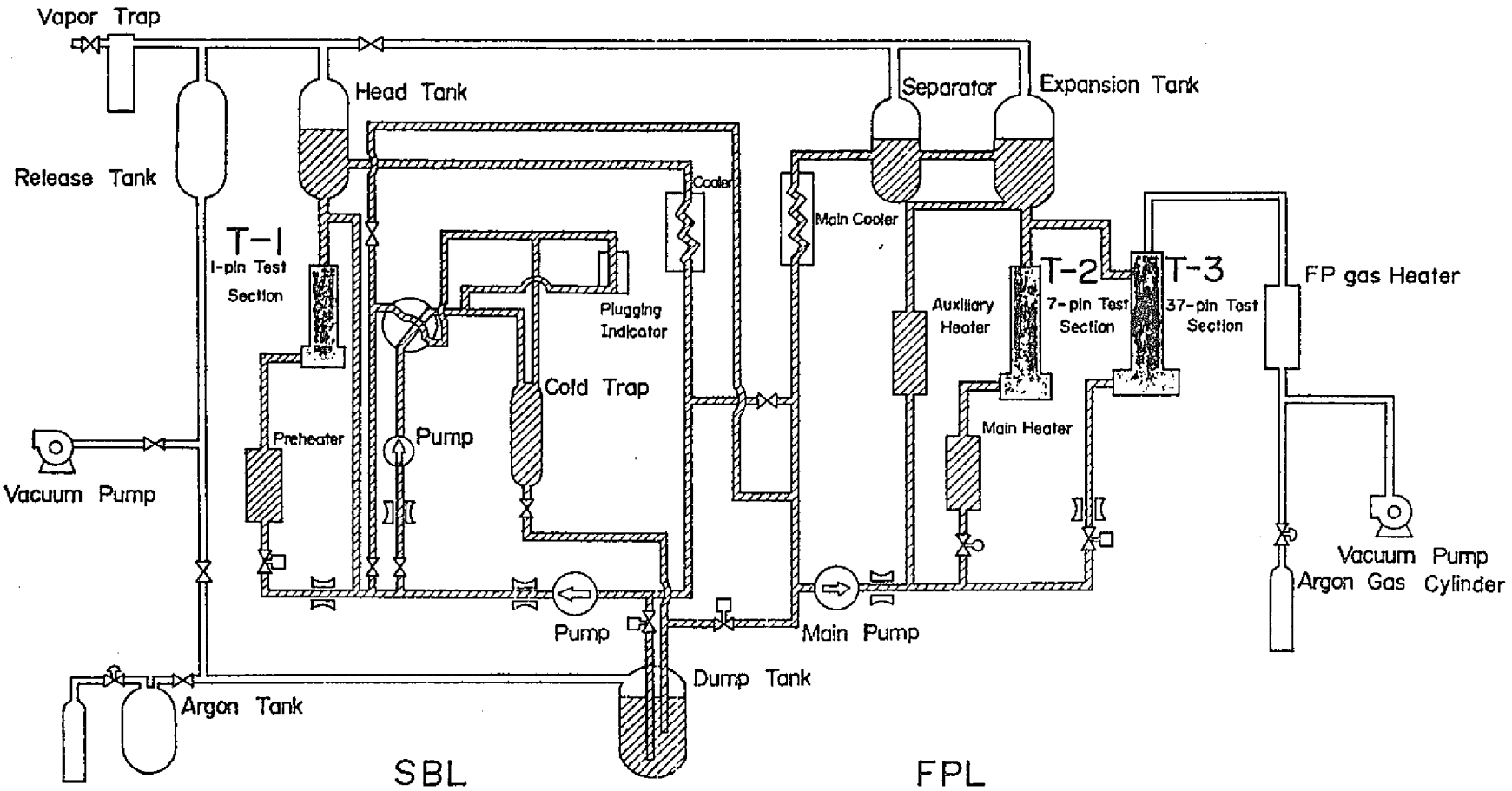

Fig. 1 Schematic diagram of sodium boiling and fuel failure propagation test loops SIENA (PNC-FS-244)

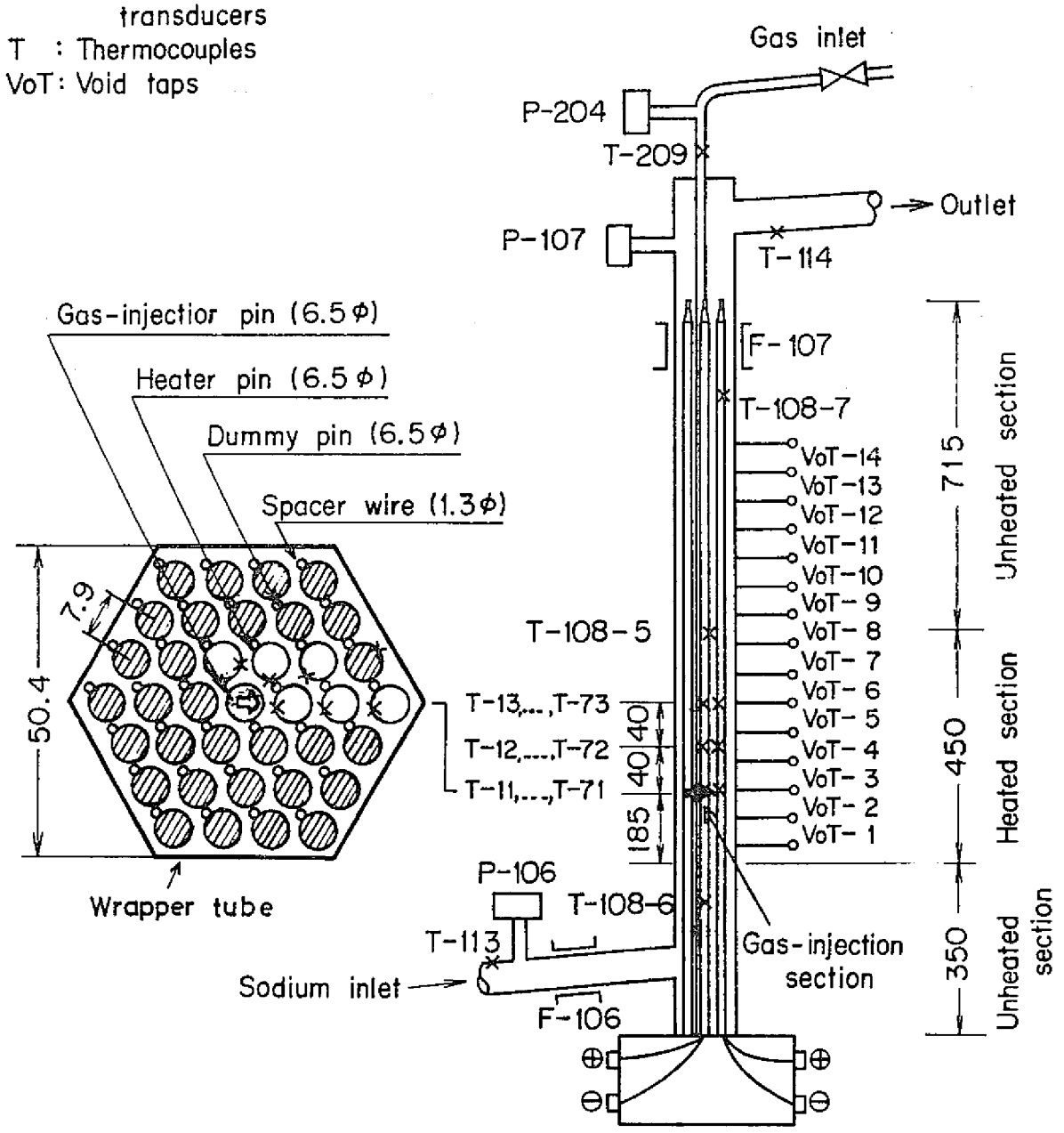

Fig. 2 Test section with a 37-pin bundle (PNC-FS-345)

into the sodium flow at a point 120mm upstream from the starting point of heated section. The outer wall of the test section vessel is fitted with compensation heaters and thermal insulators.

Speaking about the measuring sensors, on the heater pin surface are attached 0.3mm-diameter chromel-alumel grounded thermocouples T-11 - T-73 on the same sections at three places at intervals of 40mm in the axial direction as shown in Fig. 2.

The heater pin spacer wires also perform the function of thermocouples T-180-1 - T-108-7 which are 1.3mm in diameter. The outside walls of the pipes at the test section inlet and outlet are fitted with T-113 and T-114, respectively. The inlet and outlet sodium flow rates are measured by the electromagnetic flowmeters F-106 and F-107, respectively. The pressure fluctuations consequent on the gas release are measured by the strain gauge-type pressure transducers P-106 and P-107 mounted at the inlet and outlet, respectively. The potential tap-type voidmeters (Vot-1 - Vot-14) are for measuring the electrical resistance changes between the taps, which are caused by the changes in the amount of released gas. The gas-injector pin is fitted with thermocouple T-209 and pressure transducer P-204.

The signals received from those sensors were all stored in the analog and digital data recorders and were later reproduced and analyzed. The multiple-point digital recorder was also used in the continuous gas release tests and two-phase flow heat transfer tests.

Fig. 3 shows the construction of the gas-injector pin. The gas-injector pin is a tube 6.5mm in outside diameter and 3.5mm

in inside diameter which contains a 3.0mm-diameter rod simulating the fuel pellets. In the test, this rod moves to break the 0.1mm thick SUS 316 rupture film so that the gas is released through the nozzle located 5mm underneath the rupture film. In the end of the rod is embedded a 0.5mm-diameter thermocouple (T-210) for measuring the temperature of the released gas.

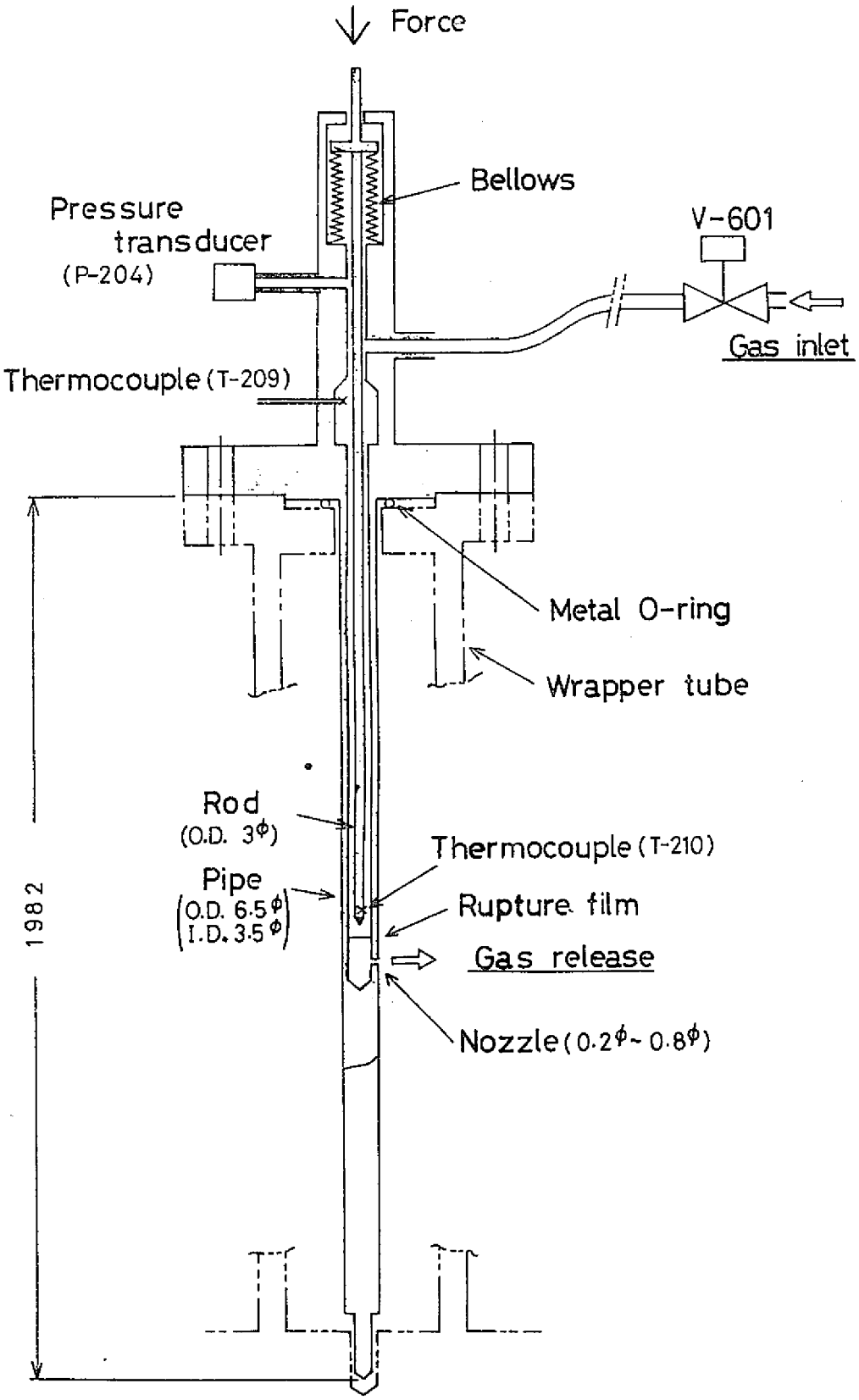

Fig. 3 Schematic diagram of gas-injector pin (PNC-FS-288)

1-3 Test facility operations

The following are the test facilities operations and modifications made in relation to the present tests.

June 3 - 4, 1975: 54th run (transient release test GR-3, continuous release test G-2101 - G-2619, 30 cases in total), 7 heater pins heated.

June 24 - 25, 1975: 55th run (transient release test GR-4, continuous release test G-3601 - G-3619, 10 cases in total)

July 10 - 11, 1975: 56th run (transient release test GR-5, continuous release test G-4101 - G-4619, 30 cases in total).

July 24, 1975: 57th run (transient release test GR-6, continuous release test G-5019 - G-5619, 7 cases in total)

Sept. 10, 1975: 59th run (transient release test GR-7, continuous release test G-6019 - G-6619, 7 cases in total)
Six heater pins were heated in this and following series of tests.

Sept. 23, 1975: 61th run (transient release test GR-9, continuous release test G-8004 - G-8604, 7 cases in total)

Sept. 30, 1975: 62th run (transient release test GR-10, continuous release test G90804 - G93004, 7 cases in total)

Oct. 7, 1975:	63th run (transient release test GR-11, continuous release test G100701 - G-106001, 7 cases in total)
Oct. 18, 1975:	The 15.9mm inside diameter pipe connecting the gas supply valve V-601 and the gas-injector pin was replaced by a 2mm-inside diameter pipe, thereby reducing the gas plenum volume from 1240cm^3 to 70cm^3.
Oct. 23, 1975:	65th run (transient release test G-12, continuous release test G-11002 and G-11602, 2 cases)
Oct. 28, 1975:	66th run (transient release test G-13, continuous release test G-12152 - G-12309, 6 cases in total)
Nov. 11 - 12, 1975:	67th run (transient release test G-14, two-phase flow heat transfer test GS-051 - GS-259, 33 cases in total)
Nov. 18, 1975:	68th run (transient release test G-15, continuous release test G-15104 - G-15609, 10 cases in total)
Nov. 20, 1975:	The test section cut off and removed from the test facilities.

Chapter 2. Transient Gas Release Tests

2-1 Test objectives

The pressure of fission gas that is generated in the fuel pin is as high as about 60 bars at the time of refueling. In the event of fuel cladding tube failure, the high-pressure gas would be transiently released into the sodium during the normal operation of the reactor and blankets the surrounding fuel pins, thus preventing the heat transfer from fuel to coolant and consequently giving rise to the possibility of the failure of other fuel pins which have been blanketed. It is also possible that mechanical damage is caused to the fuel pins due to the impingement of the gas jet on them. Since the fission gas release can be a cause of the propagation of fuel pin failure, it is necessary to make investigations on the effects of fission gas release in the fuel assembly. Following is the description of the results of transient gas release tests conducted for the above-mentioned purposes.

2-2 Test procedure

When carrying out the test, the test loop is first filled with about 200°C sodium from the dump tank and the cover pressure is set to 100mmH_2Og. After that, the sodium flow rate is set to 150ℓ/min by the main pump. The purification system pump is operated to set the cold trap flow rate to 15ℓ/min - 17ℓ/min and the cold trap blower is operated to gradually cool the cold

trap until its temperature is saturated at 150°C. The plugging temperature is measured by the plugging indicator for sodium purity. When the plugging temperature is below 150°C, the purifying operation is stopped and purification system is cut off. In some tests the purification system was not operated because there was not enough time. In this case, the temperature of sodium to be filled in the loop was lowered to 150°C. Next, the valve in the inlet of the pipe-line to the test section T-2 and auxiliary heater is closed so that the sodium may flow from the main pump → T-3 → expansion tank → separator → main cooler and back to the main pump. The main pump power output is adjusted to set the flow rate to the required value in reference to the indication of the electromagnetic flow meter. The test section inlet temperature is adjusted as required by means of the main cooler. To the gas supply system is supplied the gas from the gas cylinder, the pressure of which is calculated beforehand so the required gas pressure will be obtained after heated. Then the valve in the gas heater inlet pipe is closed and the gas is heated. Immediately before the commencement of testing, the valve V-601 located between the gas heater and the gas-injector pin is closed so that a definite amount of gas will be released into the sodium flow during the test.

The test is started by breaking the rupture film in the gas-injector pin. The gas flows downward through the circular flow channel composed of the inner wall of the gas-injector pin and the surface of the rod and is released through the nozzle into the sodium flow. In the earliest stage of the test, the sodium

which leaked through the nozzle into the small space (about $0.07cm^3$) underneath the rupture film when the loop was filled with sodium will come out with the jet of gas. After the test is started, the gas pressure in the pin is watched by the signal from the pressure transducer. When the gas pressure is found to be sufficiently reduced, V-601 is opened to supply a large amount of gas to terminate the transient release test.

2-3 Test conditions

In the previously reported two transient tests, the gas injector nozzle diameters used were 0.3mm at most and gas pressures were 33.9 bars at most. In the present tests the injector nozzle diameters were larger and the gas pressures were increased to 75.9 bars to have a larger gas release rate. The test conditions were as follows.

Nozzle diameter:	0.3, 0.5, 0.8mm
Released gas pressure:	15.9, 29.6 - 75.9 bars
Gas plenum volume:	70, $1240cm^2$
Initial gas release rate:	0.63 - 4.17g/s (354 - $2340cm^3$ (STP)/S)
Heater pin heat flux:	36.4, 77.3 - $91.6W/cm^2$
Sodium flow velocity:	1.95, 4.79 - 5.03m/s
Sodium inlet temperature:	228 - 276°C

The details of the test conditions were as shown in Table 1, which also shows the results of the two tests described in the preceding report. We performed 14 tests in total, including the previous two tests, of which only the test GR-14 used four

0.5mm-diameter gas release nozzles located 120mm upstream from the starting point of heated section. In other tests, gas was injected through only one nozzle 185mm or 225mm downstream from the starting point of.

2-4 Test results and discussions

2-4-1 Transient gas release

Fig. 4 shows the changes with time of gas plenum pressure, pin surface temperature and flow velocity at the test section inlet and outlet in a typical transient release test (GR-10).

In this test, release nozzle diameter was 0.8mm, heat flux 9.16W/cm^2, inlet flow velocity 4.95m/s, and gas plenum volume 1240cm^2. With the commencement of the test, the gas pressure began to decrease from 54.9 bars and lowered to 44.3 bars four seconds later. On the vertical axis on the right-hand side of the figure is plotted the gas release rate calculated from the rate of pressure decrease. During this period, the flow velocity at the outlet increased sharply immediately after the gas release and after reaching the maximum value of 6.8m/s it fluctuated widely centering around 5.8m/s. At the inlet, on the other hand, due to the gas release the flow velocity decreased and settled at about 4.5m/s. The figure shows the pin surface temperatures at the points of gas release and 40mm and 80mm downstream therefrom. The point of gas release was 185mm downstream from the point of inception of heating and L/De was 53.9 (L is the distance from the point of inception of heating

Tab.1 Experimental conditions of transient release tests (I)

Run Number		GR-1	GR-2	GR-3	GR-4	GR-5	GR-6	GR-7	GR-9
Date		1974.11.15	1974.12.10	1975.6.4	1975.6.25	1975.7.11	1975.7.24	1975.9.10	1975.9.23
Nozzle diameter	mm	0.3	0.2	0.3	0.3	0.5	0.5	0.5	0.5
No. of nozzles		1	1	1	1	1	1	1	1
Gas plenum pressure	bar	33.9	11.4	54.9	56.9	29.6	62.4	60.0	75.9
Gas plenum volume	cm^3	1240	26140	1240	1240	1240	1240	1240	1240
Initial gas release rate	g/s	0.39	0.10	0.63	0.66	0.76	2.00	1.92	1.83
Heat flux	W/cm^2	76.9	77.9	77.3	78.5	78.5	78.4	91.1	91.2
No. of heated pins		7	7	7	7	7	7	6	6
Sodium inlet velocity	m/s	4.84	4.85	4.87	4.89	4.82	4.92	4.94	4.92
Sodium inlet temperature	°C	268	262	275	276	265	236	225	233
Sodium outlet temperature	°C	278	272	285	286	275	246	235	243
Gas temperature	°C	(not measured)			278	266	(not measured)		
*Lg	mm	225	222	225	185	185	225	185	185

* Lg=Axial distance of gas-injection plane from starting point of heated section

Tab.1 Experimental conditions of transient release tests (II)

Run Number		GR-10	GR-11	GR-12	GR-13	GR-14	GR-15
Date		1975.9.30	1975.10.7	1975.10.23	1975.10.28	1975.11.11	1975.11.18
Nozzle diameter	mm	0.8	0.5	0,5	0.5	0.5	0.8
No. of nozzles		1	1	1	1	4	1
Gas plenum pressure	bar	54.9	62.8	64.3	31.1	15.9	62.1
Gas plenum volume	cm^3	1240	1240	1240	70	70	70
Initial gas release rate	g/s	3.69	2.01	2.06	0.81	2.04	4.17
Heat flux	W/cm^2	91.6	36.4	91.0	90.3	90.3	90.8
No. of heated pins		6	6	6	6	6	6
Sodium inlet velocity	m/s	4.95	1.95	4.79	5.03	4.95	4.84
Sodium inlet temperature	°C	237	228	245	235	235	236
Sodium outlet temperature	°C	247	238	255	245	245	246
*Lg	mm	185	185	185	185	-120	185

*Lg=Axial distance of gas-injection plane from starting point of heated section

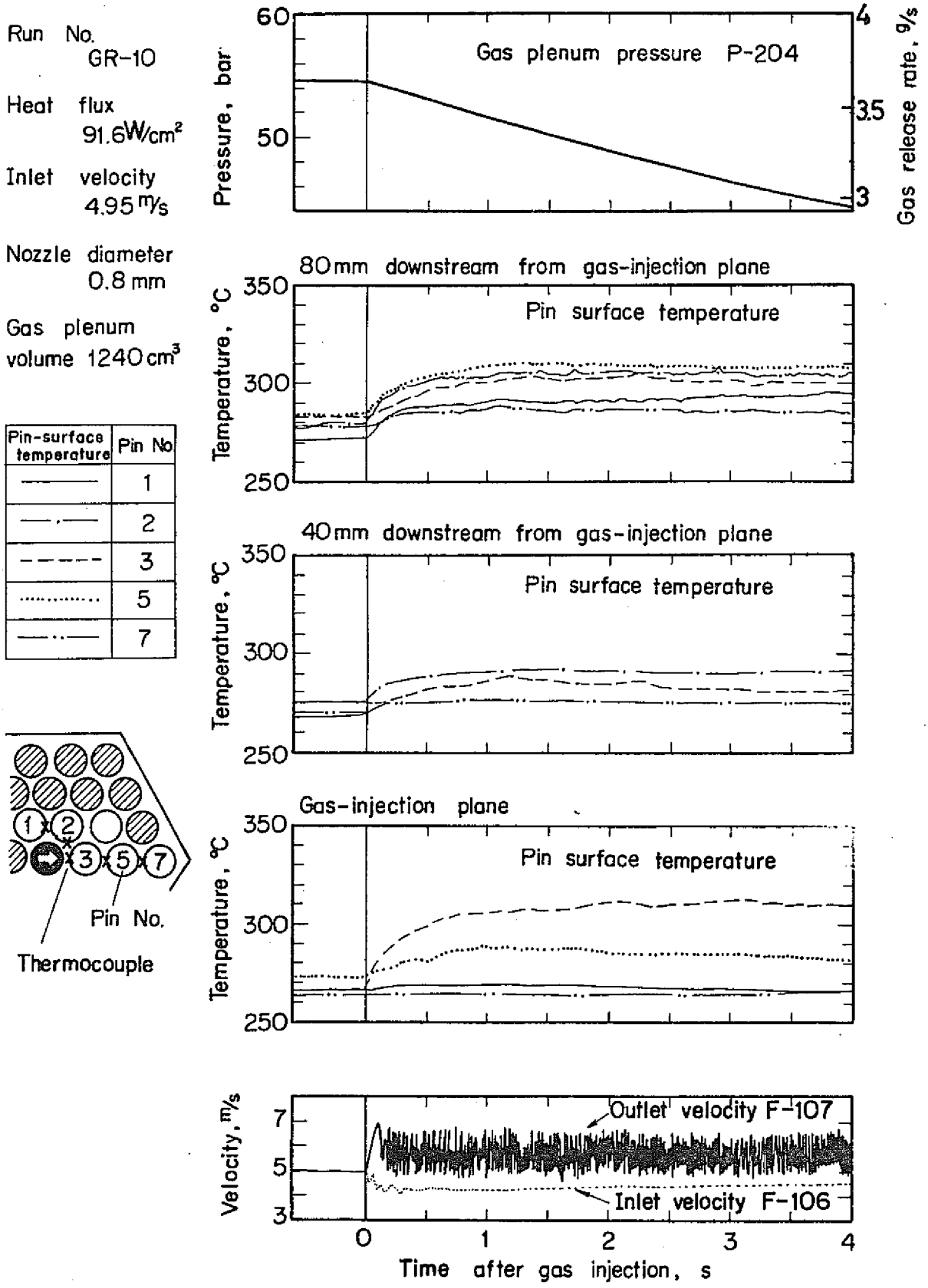

Fig. 4 Signals from flowmeters, thermocouples and pressure transducers for a transient release test; run No. GR-10 (PNC-FS-341)

and De the hydraulic equivalent diameter. With this test section, it was assumed that De = 3.43mm, considering all the wetted perimeters.). As for the temperature variations where the gas was released, temperature rose conspicuously in No. 3 pin that was directly impinged by the gas jet and only other temperature was observed in No. 5 pin located behind No. 3 pin. From this, it is considered that the thermal influence of the gas release extends at most as far as the second pin from the gas injector nozzle. The surface temperature rise began to be observed also in other pins as removed from the gas injector nozzle on the downstream side. It was found that at the section 80mm downstream from the nozzle the surface temperature rose on the surfaces of all the pins which were measured and bubbles extended also in the radial direction.

Fig. 5 shows the changes with time of inlet and outlet pressures, inlet and outlet flow velocities and void meter signals obtained in the test GR-10. The pressure peaks of 7.8 bars at the inlet and 12 bars at the outlet due to the gas release were observed. After that, both inlet and outlet pressures rose about 0.5 bar from before the gas release and settled on the level. The outlet velocity increased after gas release and reached a maximum value 0.09 second later as seen from Fig. 4 presumably because the bubbles reached the outlet flowmeter at that time. Thereafter, the sodium-gas two-phase flow velocity fluctuations were observed. Although there were large noises, the void meter signals showed that the void reached as far as VoT-10 (315mm downstream from the nozzle) about 0.03

second after the gas release and VoT-14 (715mm downstream from the nozzle) about 0.07 second after the gas release.

Fig. 6 shows the changes with time of gas plenum pressure, pin surface temperature and test section inlet and outlet flow velocities in the test GR-13 in which the gas pelnum volume was reduced to 70cm^2. Other conditions used in this test were the nozzle diameter 0.5mm, heat flux 90.3W/cm^2, and inlet flow velocity 5.03m/s. The gas plenum volume was so small that the gas pressure decreased sharply from 31.1 bars and lowered to about 10 bars 3 seconds later. Examining the changes in the outlet flow velocity during this period, it was seen that as in the test GR-10 the outlet velocity increased rapidly after the gas release and fluctuated thereafter but since the gas pressure was lower and the nozzle diameter was smaller than in GR-10, the gas release rate was about 1/4 of that in GR-10. As for the pin surface temperature, the temperature rise was largest on the gas impinged surface as in GR-10 but after its peak value was reached it lowered with the decreasing gas pressure.

2-4-2 Heat transfer coefficient on gas impinged surface

In view of the fact that the largest temperature rise due to the gas release was measured on the gas impinged surface as seen from Figs. 4 and 6, it is important to grasp the transient heat transfer coefficient for this surface from the viewpoint of reactor safety. Fig. 7 shows the changes of the gas impinged surface temperature (T-31) with the gas pressure over a longer

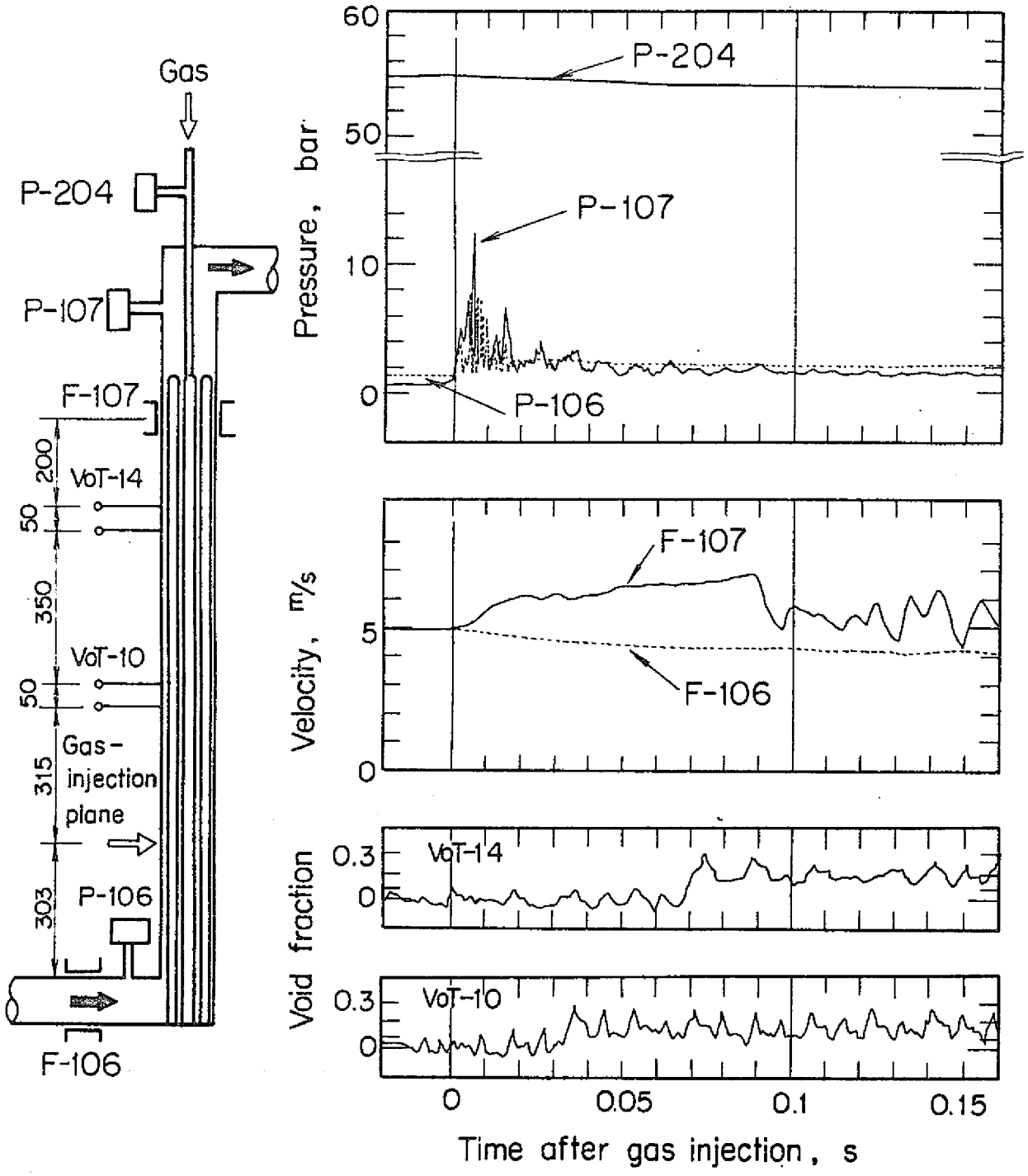

Fig. 5 Signals from pressure transducers, flowmeters and void taps for a transient release test; run No.GR-10 (PNC-FS-342)

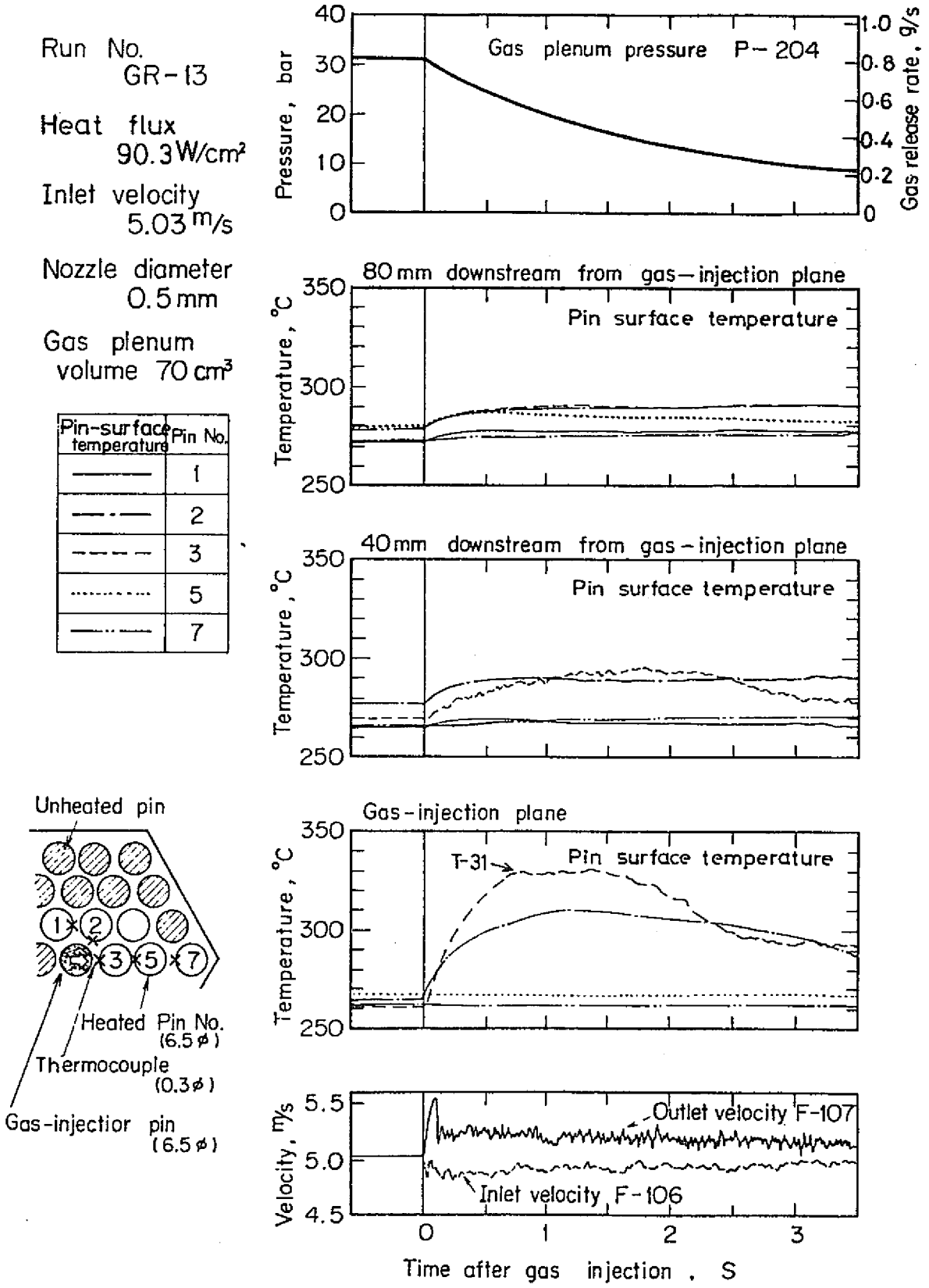

Fig. 6 Signals from flowmeters, thermocouples and pressure transducer for a transient release test; run No. GR-13 (PNC-FS-334)

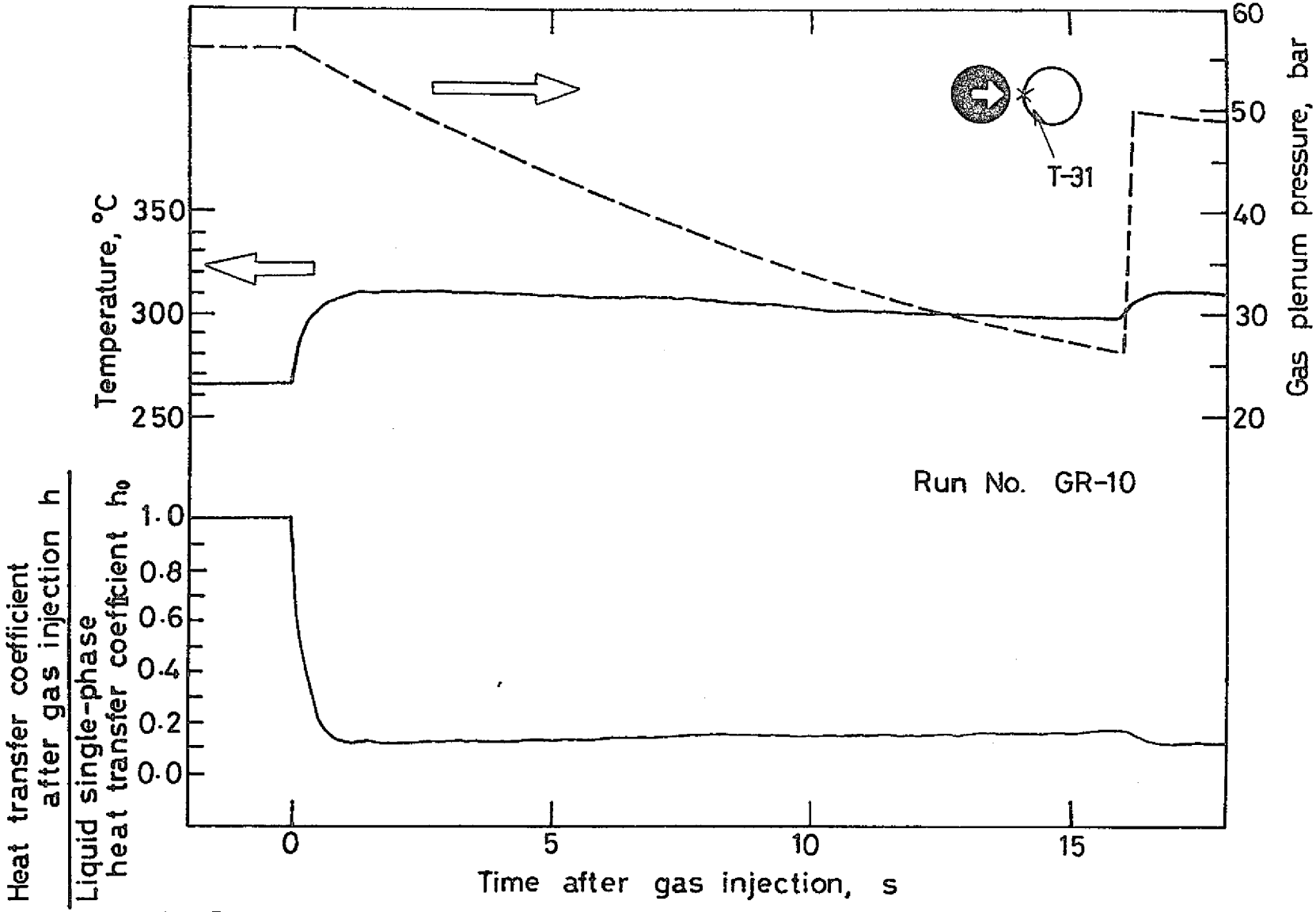

Fig. 7 Change of heat transfer coefficient corresponding to change of pin surface temperature in impingement area for a transient release test; run No. GR-10 (PNC-FS-368)

period of time in the test GR-10. The gas pressure decreased to about 26 bars 16 seconds after the commencement of the test and increased to about 50 bars owing to the opening of the gas supply valve. During this period, the impinged surface temperature remained approximately constant, suggesting that the impinged surface temperature is little dependent on gas pressure when it is on a level like this. The solid line on the bottom of the same figure shows the change with time of the ratio of heat transfer coefficient at the time of gas release to that at the time of liquid single-phase flow, h/ho, which was obtained by assuming the impinged surface temperature measured from moment to the next to be quasi-constant. To obtain h, the coolant temperature Tc was first calculated from the surface temperature Two measured at the time of liquid single-phase flow with the same inlet velocity and ho, and then h was calculated by $h/ho = (Two - Tc)/(Tw - Tc)$ on the assumption that Tc would remain unchanged after the gas release. In the above equation, Tw is the surface temperature measured after the gas release and ho was obtained from Subbotin's equation, $Nu = 5 + 0.025Pe^{0.8}$, which was used in the NORMAL code by which the internal temperature distribution of this test section at the time of sodium single-phase flow was calculated in the preceding report. Fig. 7 shows that the heat transfer coefficient decreased sharply with the gas release and lowered to about one tenth of that at the time of liquid single-phase flow. Fig. 8 shows the relation between the heat transfer coefficient obtained from the measured value of the impinged surface

temperature in the gas release test in which the inlet flow velocity was around 5m/s, assuming the impinged surface temperature to be quasi-constant as in the case of Fig. 7, and the gas pressure at that time. The position of the symbol indicating the nozzle diameter shows the point of inception of gas release. The heat transfer coefficient decreased sharply after the gas release and thereafter it remained roughly on a constant level until the end of the test. The impinged surface temperature rose transiently in the region where the heat transfer coefficient decreased sharply in the figure and it is not suitable for treating as a quasi-constant state but the temperature remained roughly constant and the solid line after a bend is considered to show approximately the relation between the gas pressure and the heat transfer coefficient on the gas impinged surface. The figure shows a tendency for the heat transfer coefficient to increase again when the gas pressure lowered below 20 bars.

So far we made investigations on the relation between the heat transfer coefficient and gas pressure, assuming that the impinged surface temperature was in a quasi-constant state even when the gas pressure decreased. Next, we will discuss the results of comparison of the temperature changes immediately after the gas release and the results of transient heat transfer analysis. Fig. 9 shows the measured values of gas impinged surface temperature in GR-10. The solid line shows the results of calculation made on the assumption that the heat transfer coefficient would changed from ho to h with the release of gas.

For use in this calculation, the heater pin transient heat transfer analysis code SURFACE was prepared. In this code, the heater is divided into 10 cells by concentric circles to calculate the change with time of the pin surface and internal temperatures when the heat transfer coefficient changes sharply. Further details of the SURFACE code are described in Appendix A. Fig. 9 shows the results of test in which h was varied as a parameter. The rate of temperature rise after the gas injection, which was obtained at h = 0.12ho, is in good agreement with the experimental results. Fig. 10 shows the comparison of the gas impinged surface temperature changes observed in the tests, in which the heat flux, inlet flow velocity and gas plenum pressure were the same as those in GR-10 but the gas injector nozzle diameter was different, with the calculated values thereof. The upper figure shows the results of the test GR-4 in which the gas injection nozzle diameter was 0.3mm. In this case h = 0.1ho and was in good agreement with the calculation. The low figure shows the results of the test GR-9 in which the gas injector nozzle was 0.5mm. In this case, h = 0.085ho, showing a good agreement between experiment and calculation. Fig. 11 shows the results obtained when the analytical calculation for the rate of gas impinged surface temperature rise in Fig. 9 and 10 was made also for the results of other tests in which the inlet flow velocity was around 5m/s. As seen from this figure, when the gas plenum pressure was higher than about 30 bars, h/ho was in the range of 0.05 - 0.15 irrespective of the magnitude of the gas pressure and the gas

injector nozzle diameter and this is in agreement with the tendency obtained previously by assuming the measured value of the gas impinged surface temperature to be quasi-constant.

Here the cooling effect by the gas jet alone will be considered. Let P_1 represents the primary pressure of gas being injected through the nozzle, P_2 the secondary pressure of the same and γ the specific heat ratio (specific heat at constant pressure/specific heat at constant volume), the gas flow will be critical, if

$$\delta \cdot P_1 \geq P_2, \quad \delta = \left(\frac{2}{\gamma + 1}\right)^{\frac{\gamma}{\gamma - 1}}$$

and its velocity will be equal to the sonic velocity. Since $\gamma = 1.66$ in the case of argon, $\delta = 0.488$. When the flow velocity is 5m/s, the pressure in the vicinity of the gas injector nozzle is about 2 bars. In the present test, the gas is considered to have been injected at the sonic velocity to impinge on the surface of the pin only 1.4mm distant from the injector nozzle. The heat transfer coefficient in the vicinity of the point of stagnation due to the parallel flow to a cylinder is given by[11]

$$Nu = 1.14 Re^{0.5} Pr^{0.4} \quad (0.5 < Pr < 5)$$

The sonic velocity of argon at 250°C is 425m/s and the Reynolds number Re is calculated to be 1.49×10^5. If Prandtl number Pr is assumed to be 0.836 and substituted into the above equation, the Nusselt number Nu = 409, from which the heat transfer

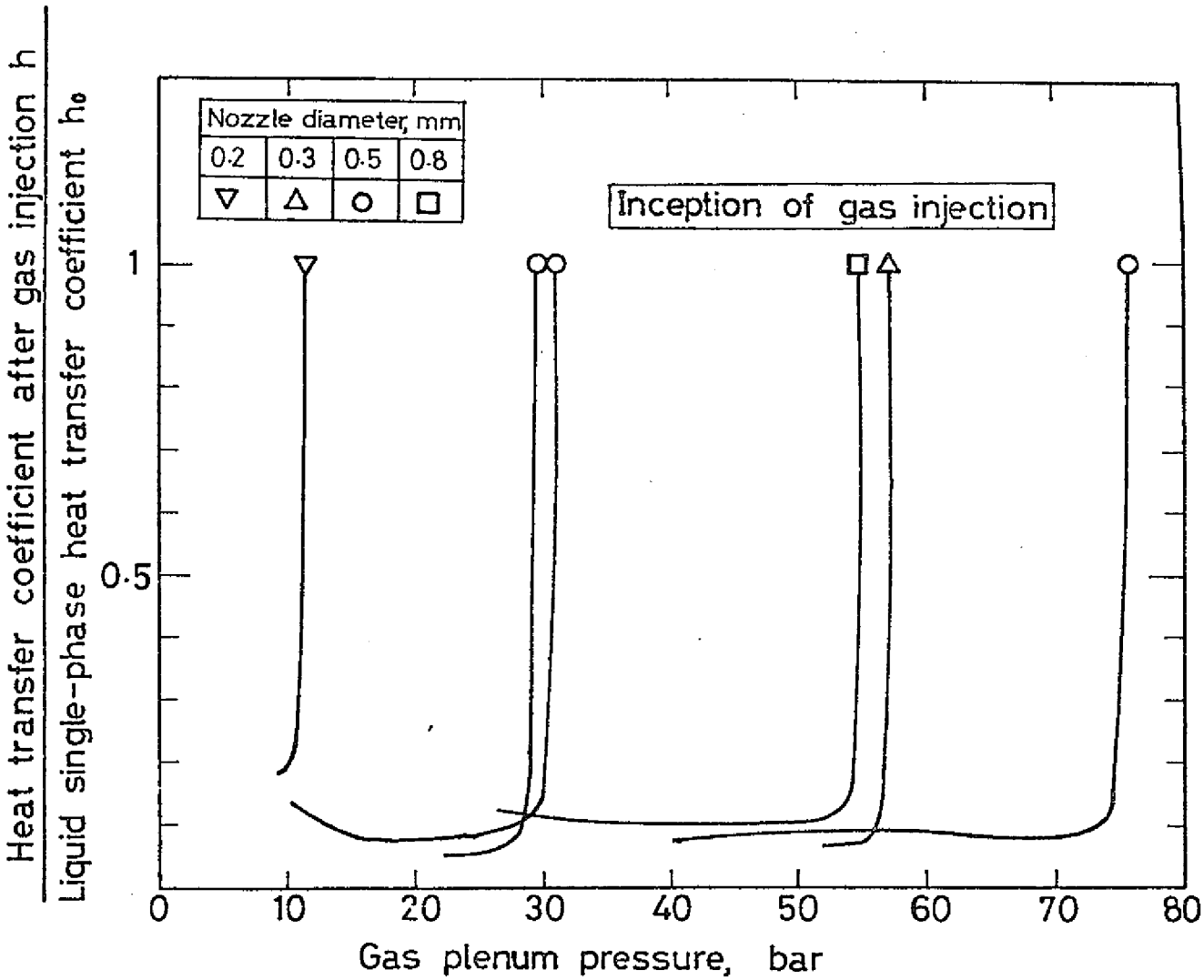

Fig. 8 Change of heat transfer coefficient in impingement area after gas release (PNC-FS-367)

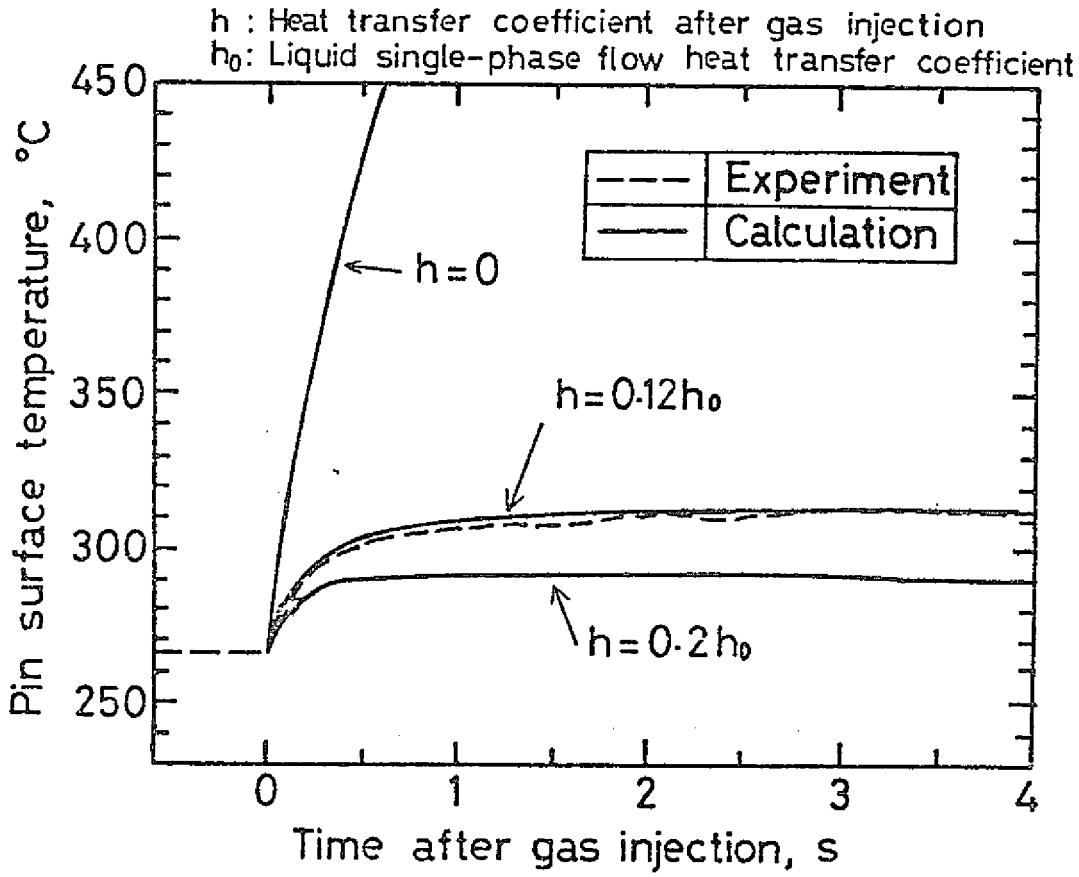

Fig. 9 Comparison of pin surface temperature rise in impingement area observed in a transient release test with the calculation; run No. GR-10 (PNC-FS-366)

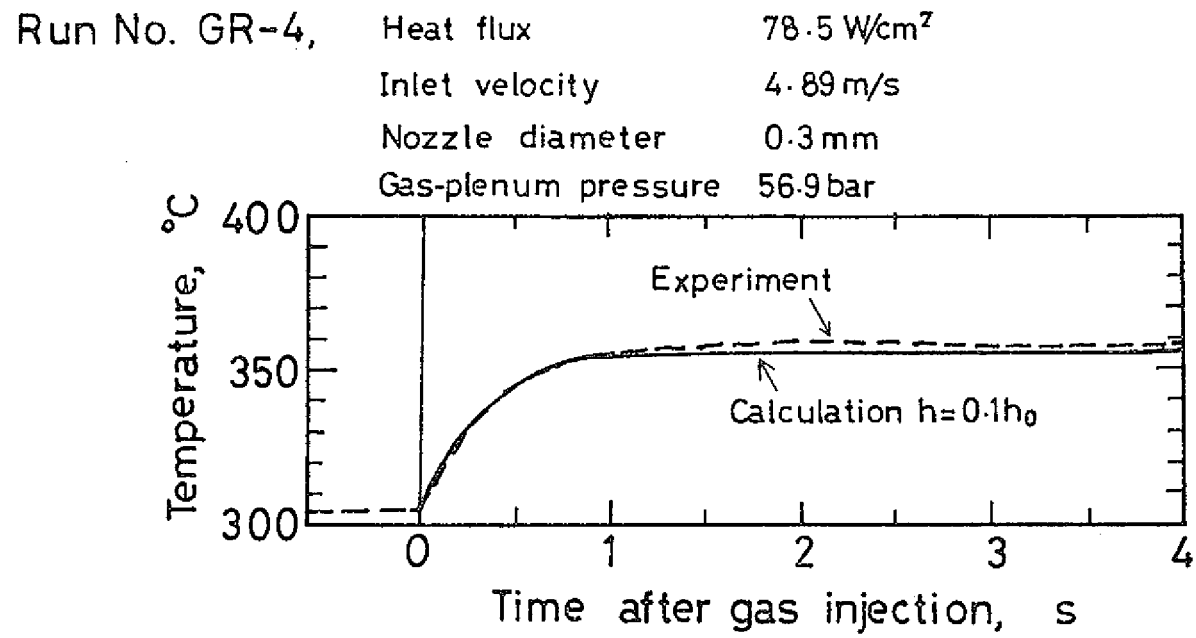

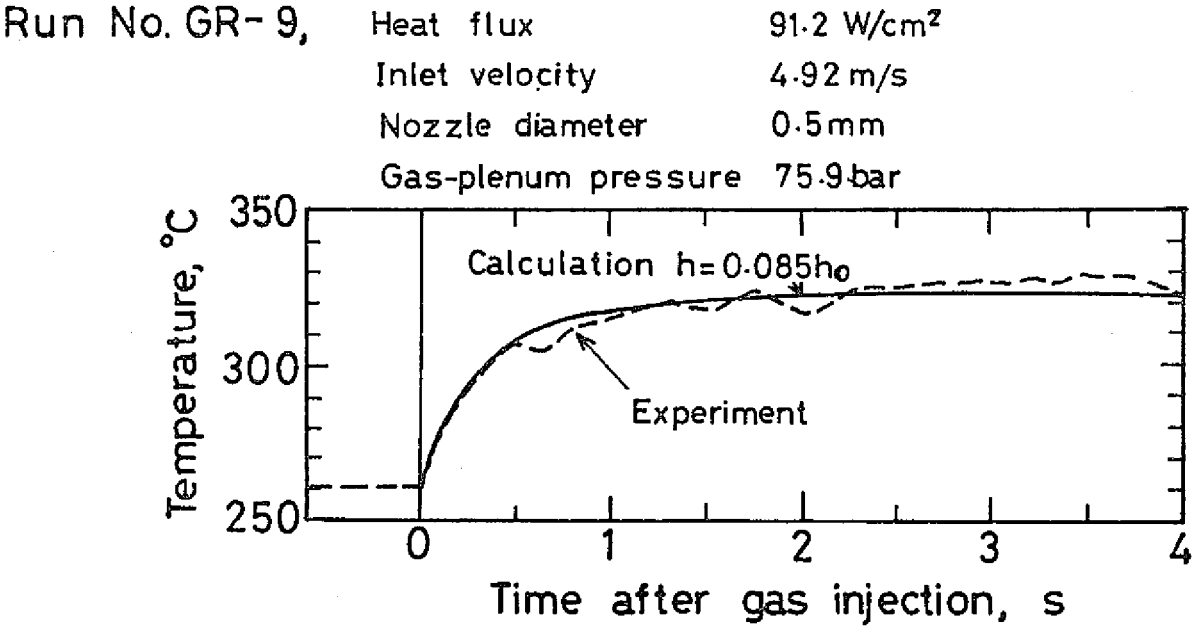

Fig. 10 Comparison of pin surface temperature rise in impingement area in transient release tests with the calculation; run No. GR-4, GR-9 (PNC-FS-365)

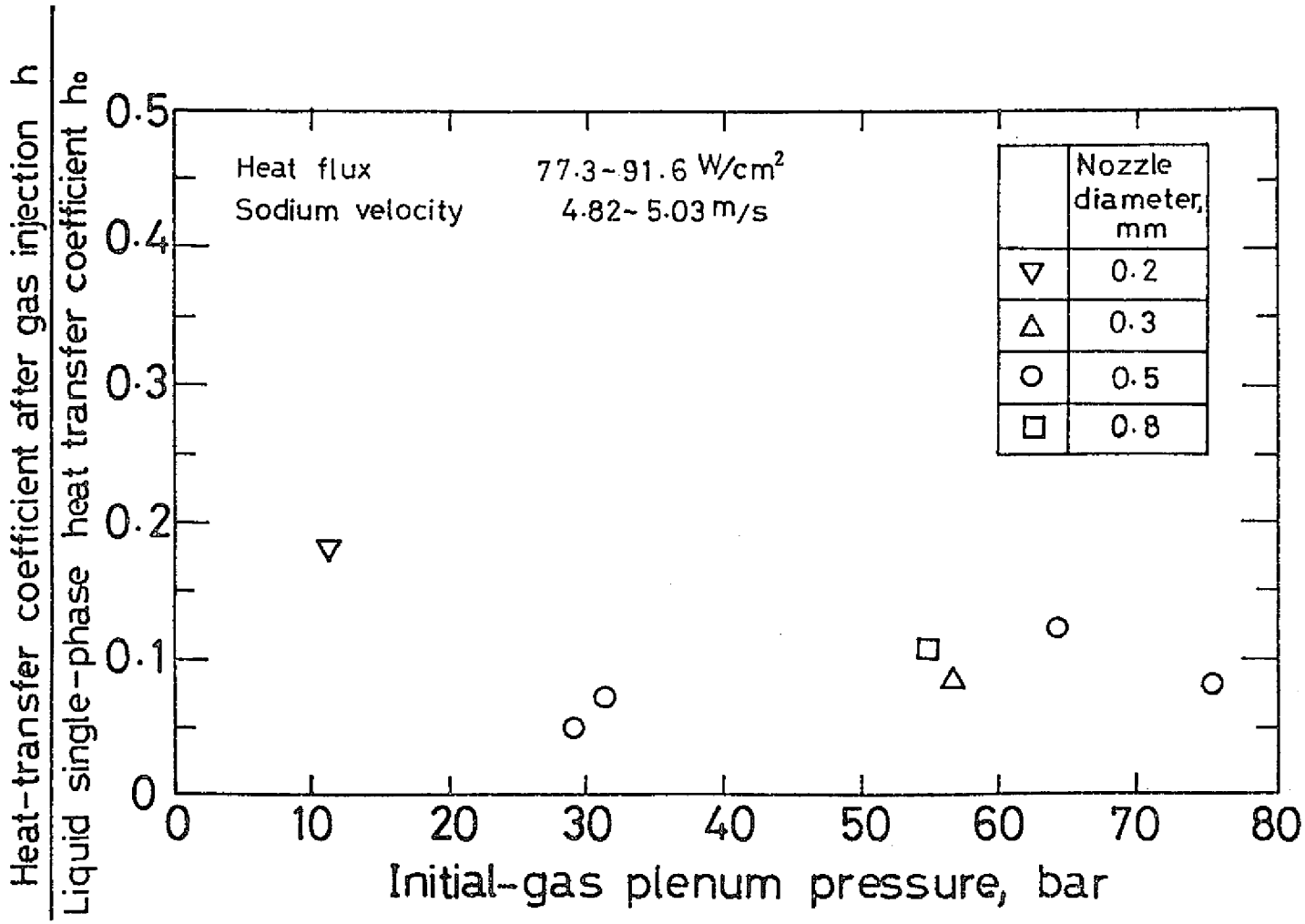

Fig. 11 Ratio of heat transfer coefficient after gas injection to liquid single-phase heat transfer coefficient in impingement area for transient release tests (PNC-FS-335)

coefficient h_G by the gas jet is calculated to be 0.14W/cm^2°C. The details of these calculations are given in Appendix B. On the other hand, the Reynolds number of the sodium single-phase flow through the test section is obtained by the following equation:

$$Re = \frac{VDe}{\nu} = \frac{5.0\ (m/s) \times 3.43 \times 10^{-3}\ (m)}{4.398 \times 10^{-7}\ (m^2/s)} = 39000$$

where De is equivalent diameter, V is flow velocity, and ν is coefficient of kinematic viscosity (a value at 250°C is used). Since the Prandtl number Pr of sodium at 250°C is 0.00655,

$$Re = Pr \cdot Re = 0.00655 \times 39000 = 255$$

The heat transfer coefficient ho of the sodium single-phase flow can be obtained by means of Subbotin's equation as follows:

$$Nu = 5 + 0.025Pe^{0.8} = 5 + 0.025 \times 255^{0.8} = 7.11$$

$$ho = \frac{\lambda Nu}{De} = \frac{0.0791\ (kW/m°C) \times 7.11}{3.43 \times 10^{-3}\ (m)} = 164\ (kW/m^2°C)$$

$$= 16.4\ (W/cm^2°C)\ \text{(Note)}$$

From this, the ratio of h_G/ho is calculated to be 0.14/16.4 = 0.009. Thus it was found that the heat transfer coefficient obtained in the present tests is more than 5 times larger than that by the gas jet alone. This is considered due to the fact that the fine drops of sodium included in the gas jet were

---

Note: From 1W/cm^2°C = 8600kcal/m^{2}h°C, 16.4W/cm^2°C = 1.41 x 10^{5}kcal/m^{2}h°C

sprayed on the impinged surface to cool it. Bell et al[1] conducted a test in which a gas injector nozzle was submerged in water in a water loop and observed the inclusion of liquid droplets into the gas jet. Hoglund et al[2] performed an in-water gas release test and obtained a good heat transfer coefficient, thereby concluding that the spray cooling is dominant on the gas impinged surface. Chawla[12] investigated the instability of the boundary between gas jet and liquid in an attempt to analytically determine the ratio of liquid included in the jet and the size of the liquid drop. When the gas comes out of the nozzle, it rapidly expands in volume and its temperature lowers and therefore it is possible to have a greater cooling effect than in the case in which a simple gas jet impinges on the target surface. However, this effect is nil or negligible, for there was no difference between the case in which the gas was injected with the heater pin not heated and the case in which there was no gas injection.

The heat transfer coefficient of gas impinged surface was was found to be greater than that of only gas jet. However in the case of sodium, the heat transfer coefficient at the gas impinged surface became smaller than that during liquid single-phase flow contorary to the case of water, which was considered due largely to the difference in heat transfer coefficient between sodium and water. Comparing the thermal conductivity and Prandtl number of 250°C sodium and 70°C water which are roughly equal in the coefficient of kinematic viscosity, sodium was found to have a thermal conductivity

of 0.0789kW/m°C and a Prandtl number of 0.0066 while they were so much different as 0.0066kW/m°C and 2.69, respectively in the case of water. Now, for the sake of comparison, we will obtain the heat transfer coefficient in the case where 70°C water flows through the test section at a velocity of 5m/s. At this time, Reynolds number is

$$Re = \frac{VDe}{\nu} = \frac{5.0\ (m/s) \times 3.43 \times 10^{-3}\ (m)}{0.417 \times 10^{-6}\ (m^2/s)} = 41100$$

For a fluid whose Prandtl number is 0.7 - 10, the turbulent flow heat transfer coefficient in a circular tube is given by the following equation from Dittus and Boelter's equation.

$$Nu = 0.023Re^{0.8}Pr^{0.4}$$

By substituting the above value of Reynolds number into the above equation, Nusselts number and heat transfer coefficient h can be obtained as follows:

$$Nu = 0.023 \times 41100^{0.8} \times 2.69^{0.4} = 168$$

$$h = \frac{\lambda}{De} \cdot Nu = \frac{0.66 \times 10^{-3}\ (kW/m°C)}{3.43 \times 10^{-3}\ (m)} \times 168 = 32.2\ (kW/m^2°C)$$

$$= 3.22\ (W/cm^2°C)$$

This value is 0.20 (= 3.22/16.4) times the value for the sodium single-phase flow. It is generally said that the water-gas two-phase flow has a better heat transfer coefficient than the water single-phase flow owing to the effects of the liquid flow velocity increase and turbulence. The same phenomenon would

probably take place also in the case of spray cooling due to the injection of gas into water.

It is also possible that the heat transfer coefficient tends to be evaluated slightly higher when obtained experimentally, for the impinged surface of the pin is heated to a high temperature but the surface on the back side and also the surfaces lower and higher from the impinged area of the same pin are not raised so much in temperature so that the heat will escape from the impinged surface to equalize the pin surface temperature. Since the similar phenomenon will take place for the actual fuel pins, the above-mentioned phenomenon is considered negligible in the evaluation of the fuel pin surface temperature rise due to the release of fission gas.

Next, we will discuss the impinged surface temperature rise in the event of the similar fission gas release occurring in the reactor core from the heat transfer coefficient after the gas injection, which has been obtained in the present tests. The smallest heat transfer coefficient obtained in the present tests is $0.82 W/cm^2 °C$ ($= 0.05 \times 16.4 W/cm^2 °C$) or 0.05 times the heat transfer coefficient for the sodium single-phase flow, which can be obtained from Subbotin's equation. The maximum heat flux during the normal operation of the Monju core is $196 W/cm^2$ (linear power 400W/cm). By using these values, the temperature rise is calculated $((196 W/cm^2)/(0.82 W/cm^2 °C))$ to be 240°C. However, since the amount of gas to be released is limited in the actual fuel pin, the release of gas under a high

pressure will end quickly(Note) and therefore the high temperature of the gas impinged pin will not last long.

Gas ejection may not take place in the actual reactor during its normal operation, for the gap between the inside wall of a new fuel pin and the fuel pellet inserted in it is 0.16mm in diameter (clad inside diameter: 5.56mm) in the Monju design and it decreases as the fuel burns in the reactor. With regard to the decrease of the gap, it is reported that the fuel-clad gap deminished from its initial diameter of 0.2mm to about 0.05mm in the vicinity of the fuel column center where the linear power was highest in the case of a fuel pin in which the burning progressed to about 400W/cm, 55,000MWD/T in the Dounreay experimental fast reactor.(14) It is needless to say that a center hole develops in the fuel pellet during that period of time but its effect is negligible. A report published by the General Electric Company said that measurements were made in the room of the gas release rate from a crack developed on the pin surface apart 170mm from the boundary between the gas plenum and the fuel column after the irradiation of the burn-up of 18,000MWD/T with the peak power of 733W/cm

---

(Note) As for the rate of decrease with time of the gas pressure when gas is released from the fuel pin at critical flow rate, the calculation results were described in the preceding report. According to the results, when the gas injection nozzle diameter is 0.5mm, for instance, the gas pressure in the fuel pin would decrease to 1/10 of the initial pressure.

in the GETR and it was found that 24 minutes were required for the gas pressure to decrease from 6.3 bars to 5.1 bars.

Murata et al[16] performed tests to obtain the frictional pressure loss coefficient when gas flowed through the circular channel and compared thus obtained result with the above-mentioned measured value to determine the effective diametrical gap for the gas flow in the failed pin and found it to be as small as 0.01mm. They reported that the effective diametrical gap was larger as the location of failure was nearer to the gas plenum and that the effective diametrical gap was 0.02mm in the pin similarly failed at the point 66mm distant from the boundary between the gas plenum and fuel column. Erp et al[17] also reported that when a fuel pin clad failure takes place in the IMFBR during its normal operation the rate of gas release is made small by the presence of the fuel pellet in the fuel pin in most cases and that a relatively high rate of gas release occurs only in the case where failure takes place in the gas plenum of a pin in which the burn-up is very high. Chawla et al[18] think that a high rate of gas release can take place in the core in the event of a pump coast down accident because they think that in this case the clad is separated from the fuel by its thermal expansion, thus causing a gap between the fuel and the clad.

2-4-3 Mechanical effects due to pressure pulse and gas release

The strain gauge-type pressure transducers (measuring frequency range: 0 - 2000Hz) made by Shinkoh Communications

Industry Co., Ltd. were set up at the test section inlet and outlet. Fig. 12 shows the values of pressure pulses measured by the inlet pressure transducer P-106 and the outlet pressure transducer P-107 in relation to the gas plenum pressure. From this, it was seen that the magnitude of the measured pressure pulse was less than 0.2 times the initial gas pressure (the maximum measured value was 12 bars at the gas pressure of 55 - 60 bars). Marked with "+" in the figure is the pressure pulse measured on the wrapper tube wall when a high-pressure gas was released from a 6.35mm-diameter aluminum or stainless steel tube inserted into the center of the hexagonal wrapper tube in the EBR-II by Koening[19] by breaking the rupture disc. In this test, the hexagonal wrapper tube was submerged in water in a tank and the height from the point of rupture to the water surface was - 711mm. The height of pressure pulse measured at the initial gas plenum pressure over 50 bars was about 0.2 times the initial gas plenum pressure. The pressure measured near the point of gas release was equal to the pressure measured in the test section vessel and there was radial dumping of pressure pulse. Kazimi[20] analyzed the results of this test, assuming the released gas to spread out in spherical form according to Relay's equation, and stated that the calculated height of the pressure pulse was in agreement with the experimental value.

Wilson et al[5] made investigations on the values of tr and tu on the assumption that if the fuel pin is to be deformed by the pressure pulse the duration time tu of the differential

pressure between both sides on the diametrical direction of the pin should be approximately equal in magnitude to the time period tr of the basic mode of resonance in the diametrical direction of the pin. So, we will make a study on the Monju fuel pin. According to the analytical solution for the pressure distribution on the cylindrical surface by the stepped pulse, tu is given by the following equation.

$$tu = 2d_2/c \quad \cdots\cdots (1)$$

where d_2 is the outside diameter of pin and c is the sonic velocity in the fluid around the pin. The approximate resonance frequency ν_r of the pin is given by

$$\nu_r^2 = \frac{\beta_0{}^4 EI}{4\pi^2 M\ell^4} \quad \cdots\cdots (2)$$

And

$$t_r = \frac{1}{\nu_r} \quad \cdots\cdots (2)'$$

where β_0 is a constant and it is π in the case of a beam supported at both ends (the pressure pulse works perpendicularly on the fuel pin and therefore the fuel pin can be considered as a beam that is supported on the pin behind through the spacer wire), E is Young's modulus, I is the moment of inertia of area, M is the mass per unit length, and ℓ is the distance between the supports (the spacer wire pitch). If calculations are made for the Monju fuel pin, d_2 = 0.65cm. Assuming that the sonic velocity in sodium c = 2.3 x 10^5cm/s (at 500°C), we obtain the

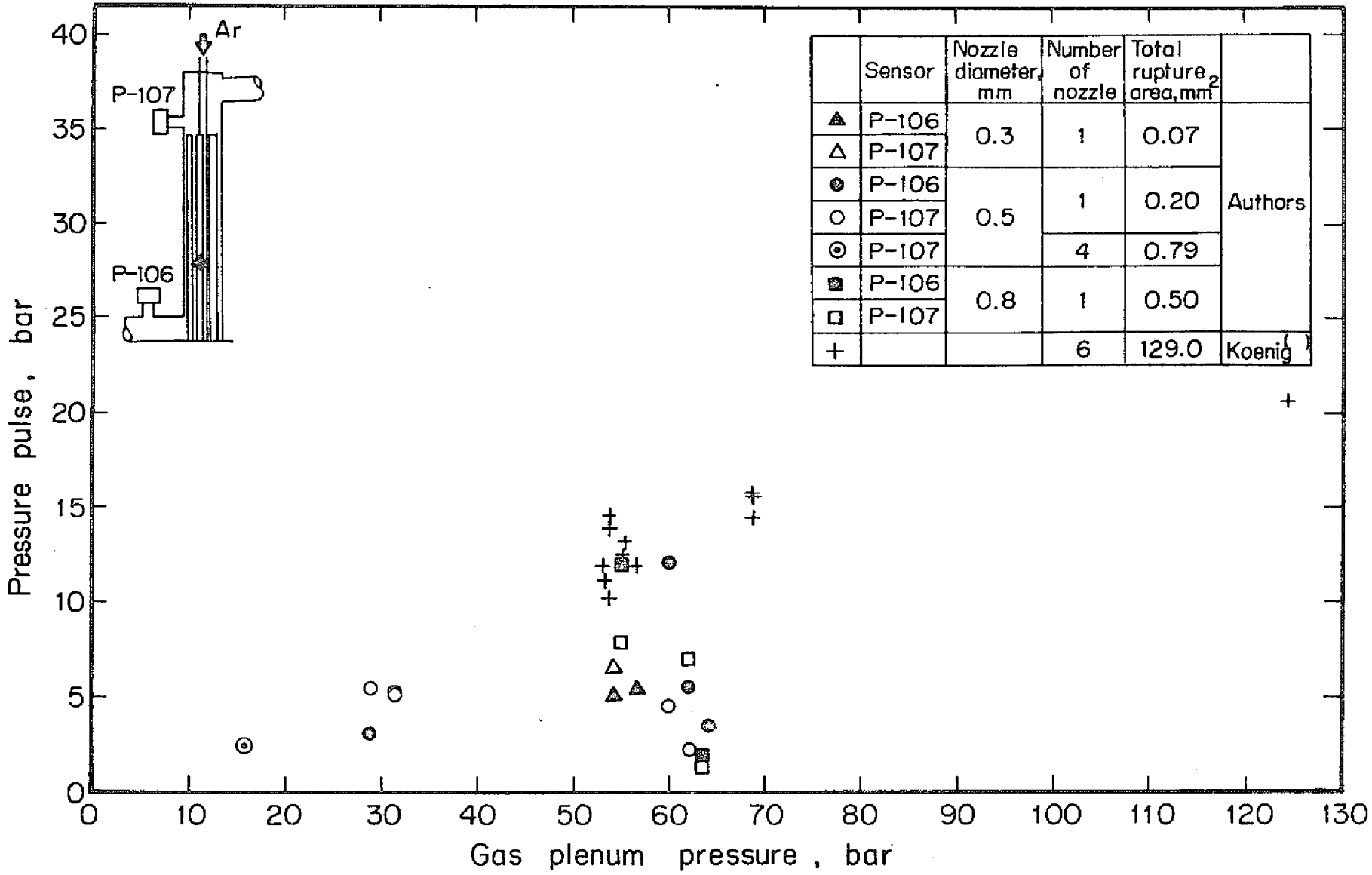

Fig. 12 Effect of gas plenum pressure on pressure pulse for transient release tests (PNC-FS-447)

following equation from equation (1):

$$tu = \frac{2 \times 0.65}{2.3 \times 10^5} = 5.9 \times 10^{-6} \text{ (s)} = 5.9 \text{ (μs)}$$

If the inside diameter (0.556cm) of the pin clad tube is represented by d_1 and the mass ($8g/cm^3$) by ρ and the spacer wire pitch is 30cm,

$$E = 15000 \text{ (kg/mm}^2\text{)} = 1.5 \times 10^{12} \text{ (dyn/cm}^2\text{)}$$
$$= 1.5 \times 10^{12} \text{ (g/cm s}^2\text{)}$$

$$I = \frac{\pi}{64} (d_2^4 - d_1^4) = \frac{\pi}{64} (0.65^4 - 0.556^4) = 0.00407 \text{ (cm}^4\text{)}$$

$$M = \rho \cdot \frac{\pi}{4} (d_2^2 - d_1^2) = 8 \times \frac{\pi}{4} (0.65^2 - 0.556^2) = 0.712 \text{ (g/cm)}$$

$$\ell = 30\text{cm}$$

$$\nu_r = \frac{\pi^2}{4} \cdot \frac{1.5 \times 10^{12} \times 0.00407}{0.712 \times 30^4} = 161 \text{ (1/sec)}$$

$$t_r = \frac{1}{161} = 0.00621 \text{ (s)} = 6.2 \text{ (ms)}$$

Hence, $tu \ll tr$ and therefore it can be concluded that the pin will not be deformed by the pressure pulse.

After completion of all the present tests, the pin bundle was removed from the test equipment and carefully inspected to find no change from normal in the pin surface condition and geometry and it was in good condition. No serious damaged was observed in the test performed by Uematsu et al[6], in which the failed pin located in the center of the 60-pin simulating assembly in the water loop was ruptured under the gas pressure

of 82 - 166 bars for the purpose of investigating the effects on the surrounding pins (filled with stainless steel pellets) and grids.

As was discussed above, there seems to be no possibility of the pins being damaged due to the mechanical effects of gas release.

2-4-4 Coolant dynamics due to gas release

Initial expulsion acceleration of sodium downstream from the gas release nozzle

Fig. 13 shows the effect of gas plenum pressure on the initial explusion acceleration of the liquid column downstream from the gas injector nozzle immediately after the gas injection. The value of the initial expulsion acceleration was obtained by differentiating the value of the expulsion acceleration measured by means of the outlet flowmeter F-107. From Fig. 13, it is seen that the higher the gas plenum pressure, the greater the initial expulsion acceleration. The solid line in the figure shows the theoretical value analytically obtained by the one-dimensional liquid column model as shown in Appendix C. In the analysis, it was assumed that the pressure of (gas plenum pressure) - (pressure loss due to the flow into and out of the gas injector nozzle) was applied to the entire section of the test section where the gas was injected, thereby one-dimensional rigid liquid column present thereabove. The experimental value is considerably smaller than the straight line showing the theoretical value. This is because where the

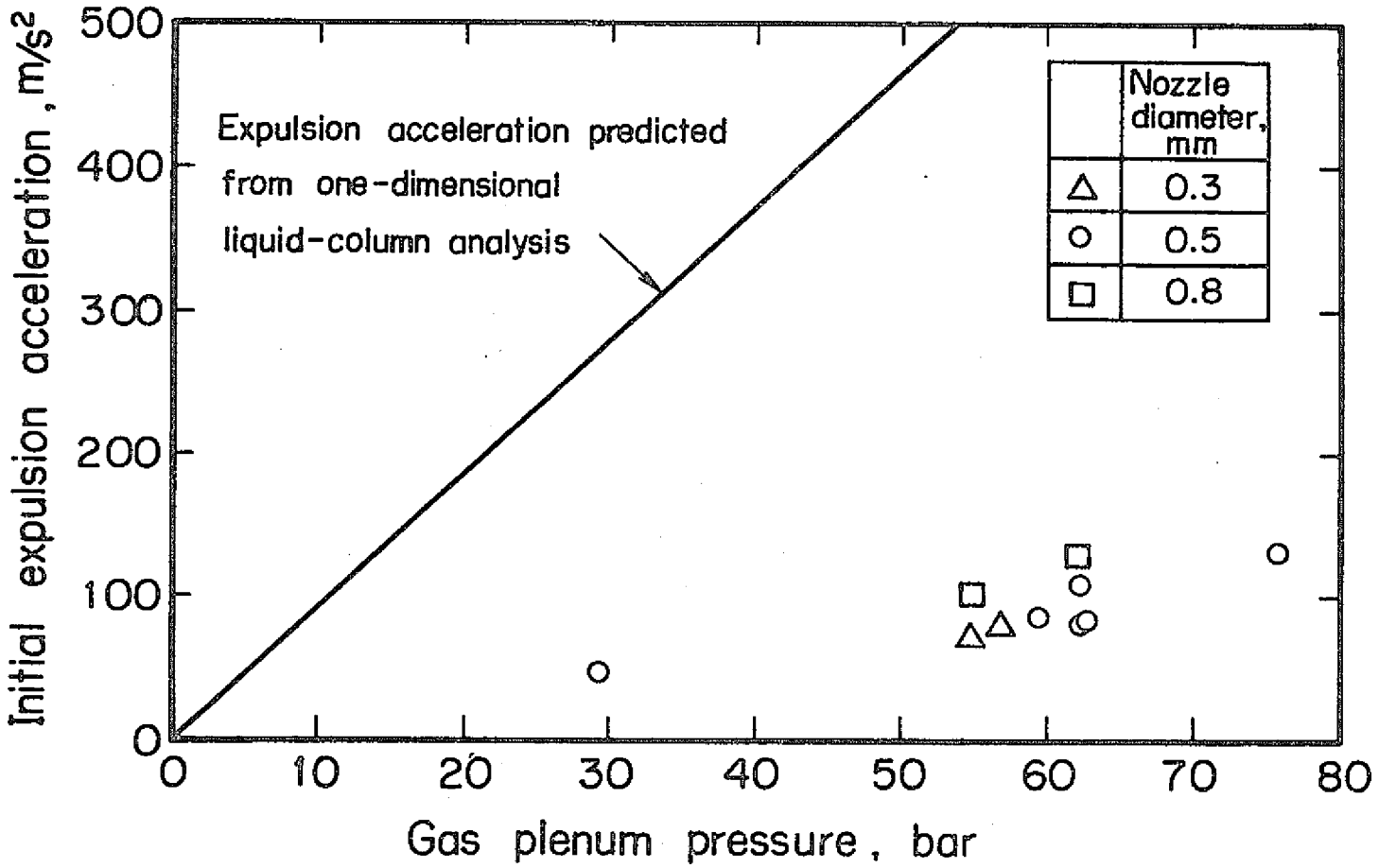

Fig. 13 Effect of gas plenum pressure on initial expulsion acceleration of liquid for transient release tests (PNC-FS-344)

gas is injected it spreads into some subchannels as is evident from the fact that the pin surface temperature change is restricted to the pin surface near the gas injector nozzle. Therefore, from this figure, it is seen that the behavior of sodium downstream from the gas injector nozzle during the transient gas release cannot be expressed by onedimensional model unless a multiple of pins fail simultaneously.

Maximum expulsion velocity of sodium downstream from the gas injector nozzle

Fig. 14 shows the difference between the maximum expulsion velocity of sodium after gas injection and the velocity before gas injection in relation to the gas plenum pressure. From Fig. 14, it is seen that the maximum expulsion velocity tends to increase as the gas plenum pressure increases. This data are rearranged by plotting the initial gas release rate on the horizontal axis in Fig. 15, which shows that the difference between the maximum expulsion velocity and the velocity before gas injection increases in proportion to the initial gas release rate.

Bubble spreading velocity

The test section is provided with 14 pairs of voidmeters in the axial direction and an electromagnetic flowmeter near the downstream end of the pin bundle. Some of the signals from these voidmeter and flowmeter are shown in Fig. 5, in which the outlet flowmeter signal increases sharply immediately after the gas injection and thereafter remains roughly constant until the

gas bubbles reach the position of the electromagnetic flowmeter. Fig. 16 shows the change with time of the upper boundary of the two-phase flow obtained from the voidmeter and outlet flowmeter signals. From this figure, it is seen that the upper boundary of the two-phase flow spreads downstream at a roughly constant velocity. When the flow velocity is constant, the greater the gas release rate is, the faster the gas bubble spread. If the bubble spreading velocity is obtained in the test GR-12, since the bubbles reached the flowmeter 0.96m downstream from the gas injector nozzle in 0.098 seconds after the gas injection, the bubble spreading velocity is calculated to be 0.98/0.098 = 9.8m/s, showing that the bubbles spread at a velocity roughly twice as fast as the flow velocity. When the flow velocity before gas injection was low (GR-11), the bubble spreading velocity was also so much lower. Voidmeters were also set up on the upstream side but they detected no void, showing that the gas bubbles spread only downstream.

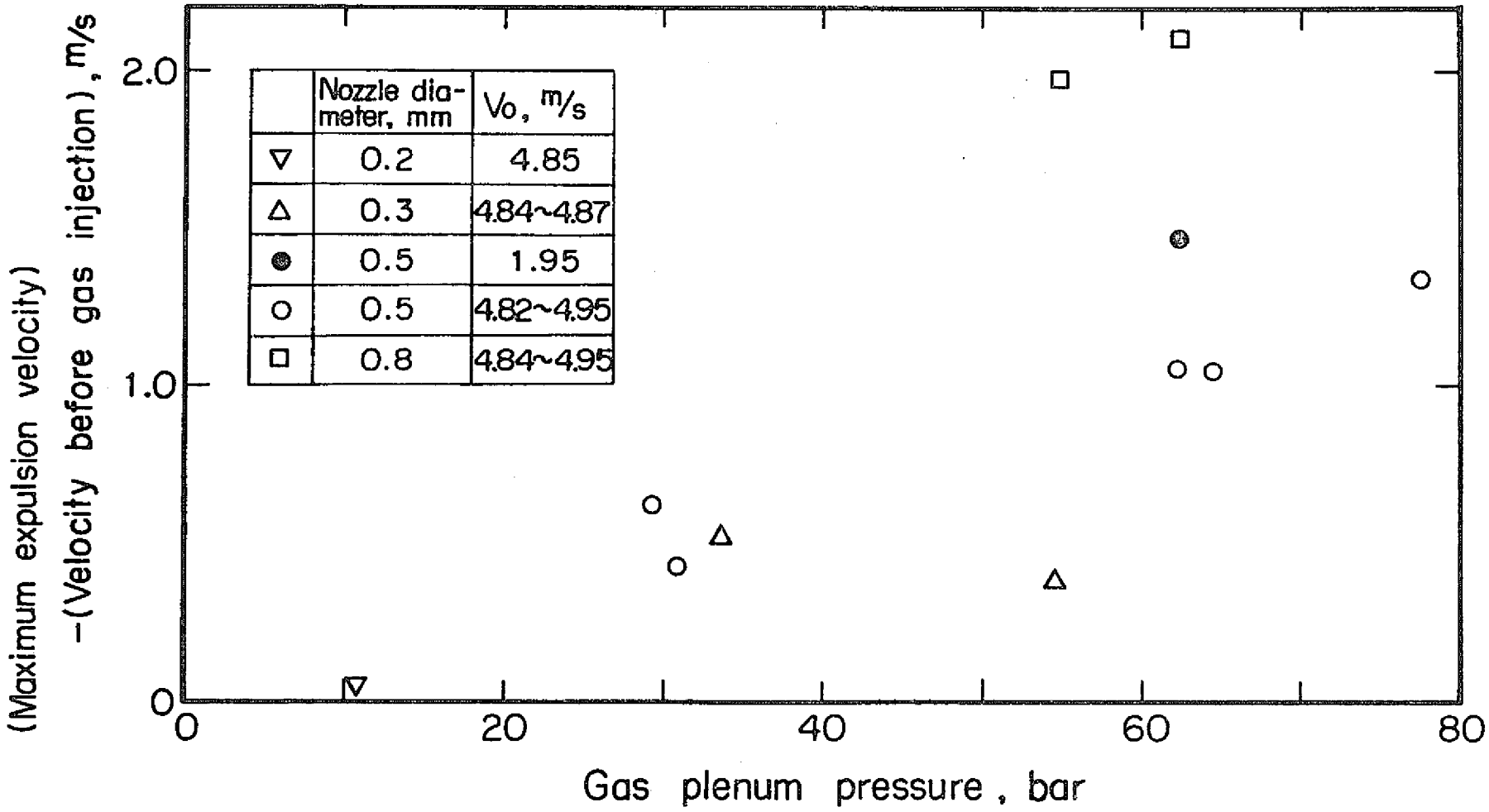

Fig. 14 Effect of gas plenum pressure on maximum expulsion velocity in transient release tests (PNC-FS-448)

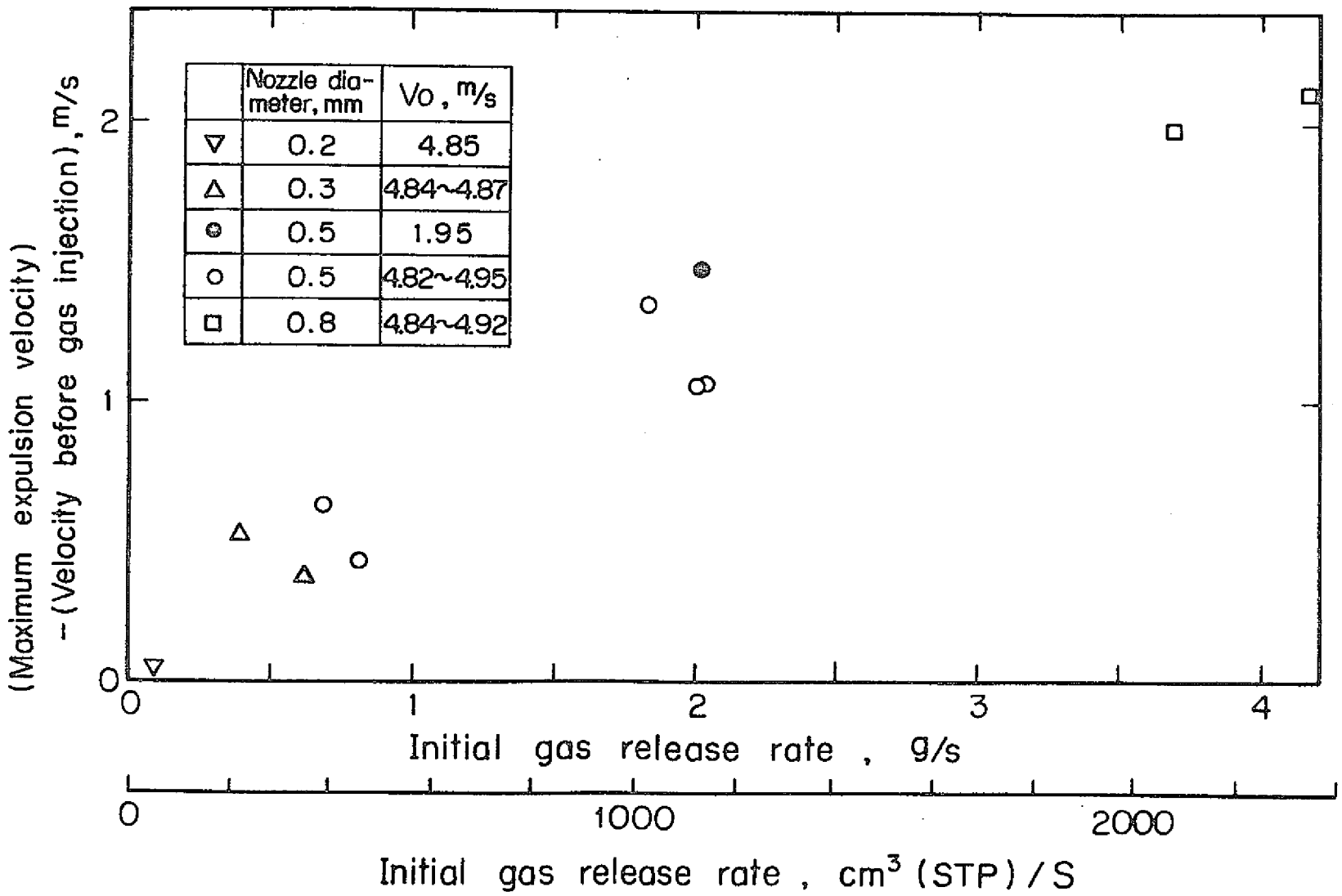

Fig. 15 Effect of gas release rate on maximum expulsion velocity in transient release tests (PNC-FS-449)

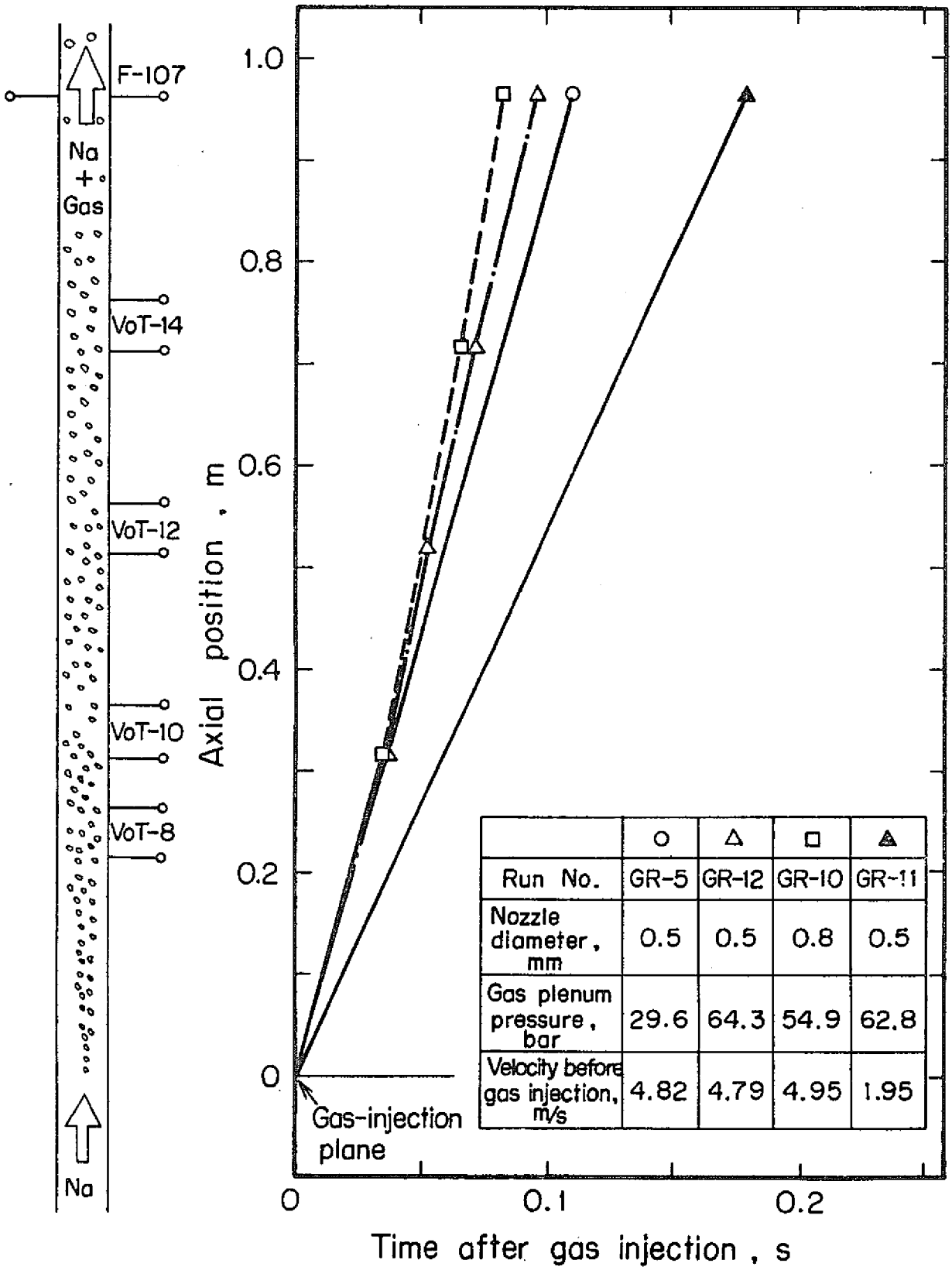

Fig. 16 Movement of upper boundary of gas bubbles described from void tap and flowmeter signals for transient release tests (PNC-FS-450)

Chapter 3. Continuous Gas Release Tests

3-1 Test objective

When fission gas is released in the fuel assembly, if the pin surface temperature does not overshoot but settles down at a certain new value after the gas injection, the continuous gas release test may suffice for the investigation of the fuel pin surface temperature rise due to the release of fission gas. This being so, for the purpose of supplementing the transient release tests, of which the number was limited, we performed the continuous gas release tests in which measurements were made of the change of heater pin surface temperature by varying the gas injector nozzle diameter, heat flux and sodium flow velocity. We also measured the outlet flow velocity fluctuations and acoustic noise for the purpose of investigating the possibility of detecting the occurrence of gas release in the reactor.

3-2 Test procedure

Prior to the gas release test, the thermocouples were calibrated by flowing isothermal sodium through the test section with no heat input into it. Next, measurements were made of sodium single-phase flow of the same flow rate and heat input as in the gas release test. To conduct the continuous gas release test, all the stop valves of the release system pipelines were opened to continuously release the gas through the

nozzle after completion of the transient gas release tests described in the preceding chapter and the sodium flow rate, heat input into the test section and released gas pressure were preset to the required values. After the various parts of the test section became constant, the test data were recorded on the multiple-point digital data recorder and analog data recorder.

3-3 Test conditions

The continuous gas release tests were carried out under the following conditions.

Gas injector nozzle diameter:	0.3, 0.5, 0.8mm
Released gas pressure:	6 - 64 bars
Gas release rate:	0.06 - 3.44g/s (34 - 1930cm^2 (STP)/s)
Quality:	1.5×10^{-5} - 3.8×10^{-3}
Heater pin heat flux:	8.0 - 92.3W/cm^2
Inlet sodium flow velocity:	0.45 - 5.07m/s
Inlet sodium temperature:	238 - 290°C

A total of 123 continuous gas release tests were carried out. The details of the tests are shown in Table 2 of Appendix D. Prior to each test, data obtained at the sodium single-phase flow with the inlet velocity and heat flux equal to those at the time of gas release were recorded. The test conditions for this test are also shown in Table 2 of Appendix D.

3-4 Test results and discussions

3-4-1 Heat pin surface temperature distribution and heat transfer coefficient

The rise in enthalpy of sodium in the test section was in good agreement with the electrical input into the heater pin. Fig. 17 shows some examples of heat pin surface temperature distribution in the continuous gas release test. Fig. 17 (a) shows the case in which the inlet flow velocity was 4.7 - 4.9m/s, the heat flux was 78 - 79W/cm^2 and the gas pressure was 11, 32 and 63 bars and the case of sodium single-phase flow and the difference from the inlet temperature is shown. The figure on the bottom of Fig. 17 (a) shows the pin surface temperature rise from the test section inlet at the gas-injection plane, the figure in the middle shows the same 40mm downstream from gas-injection plane, and the figure on the top shows the same 80mm downstream from gas-injection plane. The numbers of the pins fitted with thermocouples are shown on the horizontal axis of each figure. In this figure, it was No. 3 pin that was impinged by the gas jet and there was a conspicuous rise in the temperature on the impinged surface of this pin when gas was injected but the temperature rise 80mm downstream was roughly the same in the pins from No. 2 through No. 5. Fig. 17 (b) shows the case in which there was gas injection and the case in which there was no gas injection with the sodium flow rate being 0.5m/s and heat flux 8W/cm^2 in both cases. The sodium flow was so slow that the gas tended to spread out in the radial direction and the temperature rise due to the gas injection was observed in

all the pins in all the planes and the temperature rise on the impinged surface was smaller than that in other pins and in the downstream surface of the same No. 3 pin contrary to the case in Fig. 17 (a).

Although the relation of the gas pressure and flow velocity to the temperature rise can be investigated to some extent by these figures, in order to make clear the tendency, investigations will be made on the effects of gas pressure, flow velocity and gas release rate on temperature rise. Since it is impossible to make comparison by the measured values of temperature rise when the heat flux and flow velocity are varied, the ratio of heat transfer coefficient during gas injection to the liquid single-phase heat transfer coefficient h/ho was calculated from the measured value of the pin surface temperature by the following equation as was done in Paragraph 2-4-2.

$$h/ho = (Two - Tc)/(Tw - Tc)$$

Heat transfer coefficient of gas impinged surface

Fig. 18 shows the relation between the gas impinged surface heat transfer coefficient and gas pressure in the case the inlet flow velocity was 4.7 - 5.0m/s, which was roughly the same as in the transient gas release tests. Marked with "Δ" (nozzle diametre: 0.3mm) and "o" are the continuous gas release test data, which are distributed within the range of heat transfer coefficient ratio from 0.07 to 0.3 and when the gas pressure increased over 30 bars the values for h/ho were found within the range of heat transfer coefficient ratio from 0.07 to 0.15. Marked with

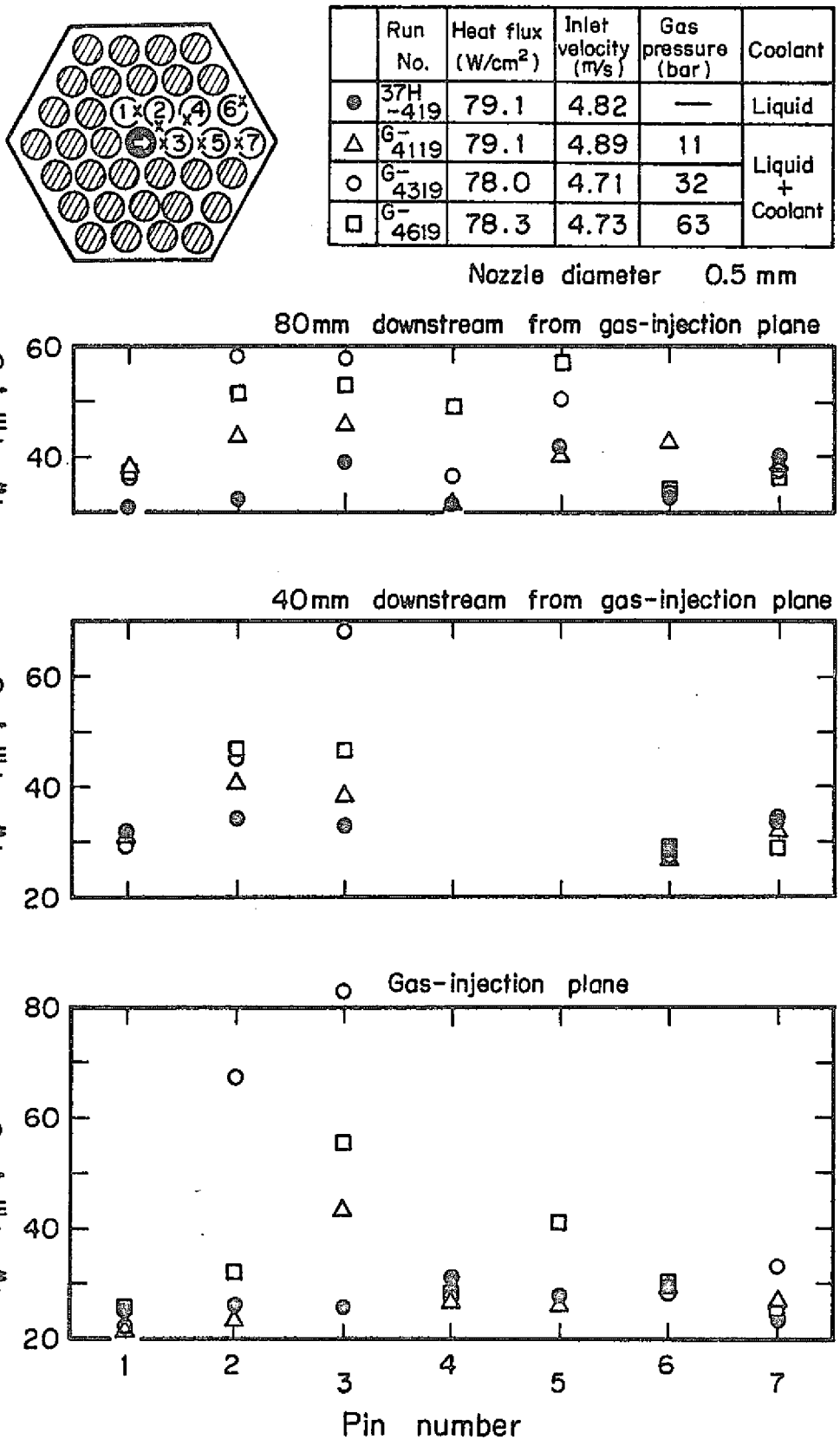

Fig. 17(a) Effect of gas plenum pressure on pin surface temperature rise for continuous release tests; Vin=4.7∿4.9m/s (PNC-FS-486)

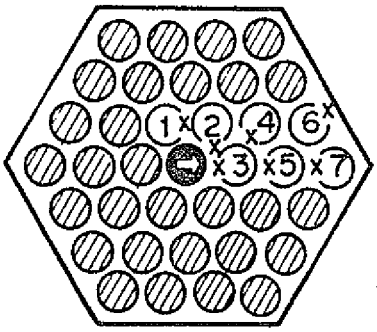

	Run No.	Heat flux (W/cm^2)	Inlet velocity (m/s)	Gas pressure (bar)	Coolant
●	37H-401	7.9	0.46	——	Liquid
△	G-4101	7.9	0.48	11	Liquid + Coolant
○	G-4301	8.0	0.49	32	
□	G-4601	7.9	0.49	63	

Nozzle diameter 0.5 mm

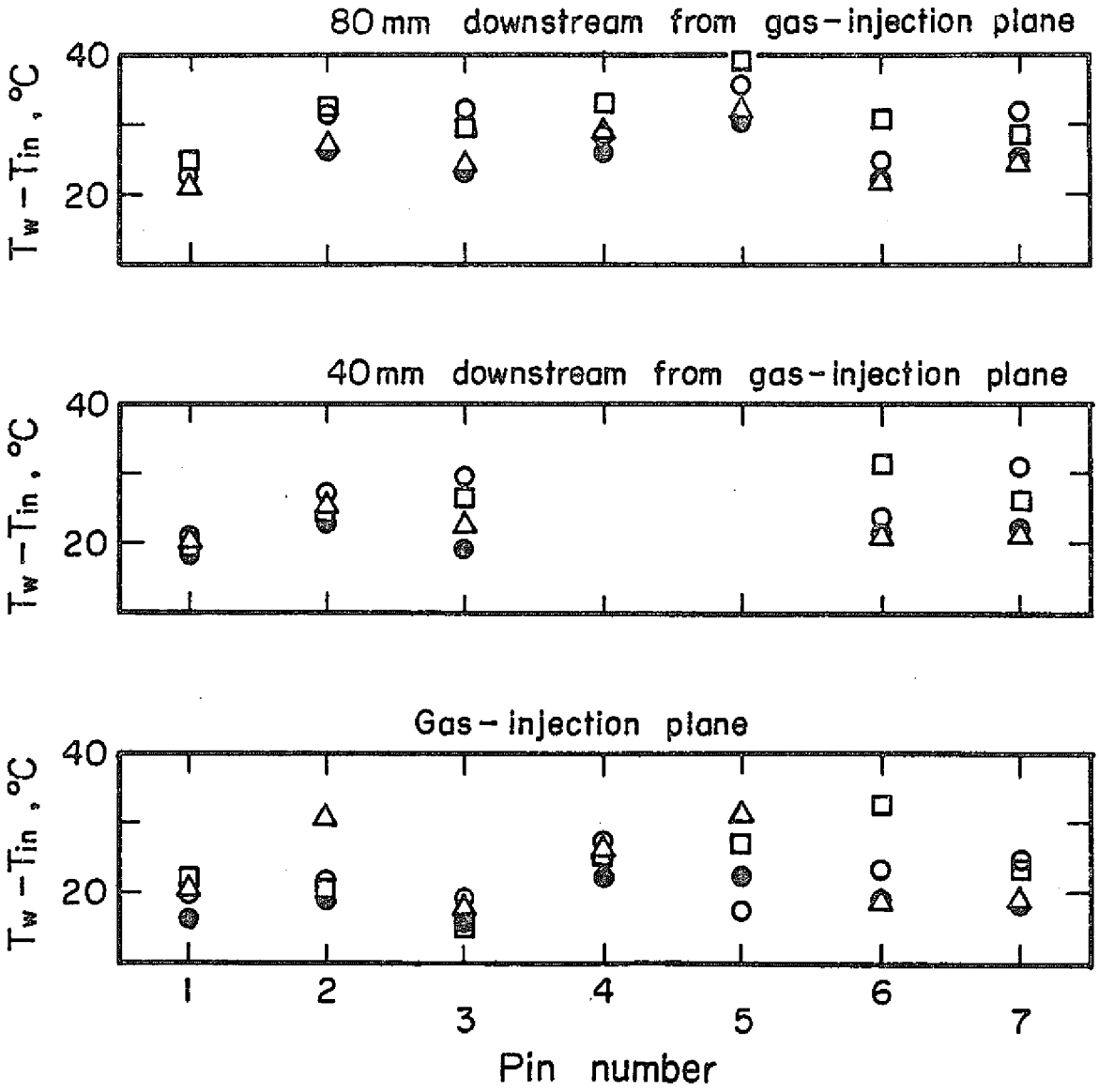

Fig. 17(b) Effect of gas plenum pressure on pin surface temperature rise for continuous release tests; Vin=0.5m/s (PNC-FS-452)

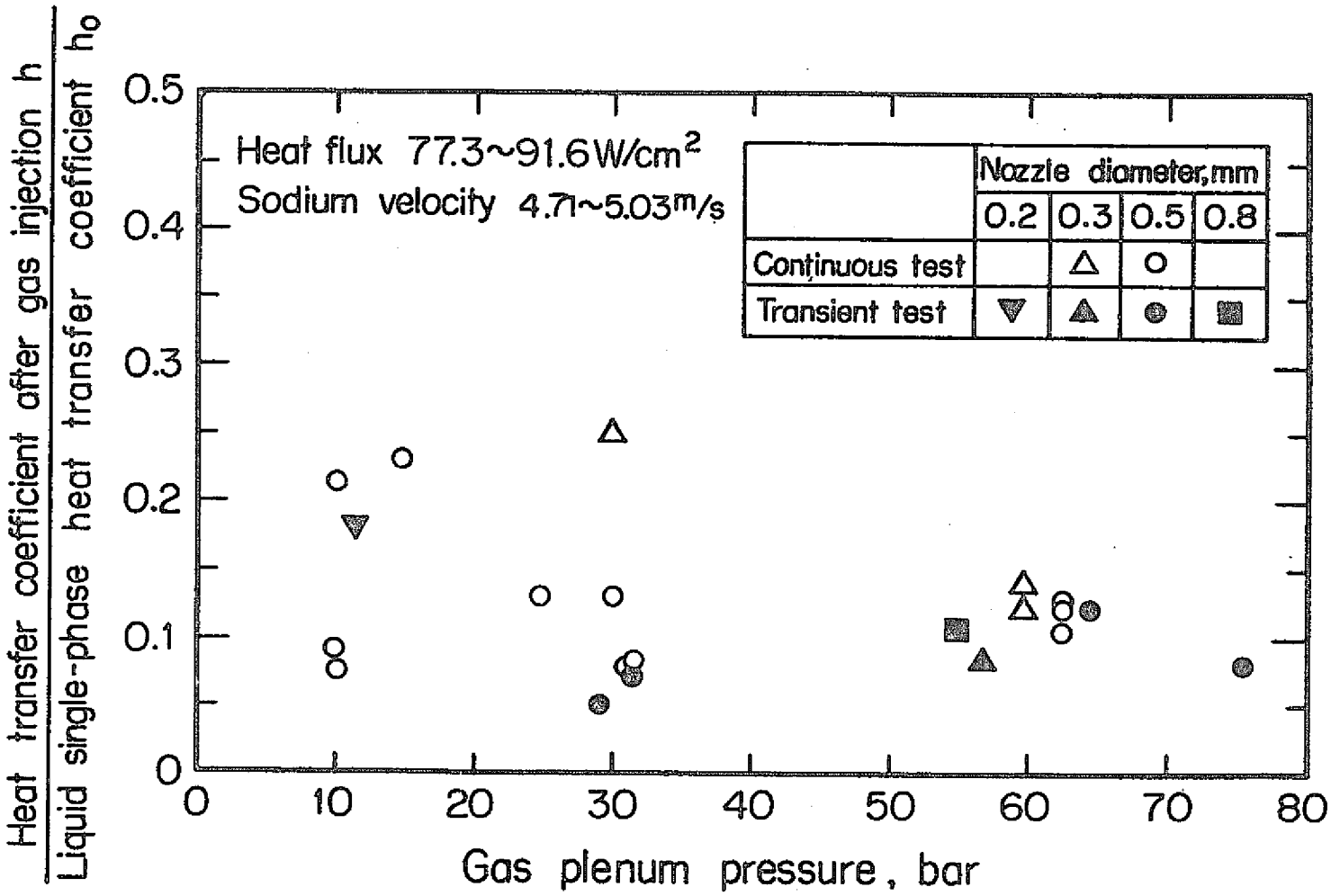

Fig. 18 Ratio of heat transfer coefficient during gas injection to liquid single-phase heat transfer coefficient in impingement area; Comparison between transient release tests and continuous release tests (PNC-FS-463)

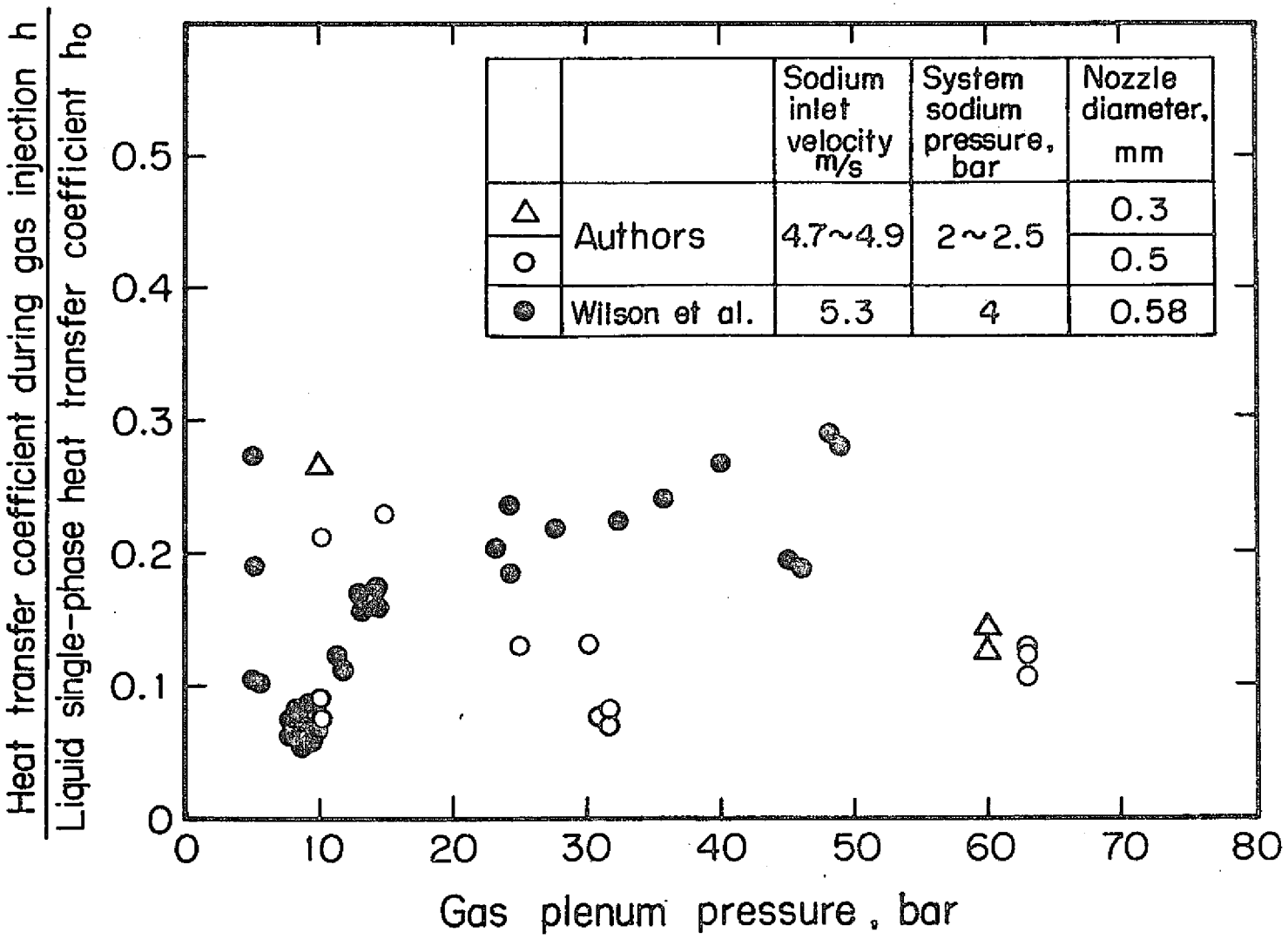

Fig. 19(a) Effect of gas plenum pressure on ratio of heat transfer coefficient during gas injection to liquid single-phase flow heat transfer coefficient in impingement area; Vin=4.7∿4.9m/s (PNC-FS-451)

"▽", "△", "o" and " " are the data obtained in the transient gas release tests, which show the values of 0.05 - 0.15 in the range of gas pressure over 30 bars, giving good agreement with the continuous gas release test results. From this finding, it seems that the continuous gas release test may be sufficient for investigating the temperature change due to the gas release. The heat transfer coefficient was found to have a tendency to restore the value in liquid single-phase flow when the gas pressure lowered below 20 bars.

Fig. 19 (a) shows the comparison of the continuous gas release test results as shown in Fig. 18 and the results of similar tests Wilson et al[5] conducted, using a 3-heater pin bundle. The tests of Wilson et al used the nozzle diameter of 0.58mm and the obtained value for h/ho ranged from 0.05 to 0.3, giving good agreement with our data. Fig. 19 (b) shows the case in which the sodium inlet velocity was 1.7 - 2.0m/s, showing the values for h/ho distributed in the range from 0.1 to 0.3. Fig. 19 (c) is the case in which the sodium inlet velocity was 0.8 - 1.0m/s and in this case the values for h/ho were scattered within the range from 0.15 to 0.55. Fig. 19 (c) also shows the data Wilson et al obtained in their tests in which the sodium inlet velocity was 1.1m/s. In this case, the values for h/ho are 0.05 to 0.4. When the sodium inlet velocity is so low like this, the relation between gas pressure and heat transfer coefficient is not clear.

Fig. 20 (a) through (c) show the relation between sodium inlet velocity and heat transfer coefficient. Fig. 20 (a) is

the case in which gas pressure Pg was 58 - 62 bars, Fig. 20 (b) is the case in which Pg was 27 - 31 bars and Fig. 20 (c) is the case in which Pg was 9 - 12 bars. From these figures, it is seen that the heat transfer coefficient tended to become smaller as the sodium inlet velocity increased. This was presumably due to the fact that as the sodium flow velocity increased it became difficult for the gas bubbles to spread in the radial direction and they were concentrated in the vicinity of the gas impinged surface and consequently the inclusion of sodium drops into the gas.

Fig. 21 shows the relation between the gas release rate and heat transfer coefficient, which shows no particularly distinct tendency.

Axial heat transfer coefficient distribution

Fig. 22 shows the axial heat transfer coefficient distribution for the gas impinged pin (No. 3) in the case in which the sodium inlet velocity was 4.7 - 4.9m/s, gas pressure 61 - 63 bars and gas injection nozzle was 0.5mm. The heat transfer coefficient was smallest where the gas was injected and did not increase very much even in the area 80mm downstream from the gas-injection plane. Fig. 22 also shows the heat transfer coefficient distribution obtained from the results of tests Wilson et al performed under the approximately the same conditions. To do the tests, they used a test section in which the gas impinged pin was fitted to it via bellows so that the pin was movable to some extent in the axial direction during the

test. Shown in Fig. 22 are the values measured by means this test section and they were restricted to the area near the gas injector nozzle.

Fig. 23 shows the effects of sodium inlet velocity and gas pressure on the heat transfer coefficient distribution. The figure on the bottom is the case in which the sodium inlet velocity was 4.7 - 4.9m/s. In this case, the heat transfer coefficient was not affected by gas pressure and it was lowest where the gas was injected. However, the heat transfer coefficient became smaller in the area downstream from the gas-injector nozzle in the case in which the sodium inlet velocity was 1.9m/s and the gas pressure was 63 bars and the case in which the sodium inlet velocity was 0.9 - 1.0m/s as shown in the figure on the top.

The decrease in the heat transfer coefficient on the gas impinged surface was due to the fact that the pin surface was covered with the gas jet instead of the flowing sodium while the heat transfer coefficient decrease in the area downstream from the gas-injector nozzle was imputable to the inclusion of gas into sodium having a high thermal conductivity. The effect of the gas jet does not extend to the area downstream from the gas-injection nozzle and it can be treated as a problem of sodium-gas two-phase flow, which will be discussed in Chapter 4.

Temperature rise due to gas release during normal operation Monju reactor

In this test, argon was used to simulate the fission gas and the temperature of the released gas was equal to that of

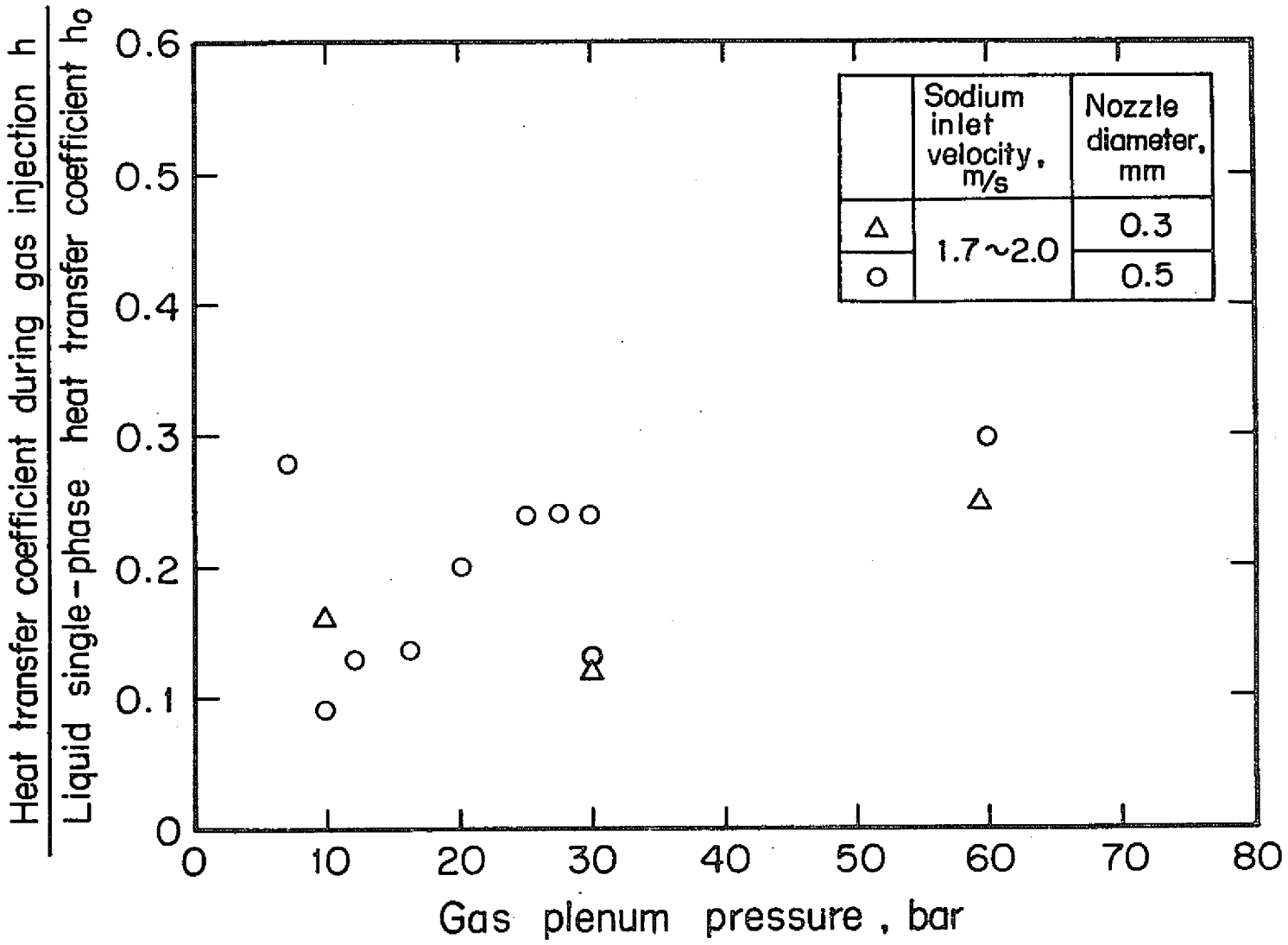

Fig. 19(b) Effect of gas plenum pressure on ratio of heat transfer coefficient during gas injection to liquid single-phase heat transfer coefficient in impingement area; Vin=1.7~2.0m/s (PNC-FS-462)

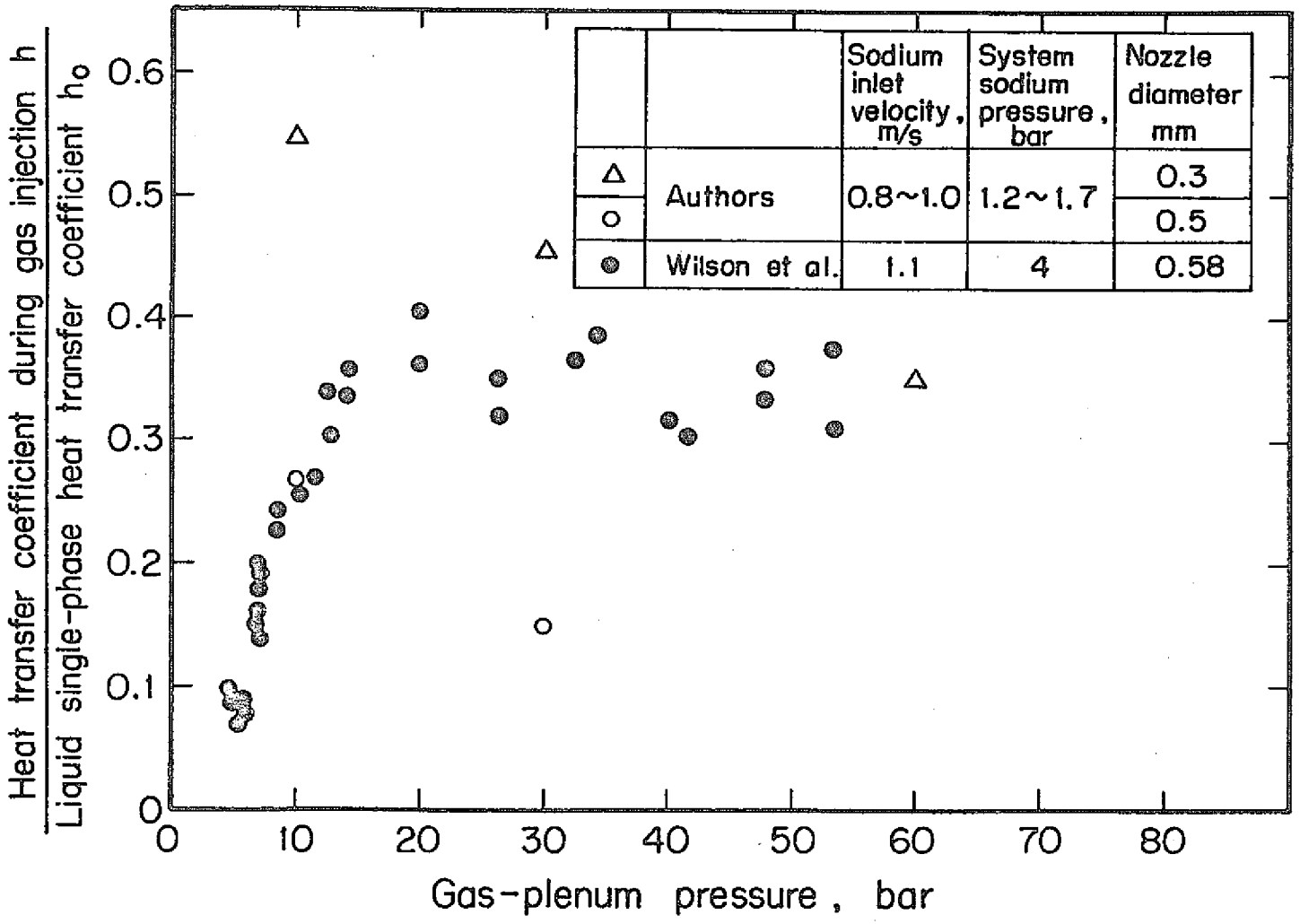

Fig. 19(c) Effect of gas plenum pressure on ratio of heat transfer coefficient during gas injection to liquid single-phase heat transfer coefficient in impingement area; Vin=0.8∿1.0m/s (PNC-FS-453)

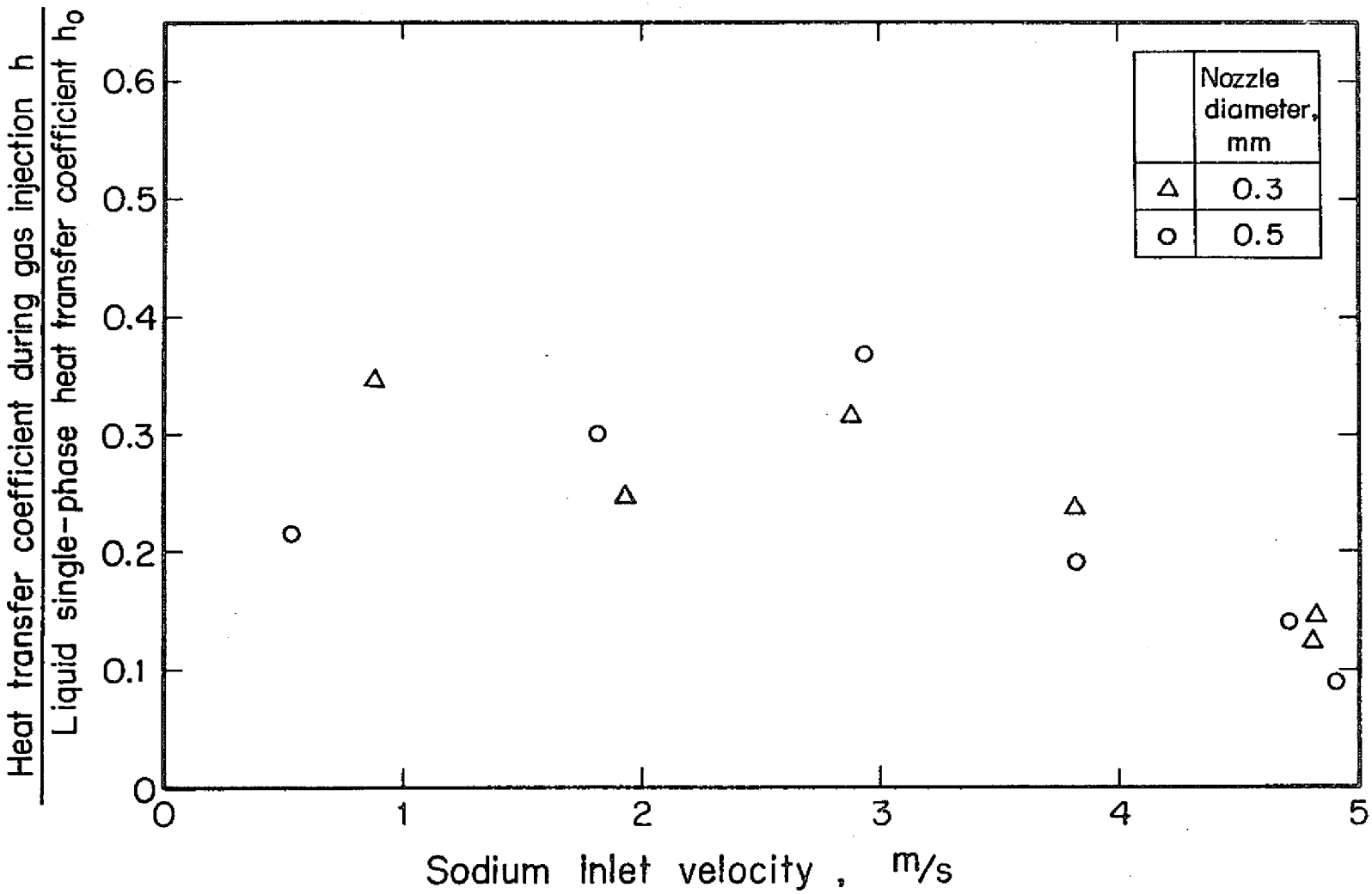

Fig. 20(a) Effect of sodium inlet velocity on ratio of heat transfer coefficient during gas injection to liquid single-phase heat transfer coefficient in impingement area; Pg=58∿62 bar (PNC-FS-454)

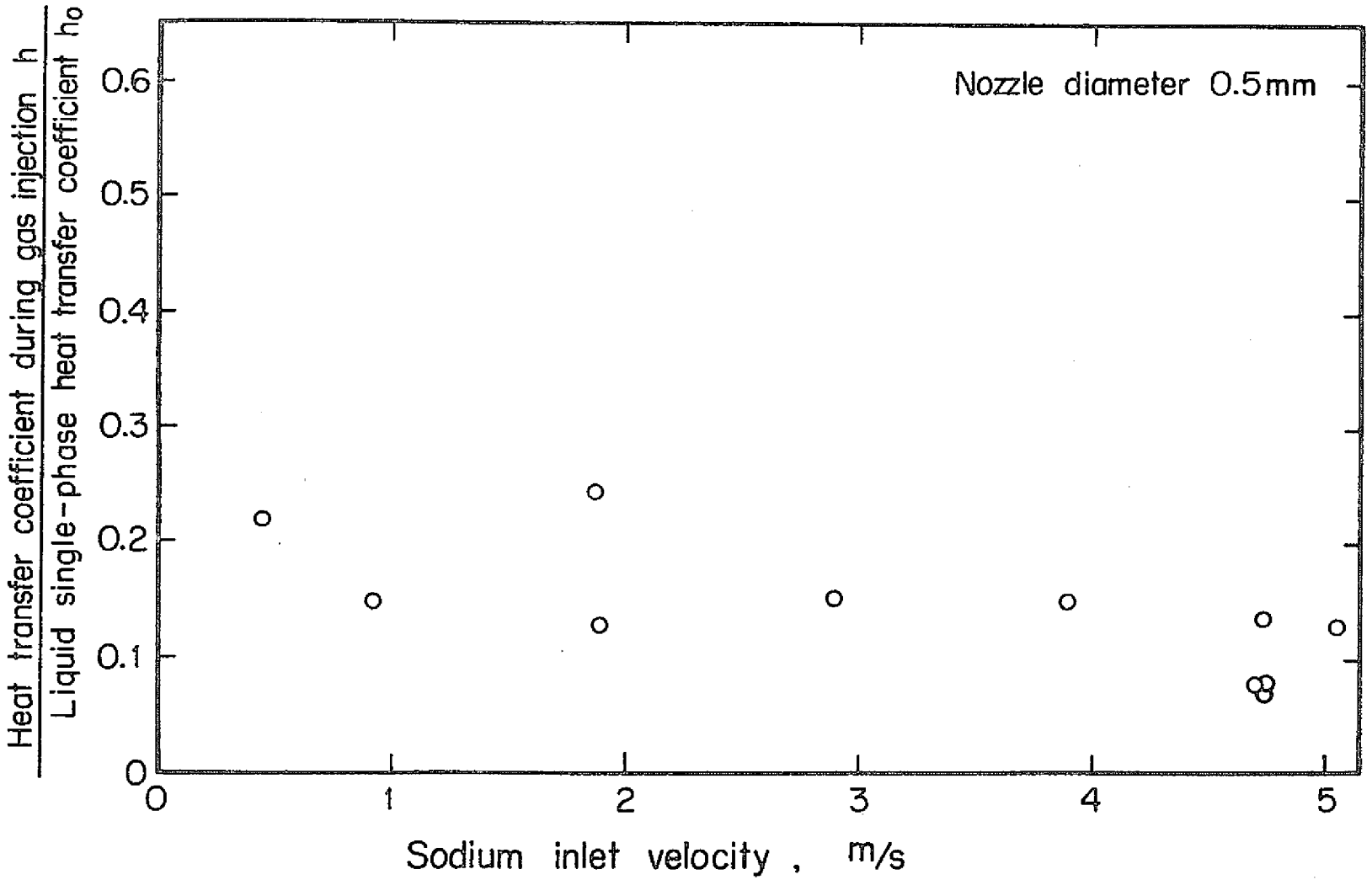

Fig. 20(b) Effect of sodium inlet velocity on ratio of heat transfer coefficient during gas injection to liquid single-phase heat transfer coefficient in impingement area; Pg=27∿32 bar (PNC-FS-455)

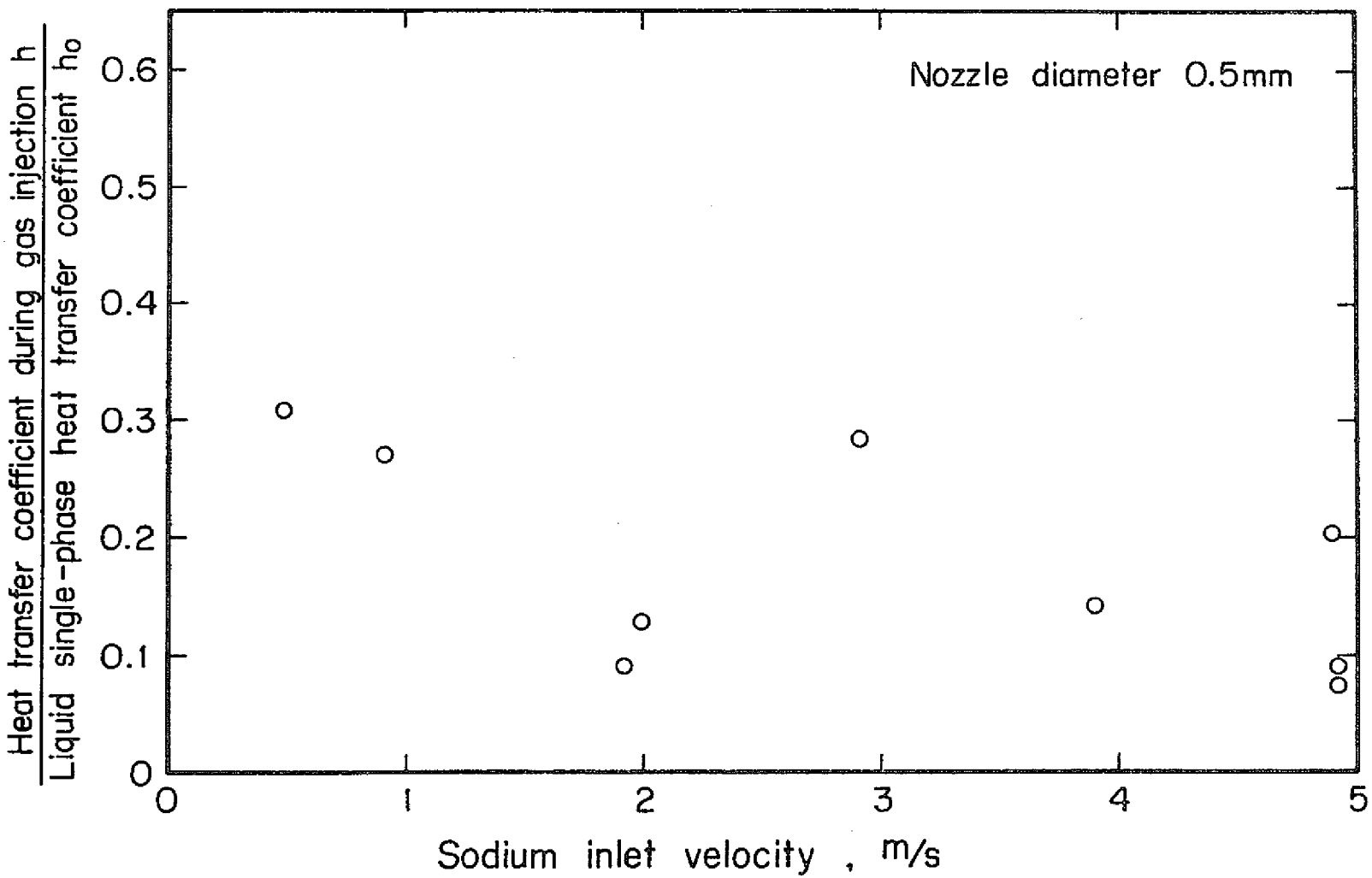

Fig. 20(c) Effect of sodium inlet velocity on ratio of heat transfer coefficient during gas injection to liquid single-phase heat transfer coefficient in impingement area; Pg=9∿12 bar (PNC-FS-456)

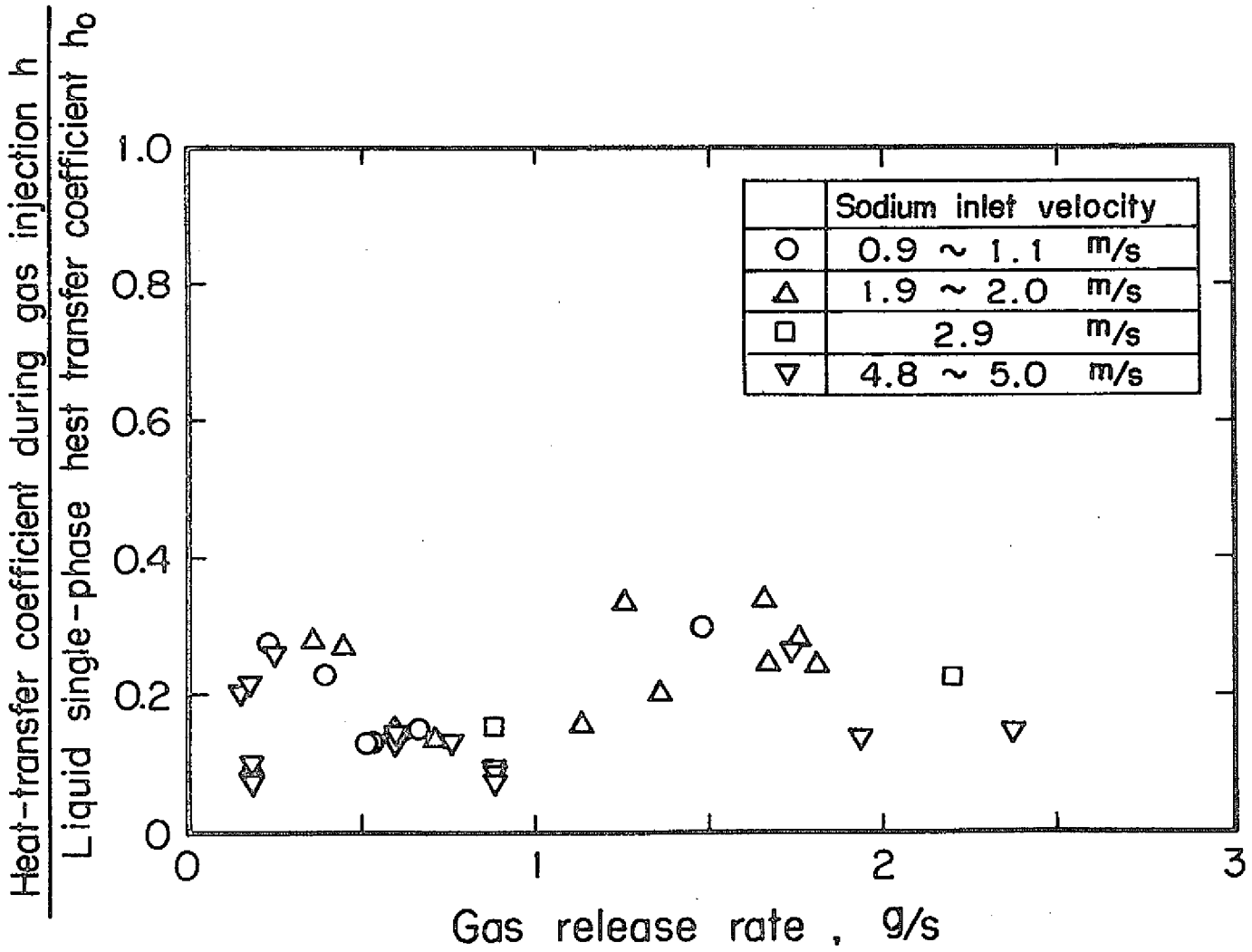

Fig. 21 Effect of gas release rate on ratio of heat transfer coefficient during gas injection to liquid single-phase heat transfer coefficient in impingement area(PNC-FS-457)

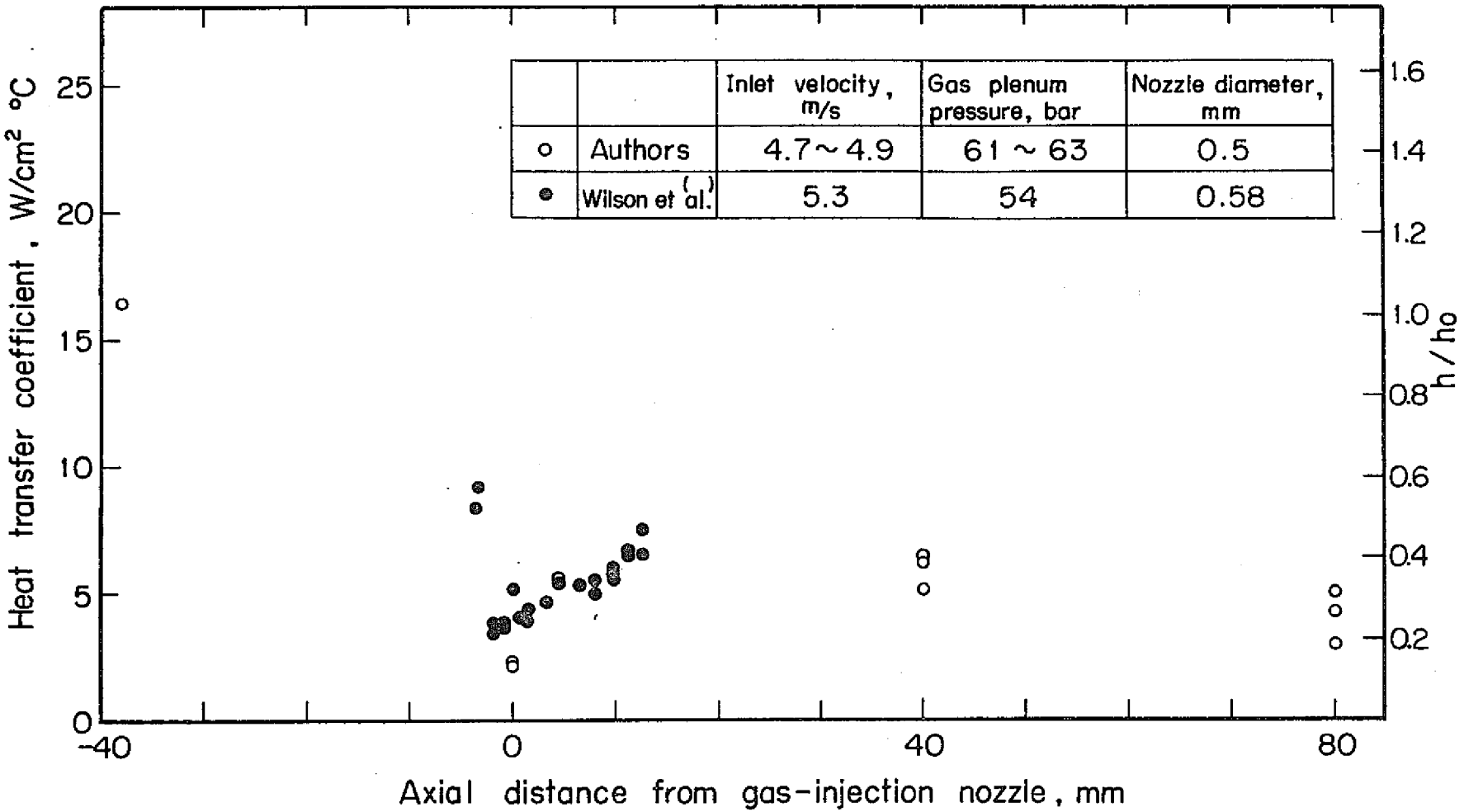

Fig. 22 Effect of relative axial position from gas-injection nozzle on heat transfer coefficient during gas injection (PNC-FS-280)

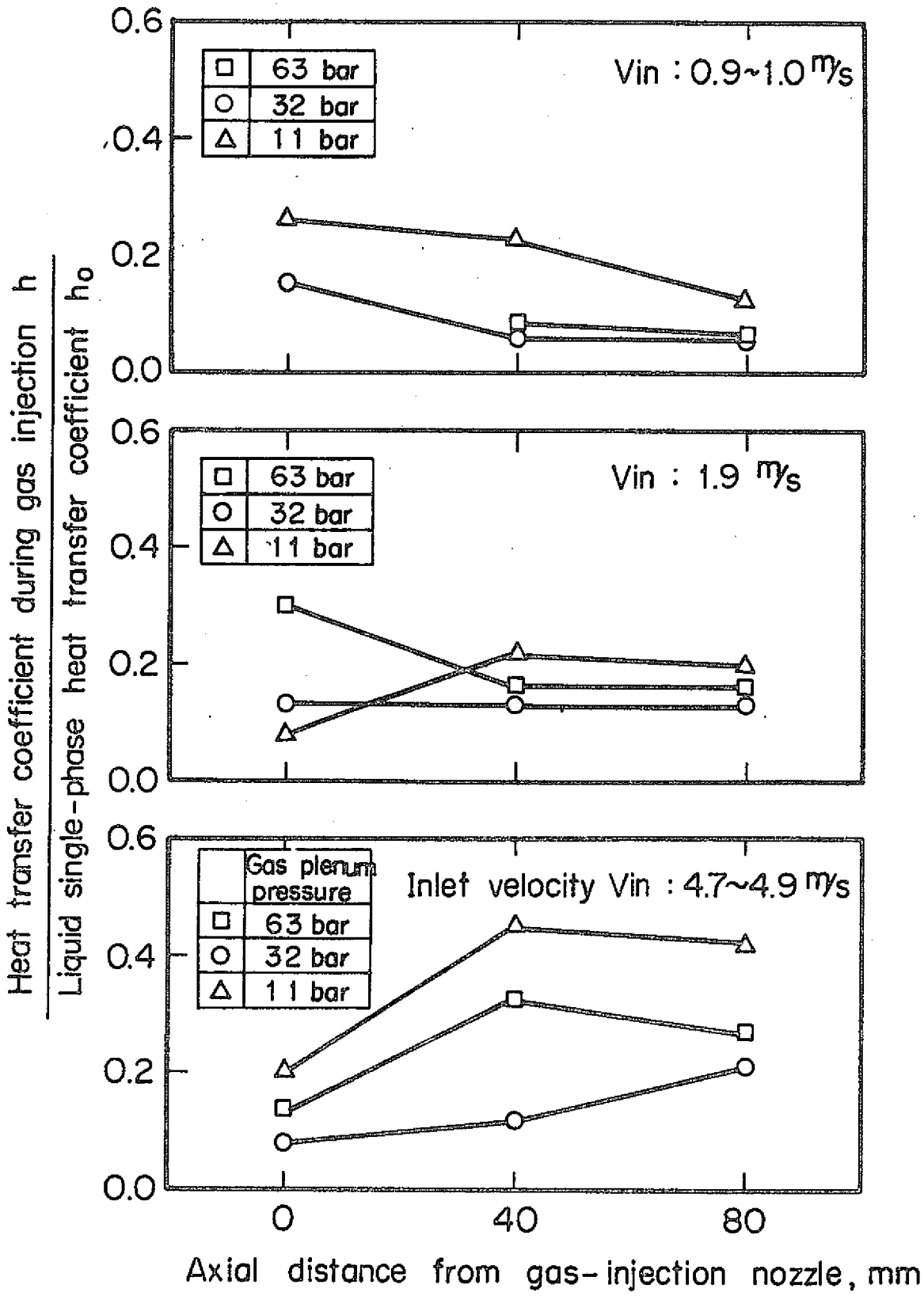

Fig. 23 Effect of gas plenum pressure on heat transfer coefficient distribution (PNC-FS-458)

the surrounding sodium. However, the actual fission gas is composed mainly of xenon and its temperature is higher than that of sodium (presumably over 700°C). The effects of gas release have been investigated by Wilson et al[5] by performing in-sodium continuous release tests in which different kinds of gases and temperatures were used. Those tests showed that there was little difference in the pin surface temperature rise between when argon was used and when xenon was used. They also reported that the gas was injected at 510°C and 720°C into the sodium at 320°C and 370°C no direct effect was caused to the gas impinged surface temperature rise. This being so, it may be concluded that the results of this test are applicable as they are in the estimation of the temperature rise in the actual reactor although the kind of gas and temperature may be different.

The minimum heat transfer coefficient of the gas impinged surface obtained in the continuous release test in which the sodium inlet velocity was 4.7 - 4.9m/s closest to the velocity during the normal operation of the Monju reactor is 1.15W/cm^2°C (= 0.07 x 16.4W/cm^2°C) or 0.07 times the single-phase heat transfer coefficient obtained by Subbotin's equation. By using this value, the temperature rise at the maximum heat flux during the normal operation of the Monju reactor is calculated to be ((196W/cm^2)/(1.15W/cm^2°C)), 170°C. However, from the results of the transient release test described in Chapter 2, we already obtained the minimum value for the heat transfer coefficient, which is 0.05 times the single-phase heat transfer coefficient

and it was extrapolated to reactor conditions, thereby calculating the temperature rise to be 240°C.

3-4-2 Outlet flow velocity fluctuation

When there occurs a gas release in the fast reactor fuel assembly, it will cause such flow velocity fluctuations as observed by means of the outlet flowmeter F-107 in the present test. So, we will consider the possibility of detecting such gas release through the outlet velocity fluctuations from the results of the present test.

Fig. 24 shows the effect of gas release rate on the root mean square of outlet flow velocity fluctuation. As for the gas release, the weight flow rate (g/s) and volume flow rate (cm^3/s) in the case where the gas in a standard state of 0°C and 1 atm were used. The figure shows the three cases in which different inlet flow velocities were used. From this figure, it is seen that even if the gas release rate was unchanged the value of the root mean square became larger because the proportion of gas in the coolant grew larger with the decreasing inlet flow velocity. When the inlet flow velocity remained unchanged, the value of the root mean square increased with the increasing gas release rate. When the inlet flow velocity was 4.6 - 4.9m/s, the value of the root mean square was 0.05 - 0.1m/s at the gas release rate of $1000cm^3$ (STP)/s.

Now we will discuss the amount of fission gas to be accumulated in the Monju fuel pin. In the Monju adjustment design,

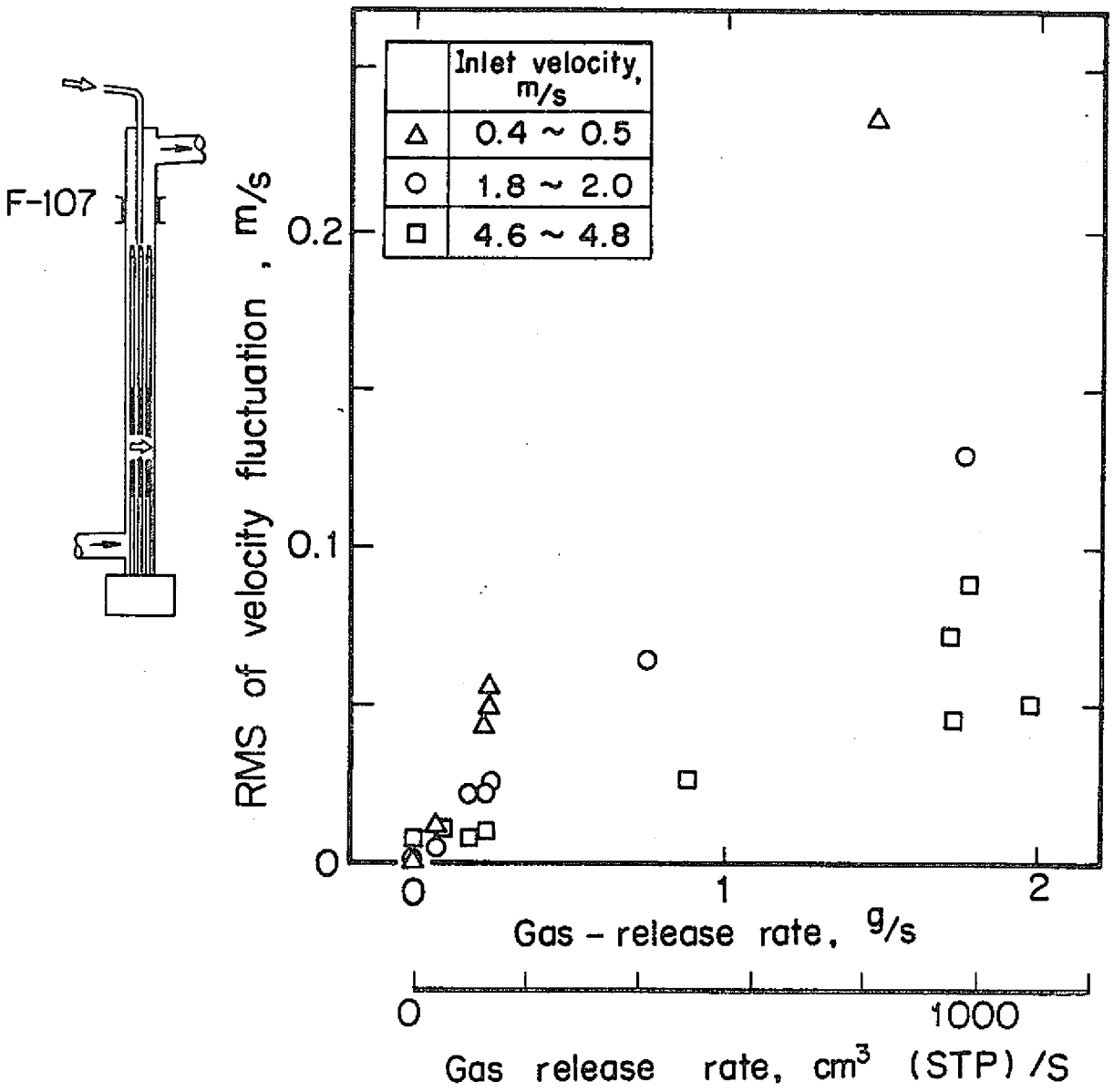

Fig. 24 Effect of gas release rate on root mean square of outlet flow velocity fluctuation for continuous release tests (PNC-FS-459)

the fuel clad tube inside diameter is 5.56mm, gas plenum length 1150mm, pellet diameter 5.4mm and the pellet insertion length is 1580mm, therefore, the volume of gas in the fuel pin before it is used is

$$1150 \times \frac{\pi}{4} \times 5.56^2 + 1580 \times \frac{\pi}{4} (5.56^2 - 5.4^2) = 30100\text{mm}^3$$

$$= 30.1\text{cm}^3$$

As the burning of the fuel progresses, the fuel will be deformed. If the volume of gas present in the fuel pin at the time of refueling is assumed to be 30cm^2, the pressure in the fuel pin to be 60 bars and the temperature to be 770°C to make calculations easier, the amount of gas present in the fuel pin in a standard state is calculated to be as follows:

$$30 \times \frac{273}{273 + 700} \times \frac{60}{1} = 505\text{cm}^3$$

Suppose that a rupture hole larger than 1mm in diameter develops in the fuel clad tube and the fission gas flows to the hole without being hindered by the charge materials and released into the sodium, a gas release rate over 500cm^3 (STP)/s is possible since the gas release comes to an end in one second (Refer to Fig. 23 in the previous report) but normally it is far lower than the above value as was stated in Paragraph 2-4-2. Contrary, in the case where the gas is released at a very high rate, it is possible that the gas release will end so soon that it will be impossible to detect the accident. Since this test system uses a 37 fuel pins while the Monju fuel assembly

has 169 fuel pins, even if a release of fission gas at the same rate as in this test should happen in the reactor core, the effect of gas release of the flow rate fluctuation would be so much smaller as about 20% of the value obtained in the present test (37/169 = 0.22). Such being the case, even if a flowmeter is installed at each fuel assembly, it would be difficult to detect a fission gas release unless many fuel pins fail at the same time and the gas release continues for a long time.

The flowmeters used in the present test were of the electromagnet type while eddy-current type flowmeters are used in the actual reactor. We are planning to use the eddy-current type flowmeters, too, in the fission gas release tests to be performed in the future, thereby to make investigations on their responses.

3-4-3 Acoustic noise

The acoustic noise caused by the injection of gas was measured by means of the accelerometer (Kistler 815A) that was installed on the expansion tank. In the preceding report, we reported that the increase in acoustic noise due to the gas injection was small, that is, the intensity of noise was less than two times that at the time of sodium single-phase flow within the range of gas release rate up to 0.6g/s. Fig. 25 shows the acoustic noise level measured by the accelerometer Ac-101 in the present test.

From this figure, it is seen that the acoustic noise level increased with the increase in the gas release rate irrespective

of the inlet flow velocity and the noise level measured when the release rate was over 3g/s (1700cm^3 (STP)/s) was about 6 times higher than at the time of sodium single-phase flow. It is hard to think of such a high gas release rate in the actual reactor core but it is possible for the noise level to increase so much as detectable even though there would be no increase more than 10 times as in the case of sodium boiling.[21] Fig. 26 shows the frequency spectra of the measured acoustic noise, which shows that the acoustic noise level increased at all frequencies. However, the gas which had been included in sodium in the test section was separated out into the cover gas in the expansion tank on which the accelerometer was installed, and therefore it is possible for the accelerometer to have picked up the separated sound. For this reason, we are planning to measure the acoustic noise level by installing the accelerometer on the main body of the test section in the fission gas release tests to be carried out in the future.

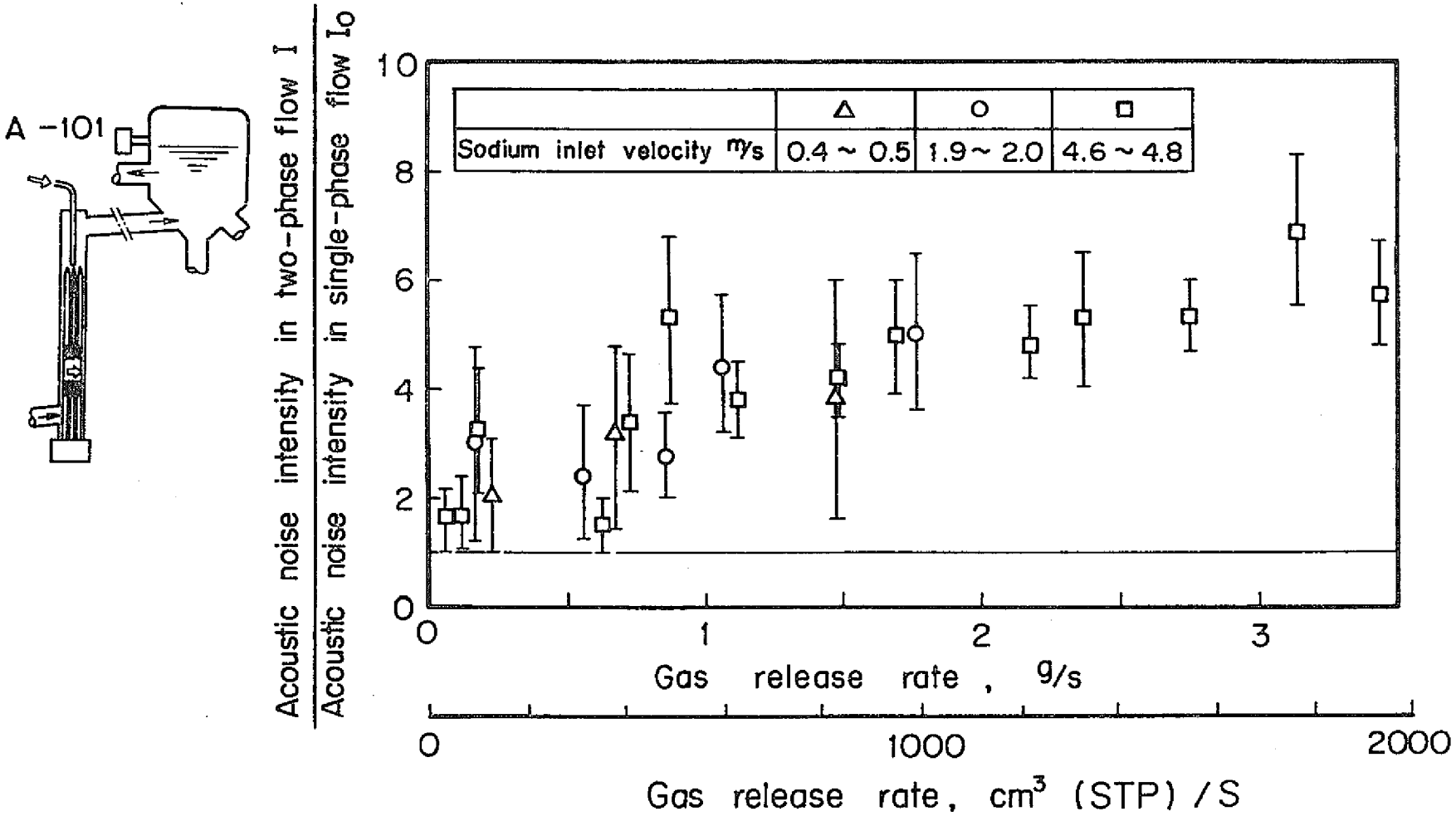

Fig. 25 Effect of gas release rate on intensity of acoustic noise for continuous release tests (PNC-FS-460)

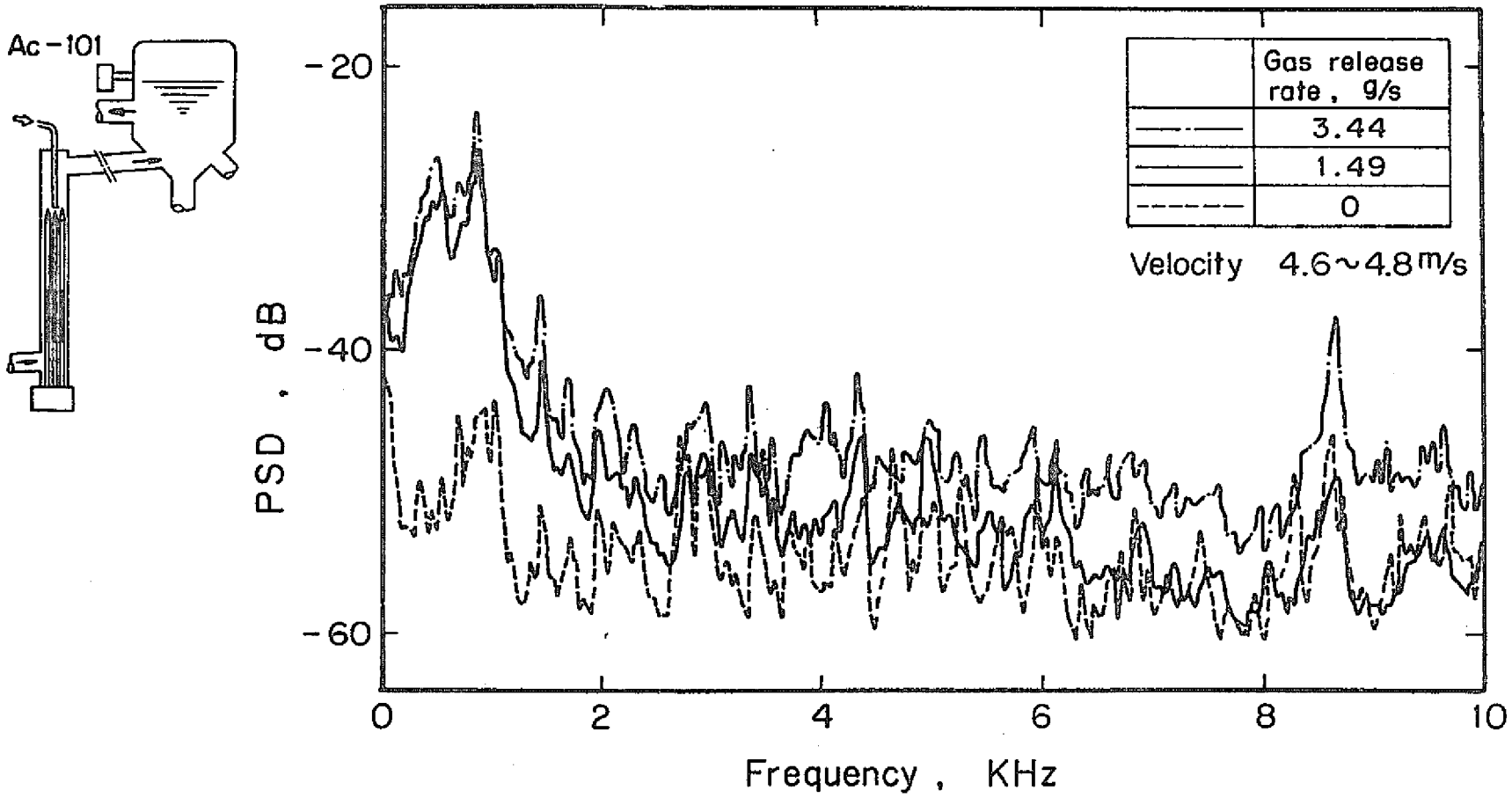

Fig. 26 Frequency spectra of acoustic noise for continuous release tests (PNC-FS-461)

Chapter 4. Sodium-Gas Two-Phase Heat Transfer Tests

4-1 Test objectives

The fission gas which has been released through the rupture hole developed in a fuel pin, after impinging on the surrounding fuel pins, flows downstream, gradually spreading out in the radial direction. Such being the case, the sodium-gas two-phase heat transfer rather than the gas jet itself becomes a problem for the surfaces of the pins downstream from the point of gas release. Therefore, in order to determine the relation between the ratio of gas included in sodium and the sodium-gas two-phase heat transfer coefficient, we conducted heat transfer tests in which gas was mixed uniformly into sodium in the upstream flow in the test section. The sodium-gas two-phase heat transfer also becomes a problem when sodium flows through the reactor core and the results of the present tests are applicable in such a case.

4-2 Test procedure

Four 0.5mm-diameter gas releasing holes were prepared crosswise on the gas-injector pin 120mm upstream from the starting point of heating section and the gas was injected through these holes into the sodium flow channel. The test procedure was the same as that used in the continuous gas release test. The sodium flow rate, heat input into the test section and released gas pressure were set to the required

values and the obtained data were recorded on the multiple-point digital recorder and digital data recorder after the temperature of all the parts of the test section became constant.

4-3 Test conditions

The test conditions were as follows.

Gas release rate:	0.29 - 2.05g/s (162 - 1150cm^2 (STP)/s)
Quality:	7.1 x 10^{-5} - 4.5 x 10^{-3}
Heater pin heat flux:	9.1 x 93.8W/cm^2
Sodium inlet flow velocity:	0.5 - 5.0m/s
Sodium outlet flow velocity:	221 - 279°C

The details are shown in Table 3 in Appendix E. A total of 33 tests were carried out. Prior to the two-phase flow test, the sodium single-phase flow data were recorded with the same heat flux and inlet flow velocity as during the gas injection. The conditions in this test are also shown in Table 3. The sodium was charged to the test facility from the dump tank at 160°C.

4-4 Test results and discussions

4-4-1 Quality and void fraction

Fig. 27 shows the voidmeter and outlet flowmeter signals obtained in the tests in which the inlet flow velocity was (a) 0.5m/s and (b) 2.0m/s. The figure at the left is the case of

liquid single-phase flow and the two others at the right are the case of two-phase flow. As the void fraction increased, the signal fluctuated sharply. The value of void fraction plotted on the vertical axis was obtained on the assumption that the electric conductivity of sodium-gas two-phase flow conforms to Maxwell's equation. It is seen that the outlet flowmeter signal also increased and fluctuated sharply due to the mixing of gas into the sodium flow. Fig. 28 shows the root mean square of flow velocity fluctuations measured by means of inlet flowmeter F-106 and outlet flowmeter F-107. From this figure, it is seen that there was no difference in the inlet velocity between single-phase flow and two-phase flow but the value of the root mean square increased with the increasing quality in the outlet flow velocity. The void fraction was obtained by means of the electromagnetic flowmeter method(Note) from the mean value of the above outlet velocities and the inlet velocity.

Fig. 29 shows thus determined relation between quality X and void ratio α. The symbols in this figure indicate the different inlet velocities, that is, "o" and "●" represent the velocity of 0.5m/s, "Δ" and "▲" 1m/s, "□" and "■" 2m/s, and "▽" and "▼" 5m/s. Of these symbols, the white ones show the values obtained by the electromagnetic flowmeter method and the black ones by means of voidmeter. As seen from this figure,

---

(Note) With the electromagnetic flowmeter method, α is calculated by means of the equation $V_{out} = V_{in}/(1 - \alpha)$, in which V_{in} is inlet velocity and V_{out} outlet velocity.

these two sets of values are in good agreement with one another when quality was approximately 10^{-3} and the void fraction below 0.2 while the values obtained by the electromagnetic flowmeter method are far lower than those obtained by the void-meter method when the quality and void ratio are higher. This tendency also has been observed in the tests performed by some other researchers. For instance, Ochiai et al[9] obtained such a curve as shown by the dot-dash-line given in the figure from the results obtained by the electromagnetic flowmeter method and the gamma-ray penetration method. The broken line in the same figure shows the experimental values obtained by Milliot et al[22] and the solid line shows the calculated values obtained by means of Nishino-Yamazaki's equation.[23] By Nishino-Yamazaki's equation, the two-phase flow slip ratio (gas phase flow velocity/liquid phase flow velocity) can be obtained by

$$S = 1/2 \left\{1 + \sqrt{1 + 4 \frac{X}{1 - X} \cdot \frac{\rho\ell}{\rho g}}\right\} \quad \cdots\cdots\cdots\cdots\cdots\cdots \quad (3)$$

For two-phase flow, the following equation holds in general:

$$S = \frac{\rho\ell}{g} \cdot \frac{1 - \alpha}{\alpha} \cdot \frac{X}{1 - X} \quad \cdots\cdots\cdots\cdots\cdots\cdots\cdots\cdots \quad (4)$$

And the relation between quality X and void ratio α was calculated by means of equations (3) and (4). In the above equations, $\rho\ell$ and ρg are the density of gas phase and liquid phase, respectively. In arranging the data of the present test, the void fraction at the quality over 10^{-3} was calculated by the use of

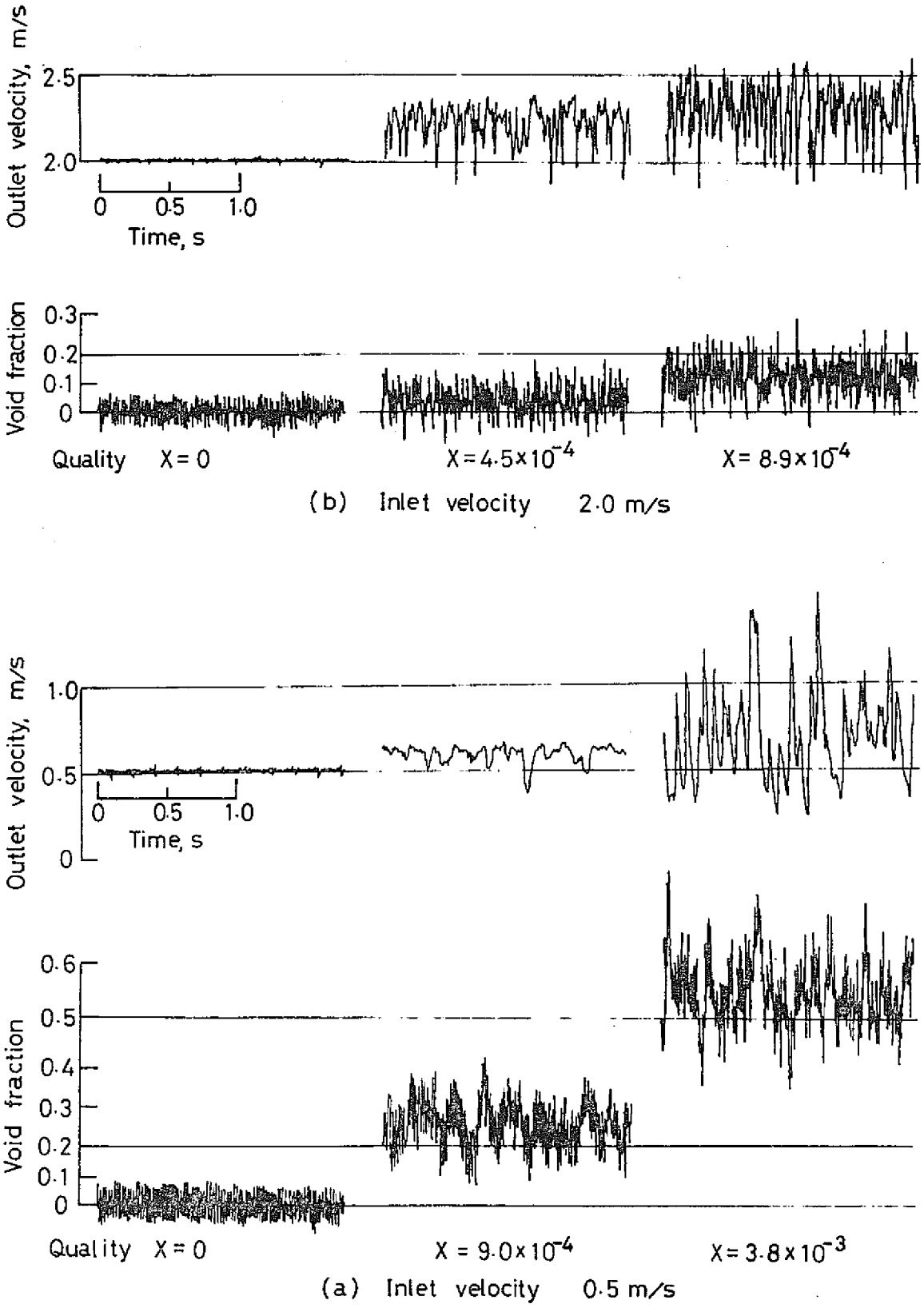

Fig. 27 Signals from voidmeter and outlet flowmeter for two-phase heat transfer tests (PNC-FS-326)

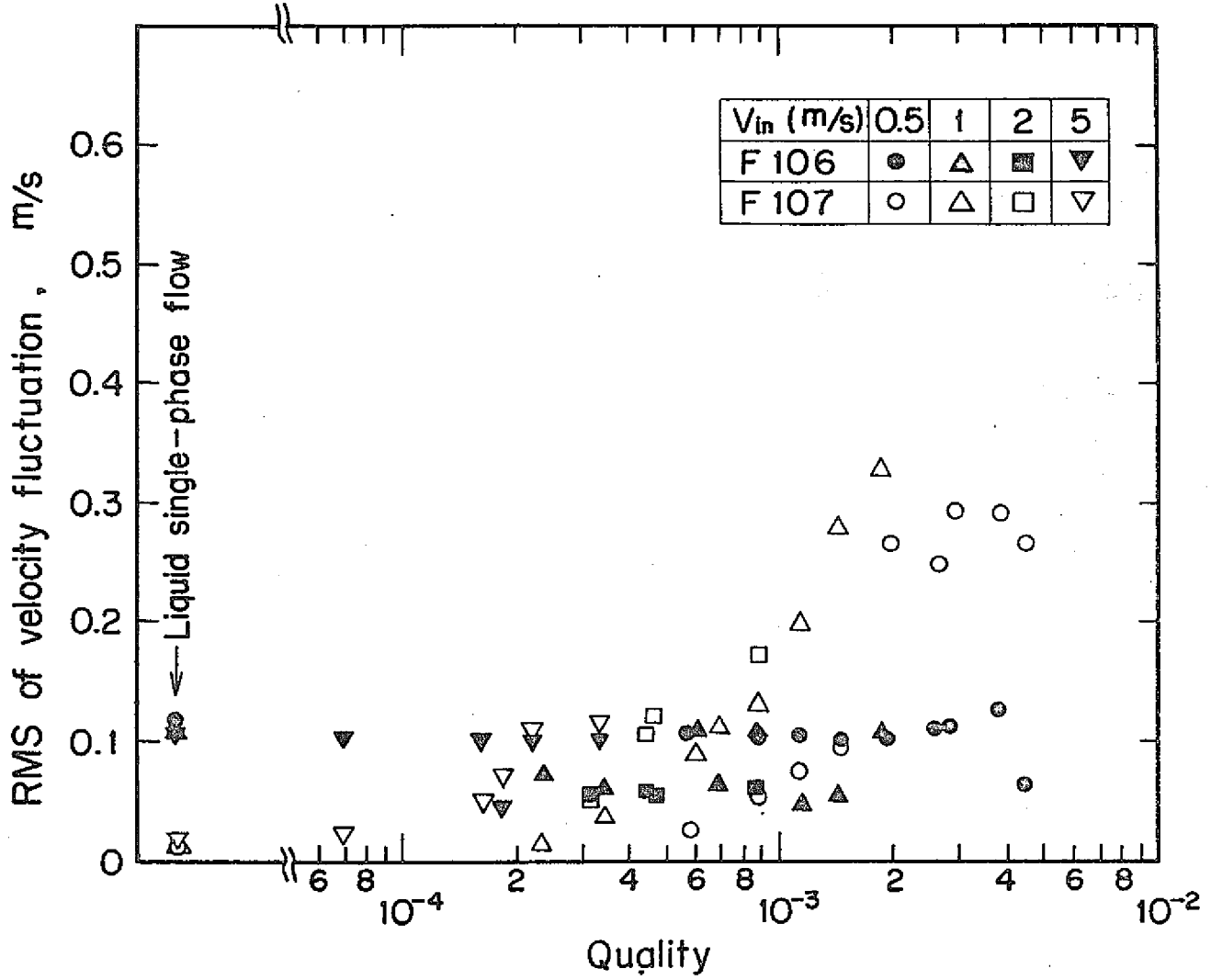

Fig. 28 Root mean square of inlet and outlet velocity fluctuations for two-phase flow heat transfer tests (PNC-FS-320)

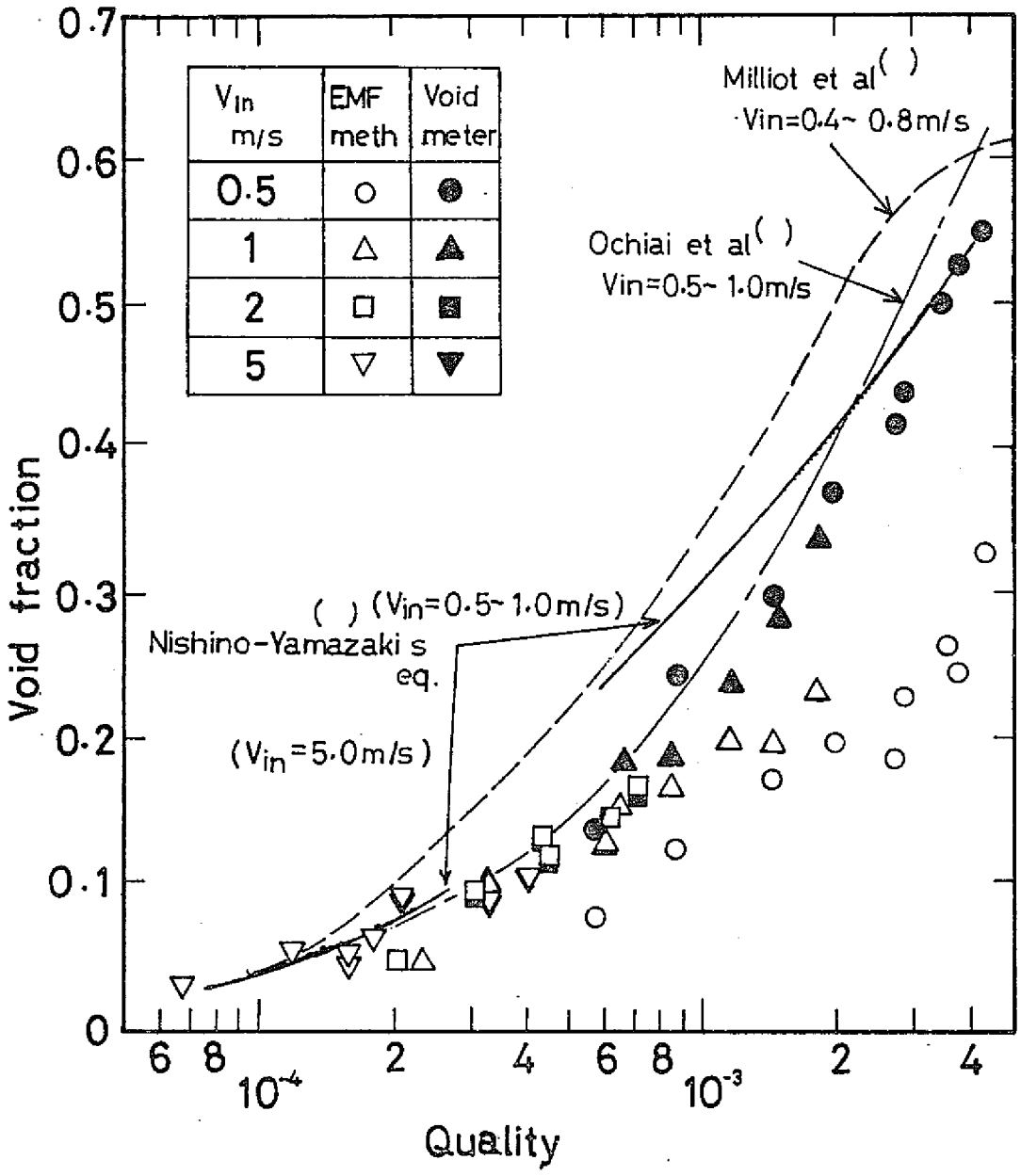

Fig. 29 Relation between quality and void fraction (PNC-FS-300)

the void method. As for the mode of the two-phase flow in the present test, it is considered to be the slag flow at the void ratio over 0.2 or so and the gas bubble flow at the void ratio lower than that. This also can be inferred from the fact that in Fig. 27 the flowmeter signal fluctuates in a regular pattern when the voidmeter signal is below 0.2 and that in Fig. 9 the results obtained by the electromagnetic flowmeter method (in which the two-phase flow was assumed to be the gas bubble in the flow mode) are not in agreement with the results obtained by the voidmeter.

4-4-2 Sodium-gas two-phase heat transfer coefficient

Fig. 30 shows the effect of quality on the ratio of two-phase heat transfer coefficient h_{TP} to liquid single-phase heat transfer coefficient ho, which was obtained from the values measured by means of the thermocouple T-33 on the surface of a pin near the center of the bundle and the thermocouple T-73 on a pin in the periphery of the bundle. Both T-33 and T-73 were installed on the plane 265mm downstream from the starting point of heated section (385mm downstream from where gas was mixed into the sodium flow). When obtaining h_{TP}, the coolant temperature was obtained from the surface temperature, which was measured in the case of liquid single-phase flow with the same inlet flow velocity as was done in Paragraph 2-4-2, and ho and the coolant temperature were assumed to remain unchanged in two-phase flow, too. The figure shows that h_{TP}/ho becomes smaller with the increasing quality both for T-33 and T-73,

except that the heat transfer for T-73 is slightly better than in the liquid single-phase flow within the region where quality is very small. The reason why the value of h_{TP}/ho was smaller in the case of T-33, showing little effect of flow velocity, was presumably that the gas bubbles were concentrated mostly near the central flow channel. The difference in the values obtained by T-33 and T-73 became almost nil and the value of h_{TP}/ho became nearly 0.1 when the flow velocity was 0.5m/s and quality became larger than 2×10^{-3}.

Fig. 31 shows the arrangement of the data obtained by T-33 by plotting the void fraction on the horizontal axis. In the figure, the black marks show the results of the sodium-argon two-phase heat transfer test Ochiai et al[9] performed, using a circular flow channel (inner diameter of 22mm) with the outer wall heated. The data of Ochiai et al show that when the void fraction increased h_{TP}/ho first decreased and reached its minimum value (approximately 0.6) at the void fraction of 0.2 and thereafter the heat transfer coefficient tended to increase again.

In the same figure, the solid line shows the calculated values obtained by the model proposed by Hori et al[24]. The model of Hori et al assumes that $\lambda_{TP} = \lambda_o (1 - \alpha)/(1 - 0.5\alpha)$, in which α is void fraction, on the assumption that the thermal conductivity λ_{TP} for sodium-gas two-phase flow conforms to Maxwell's equation. And the two-phase flow velocity V_{TP}, density ρ_{TP} and specific heat C_{pTP} are assumed to be $V_{TP} = Vo/(1 - \alpha)$, $\rho_{TP} = \rho_o (1 - \alpha)$ and $C_{pTP} = C_{po} (1 - \alpha)$, respectively and they

are substituted into the equation of liquid single-phase heat transfer coefficient to calculated h_{TP}/ho. In the above equations, Vo, C_{po} and λ_o are the values at the time of liquid single-phase flow. If arranged by the use of Subbotin's equation for the equation of heat transfer coefficient (the details are shown in Appendix E), we obtain the following equation:

$$\frac{h_{TP}}{h_o} = \frac{1 - \alpha}{1 + 0.5\alpha} \cdot \frac{5 + 0.025 \{P_{eo} (1 + 0.5\alpha)\}^{0.8}}{5 + 0.025 P_{eo}^{0.8}}$$

where P_{eo} is Peclet number in the case of liquid single-phase flow. As for the calculated values, those in the case of laminar flow with Peclet number below 30 and those with Peclet number of 256 (they correspond to the flow velocity below 0.6m/s and at 5m/s in the test section, respectively) and there is little difference between these two sets of values. Fig. 31 shows that our data are lower than the data of Ochiai et al and the values calculated by the model of Hori et al. This is presumably due to the fact that in calculating the values of h_{TP} and h_o we assumed the coolant temperature would remain unchanged in two-phase flow, but in the case as the present test in which sodium-gas two-phase flow moves through the pin bundle wrapped with spacer wire, gas trapped by the wire to reduce the mixing, thereby causing a local coolant temperature rise. This is evident from Fig. 32, which shows the ratio of coolant temperature rise in two-phase flow to that in single-phase flow, which were measured by means of the thermocouple T-108-2, which also performed the function of spacer wire, located 265mm downstream

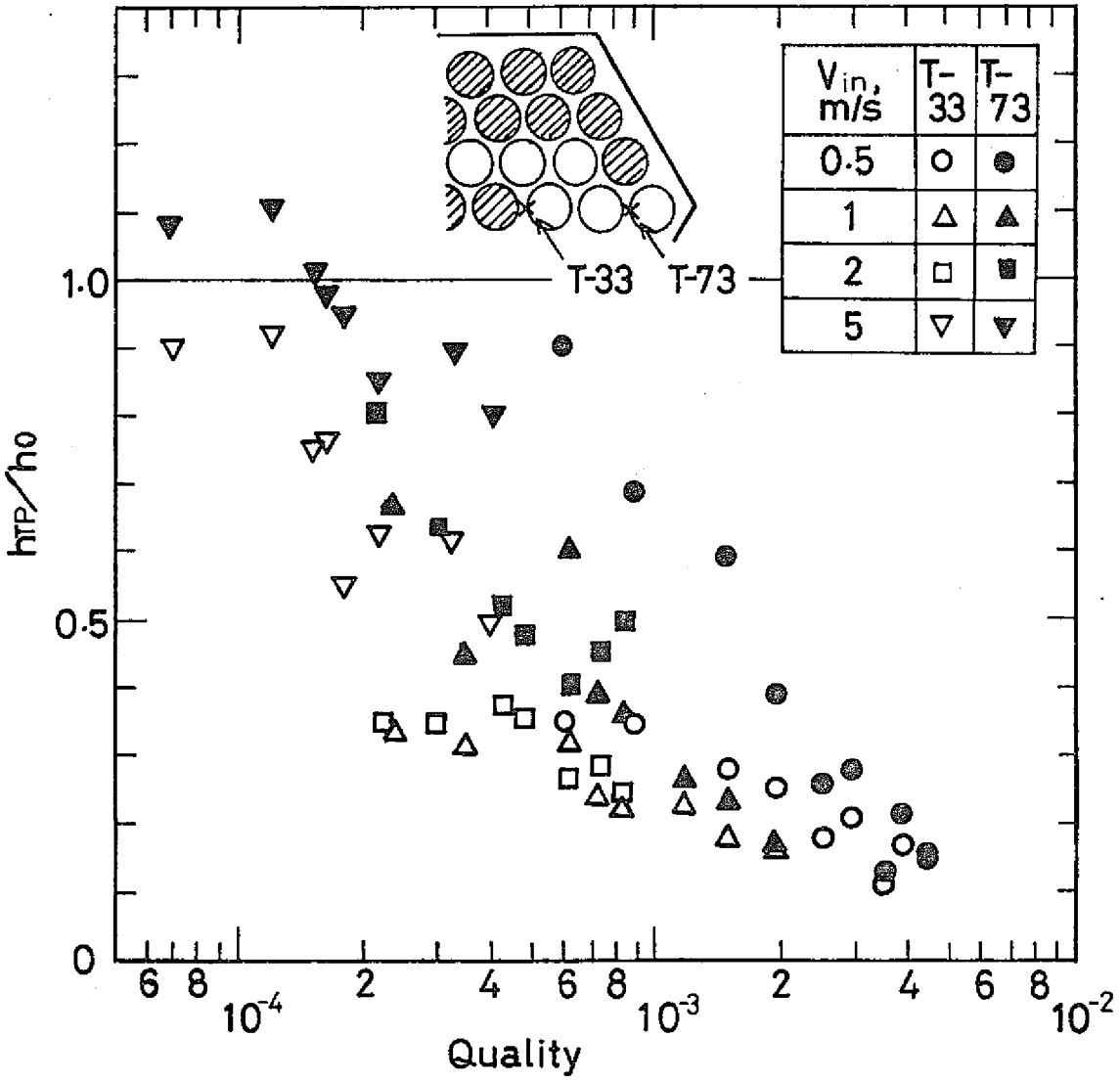

Fig. 30 Effect of quality on ratio of two-phase heat transfer coefficient h_{TP} to liquid single-phase flow heat transfer coefficient h_O (PNC-FS-301)

from the starting point of heated section and the thermocouple T-63 on the dummy pin. In this figure, Tin on the vertical axis is inlet temperature, T_{CO} coolant temperature in single-phase flow and T_{CTP} is coolant temperature in two-phase flow. From this figure, it is seen that in two-phase flow the coolant temperature measured by T-108-2 on the heater pin rose while that measured by T-63 lowered. This was due to the fact that the mixing between flow channels was reduced due to the inclusion of gas into sodium. Such being the case, the sodium-gas two-phase heat transfer coefficient which was obtained in the present test is considered to be somewhat lower than the actual value.

In order to evaluate precisely the sodium-gas two-phase heat transfer coefficient in a narrow flow channel, it is necessary to perform a test with simple channel geometry without any mixing between channels. For this reason, we are now performing the sodium-gas two-phase heat transfer tests, using a test section with a narrow circular flow channel which is formed by inserting a heater pin in the center of a circular tube. Two kinds of heater pins, one with spacer wire and the other with no spacer wire, are used to investigate also on the effect of spacer wire. These tests are being carried out in cooperation with Mitsui Shipbuilding & Engineering Co., Ltd., using the sodium loop at the Chiba Laboratory of the company.

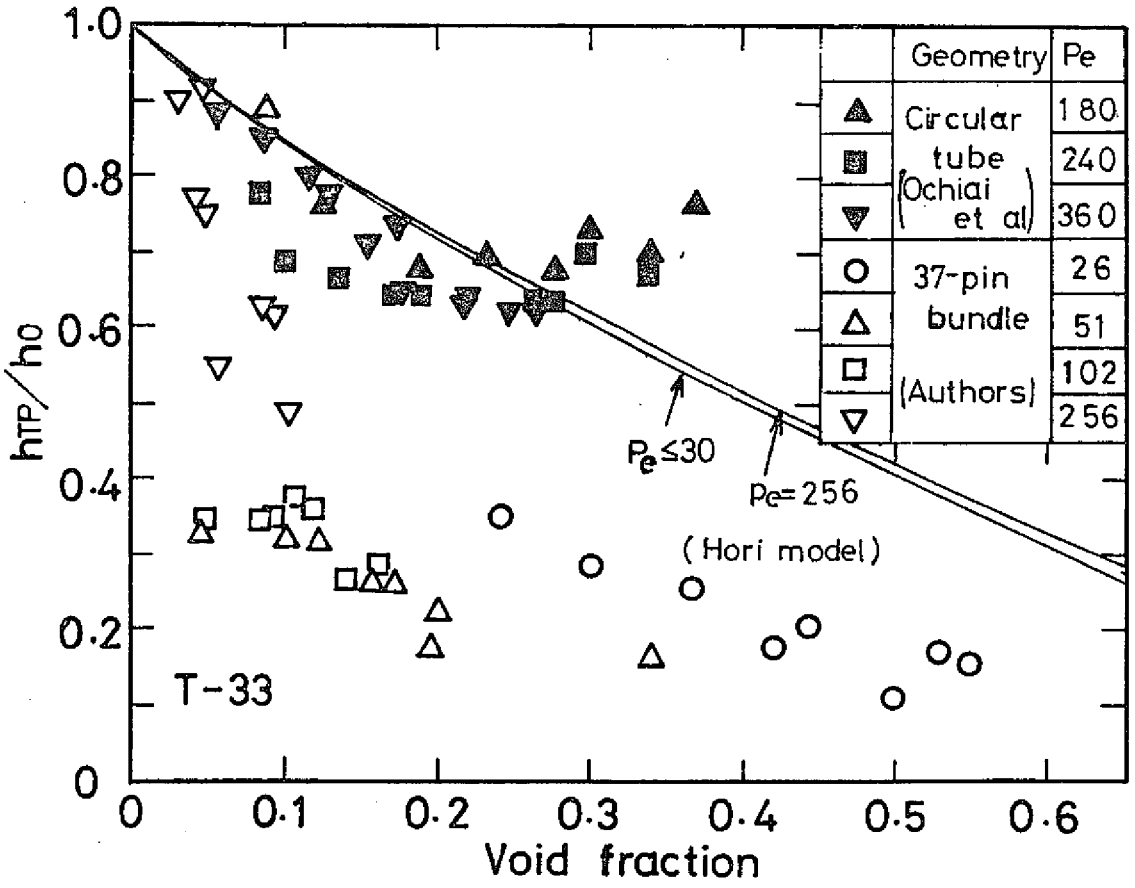

Fig. 31 Effect of void fraction on ratio of two-phase heat transfer coefficient h_{TP} to liquid single-phase heat transfer coefficient h_0 (PNC-FS-302)

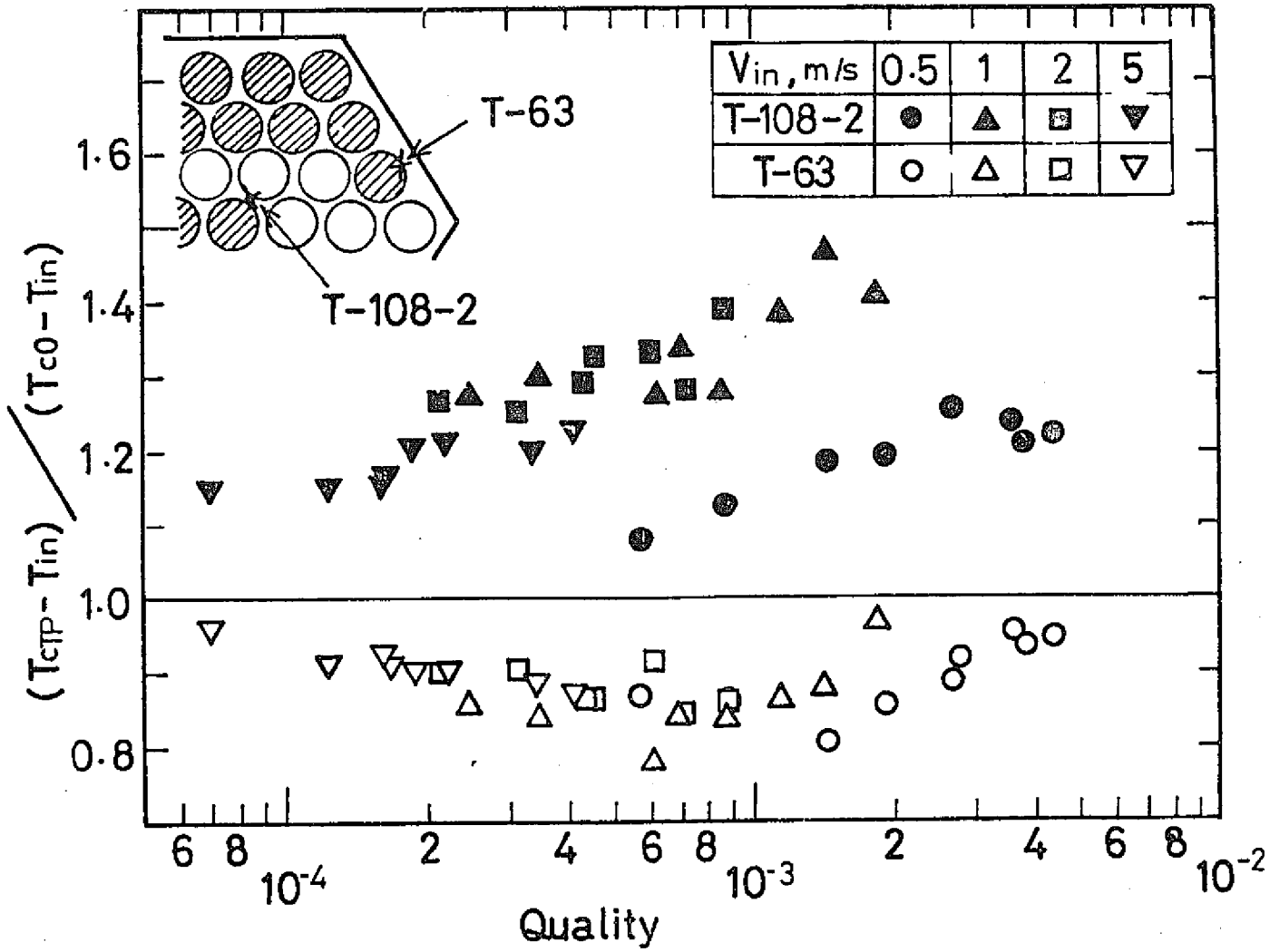

Fig. 32 Effect of quality on ratio of coolant temperature rise in two-phase flow to that in liquid single-phase flow
(PNC-FS-303)

Conclusions

After the previously reported tests, we have carried out another series of tests for making investigations on fission gas release, using normal 37-pin bundle and such test conditions that the gas injector nozzles were made large in diameter (0.3, 0.5, 0.8mm) and the gas pressure was increased in transient release tests (29.6 - 75.9 bars) so that tests were made at higher gas release rates than in the tests described in the preceding report. From thus measured temperature, pressure, flow velocity and acoustic noise fluctuation, the following things have been found. However, when these test results are applied to the actual reactor conditions, it is necessary to pay attention to the fact that the actual fission gas is composed mainly of xenon but the present tests used argon (with a density about 30% of that of xenon).

1. Transient gas release tests (Test conditions: flow velocity 1.95 - 5.03m/s, initial gas release rate 0.63 - 4.17g/s)

1-1 The surface temperature rose due to gas injection. The greatest temperature rise was observed on the gas impinged surface. The heat transfer coefficient after gas injection which was obtained by analyzing the impinged surface temperature fluctuation by the SURFACE code was 0.05 to 0.15 times that in sodium single-phase flow. Extrapolating the test results to the actual reactor conditions (200W/cm^2, 5m/s), the pin surface temperature rise due to gas injection was calculated to be less than 240°C.

1-2 The pressure pulse due to gas injection was found to be less than 0.2 of the initial gas plenum pressure. After completion of a total of 14 transient release tests, the pin bundle was removed from the test facility and subjected to careful inspection and it was found to be free from damage and deformation and in good condition, from which there is no possibility conceivable of pin damage due to the mechanical effect of gas release.

1-3 The sodium inlet velocity increase due to gas injection was greater as the gas plenum pressure increased but the experimental value thereof was considerably smaller than the theroretical value obtained by the one-dimensional liquid-column model. The difference in the sodium outlet velocity between before and after gas injection increased in proportion to the gas release rate. The gas bubbles did not spread upstream but spread nearly straight downstream as time went on. When the flow velocity was around 5m/s, the time necessary for the gas bubbles to reach the flowmeter located 0.96m downstream from the gas injector nozzle was 1/2 of the time required for the sodium flow to reach the same flowmeter before gas injection.

2. Continuous gas release tests (Test conditions: inlet velocity 0.45 - 5.07m/s, gas release rate 0.06 - 3.44g/s)

2-1 The gas impinged surface heat transfer coefficient tended to decrease when the inlet flow velocity was high.

When the inlet flow velocity was about 5m/s, if the gas pressure rose higher than 30 bars, the heat transfer coefficient was 0.07 - 0.15 times that in sodium single-phase flow and this value was in agreement with the results of the transient release tests performed with the same inlet velocity of 5m/s, showing that the continuous release test may be sufficient for investigation of the temperature changes due to gas release. The heat transfer coefficient was found to have a tendency to slightly increase again when the gas pressure lowered below 20 bars. The relation between gas pressure and heat transfer coefficient was not clear when the inlet velocity was lower than 2m/s.

2-2 The outlet flow velocity fluctuation observed by the electromagnet-type flowmeter increased with the increasing gas release rate and the value of the root mean square of the flow velocity fluctuation at the gas release rate of $1000cm^3$ (STP)/s was 0.05 - 0.1m/s when the inlet velocity was about 5m/s. However, in the actual fuel assembly the maximum amount of fission gas content per fuel pin is $500cm^3$ (STP) and there are five times as many pins as in the present test system, therefore, the actual flow velocity fluctuation is considered to so much smaller.

2-3 As the gas release rate increased, the acoustic noise level measured by the accelerometer installed on the expansion tank rose and the acoustic noise level when the gas release rate was $1000cm^3$ (STP)/s was about 5 times higher

than when there was no gas injection. However, it is possible for the acoustic noise to include the sound that is produced when gas is separated from sodium, and therefore it is necessary to make further measurements in the main body of the test section.

We would like to conclude this report by expressing our gratitude to all the persons who have extended their cooperation to us in carrying out the present tests.

References

(1) R. Bell, B.E. Boyce and J.G. Collier:
The Structure of a Submerged Impinging Gas Jet, J. Brit Nucl. Energy Soc., Vol. 11 (2), pp. 183 - 193 (1972)

(2) B.M. Hoglund, R.P. Anderson and L. Bova:
Experimental Study of a Gas Jet Penetrating a Liquid Coolant and Impinging on a Heated Surface, ANL-7734 (March 1971)

(3) T.C. Chawla and B.M. Hoglund:
A Study of Coolant Transients During a Rapid Fission Gas Release in a Fast Reactor Subassembly, Nucl. Sci. Eng., Vol. 44, pp. 320 - 344 (1971)

(4) J.B. van Erp, C.J. Roop and P.L. Zaleski:
Simulation of Slow Gas Release in an LMFBR Fuel Subassembly, Trans. Amer. Nucl. Soc., Vol. 14 (1), pp. 277 - 278 (1971)

(5) R.E. Wilson, J.B. van Erp, T.C. Chawla, E.L. Kimont and R.D. Baldwin:
Experimental Evaluation of Fission-Gas Release in LMFBR Subassemblies Using an Electrically Heated Test Section with Sodium as Coolant, ANL-8036 (July 1973)

(6) K. Uematsu, Y. Kumaoka, K. Miyaguchi, T. Uemura and Y. Yamamoto:
Experimental Study on the Consequences of Fuel Cladding Failure - PART II, Atomic Fuel Corporation AFCPU-REPORT - 023 (1967)

(7) K. Miyaguchi, S. Uruwashi, Y. Yamamoto and S. Kondo:
Experimental Study on the Consequences of Fuel Cladding Failure - PART IV, PNC SN941 75-100 (Nov. 1975)

(8) T. Mizushina, T. Sasano, M. Hirayama, N. Otsuki and M. Takeuchi:
Effect of Gas Entrainment on Liquid Metal Heat Transfer, Int. J. Heat Mass Transfer, Vol. 7, pp. 1419 - 1425 (1964)

(9) M. Ochiai, T. Kuroyanagi and K. Furukawa:
Sodium-Argon Two-Phase Vertical Ascending Flow Heat Transfer Coefficient, 7th Japanese Heat Transfer Symposium II-10.3 (May 1970)

(10) K. Haga, Y. Kikuchi, Y. Daigo, M. Okouchi and M. Hori:
Out-of-pile Experiments of Fission Gas Release in Fast Reactor Fuel Assemblies-1 Preliminary Experiments in a Normal Pin Bundle, PNC SN951 77-04 (Aug. 1977)

(11) Y. Katto:
Introduction to Heat Transfer, p. 148, Yoken-do (1976)

(12) T.C. Chawla:
Rate of Liquid Entrainment at the Gas-Liquid Interface of a Liquid Submerged Sonic Gas Jet, Nucl. Sci. Eng. Vol. 56 pp. 1 - 6 (1975)

(13) Handbook of Mechanical Engineering, Vol. 11, p. 24, Mechanical Engineering Society of Japan (1975)

(14) S. Seki, J. Komatsu, K. Inoue, M. Hasegawa, H. Satake and T. Sugiyama:
DFR 332/6 Post Irradiation Tests (No. 2) Metallographical Test Results, PNC ZN76-85 (Aug. 1976)

(15) K.E. Gregoire, P.E. Novak and R.E. Murata:
Failed Fuel Performance in Naturally Convecting Liquid Metal Coolant, GEAP-13620 (June 1970)

(16) R.E. Murata, K.E. Gregoire and C.N. Craig:
Friction Factors and Model for Gas Release from Failed LMFBR Fuel Rods, GEAP-13989 (Sept. 1973)

(17) J.B. van Erp, T.C. Chawla and H.I. Fauske:
An Evaluation of Pin-to-Pin Failure Propagation due to Fission Gas Release in Fuel Subassemblies of Liquid-Metal-Cooled Fast Breeder Reactors, Nucl. Eng. and Design. Vol. 31, pp. 128 - 150 (Nov. 1974)

(18) T.C. Chawla, W.L. Chen, M.A. Grolmes, G.M. Hauser, H.K. Fauske:
The Effects of Fission-Gas Release in LMFBR Subassemblies During Hypothetical Loss-of-Flow Accidents, Trans. Amer. Nucl. Soc., Vol. 18 (2), pp. 257 - 258 (1974)

(19) F.F. Koenig:
Reactor Development Program Progress Report, ANL-7900 1.32 - 1.34 (1971)

(20) M.S. Kazimi:
Analysis of Pressure Pulse Generation Due to Gas Release from Failed Fuel Pins in a Liquid-Metal Fast Breeder Reactor, Nucl. Sci. Eng., Vol. 59, pp. 1 - 11 (1976)

(21) Y. Kikuchi, Y. Daigo, K. Haga, M. Okouchi, T. Komaba and M. Hori:
Sodium Boiling Experiments (7) Local boiling of Sodium behind Local Flow Blockage in a Seven-Pin Bundle, PNC SN941 76-66 (June 1976)

(22) B. Milliot, J. Lazarus and J. Ph. Navarre:
Void Fraction Measurements in a Two-Phase Flow NaK/Argon, Proceedings of "Conference Internationale sur la Surete des Reacteurs a Neutrons Rapides," II-B/3 (Aix-en-Provence, Sept. 1967)

(23) Nishino and Yamazaki:
A New Method of Estimating the Vapor Volumetric Fraction in the Boiling System, Atomic Energy Society of Japan Journal Vol. 5, No. 1, pp. 39 - 49 (1963)

(24) M. Hori and A.J. Friedland:
Effect of Gas Entrainment on Thermal-hydraulic Performance of Sodium Cooled Reactor Core, J. Nucl. Sci. Technol., Vol. 7 No. 5 pp. 256 - 263 (May 1970)

Appendix A Heater Pin Transient Heat Transfer Analysis Code SURFACE

1. Brief description of SURFACE code

This is a code for use in the calculation of the changes of heat on the surface and in the heater pin when the heat transfer coefficient has suddenly changed due to the gas impingement on the pin. This code considers only the diametrical heat distribution, not the axial transfer of heat.

A cross section of the heater pin (made by Sukegawa Electrical Industry Co., Ltd.) which was used in the tests is shown in Fig. A-1.

In the SURFACE code, the pin is divided into 10 cells by concentric circles (clad is divided into three, insulator outside the heating element into four, heating element not divided, and insulator inside the heating element into two). Apart from the above, a special region having no thickness is considered for the pin surface. The coefficient of overall heat transmission is considered for the boundary of cells different in material.

As for the calculation procedure, the temperature distribution in the steady state is first obtained. Next, the heat transfer coefficient is varied to a certain value (give by a coefficient several times the value in the steady state) to proceed to transient calculations and convergence calculations are made for each time step, proceeding to the next step when the given convergence is satisfied.

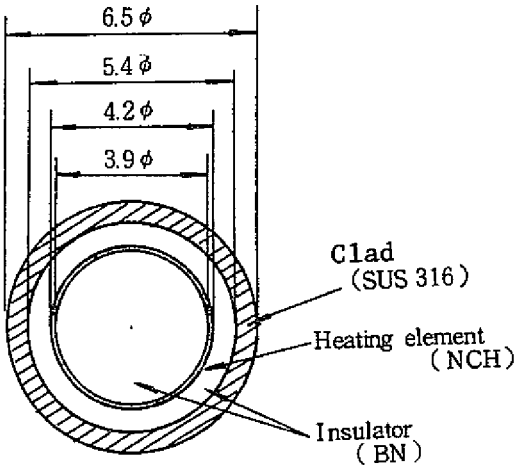

Fig. A-1 Cross section of heater pin

2. Calculational results

The gas impinged surface temperature changes were measured in transient gas release test GR-10 and the calculated values thereof were shown in Fig. 9 in this report. Fig. A-2 shows the calculated values of temperature in the gas impinged pin at h = 0.12 ho, 0.0, 0.2, 1.0 and 2.0 seconds after the gas injection. After the gas injection, the temperature in the vicinity of the pin surface rose sharply and the effect of gas injection appeared also inside the pin with the lapse of time and 2.0 seconds later the temperature in the pin settled down on a new level.

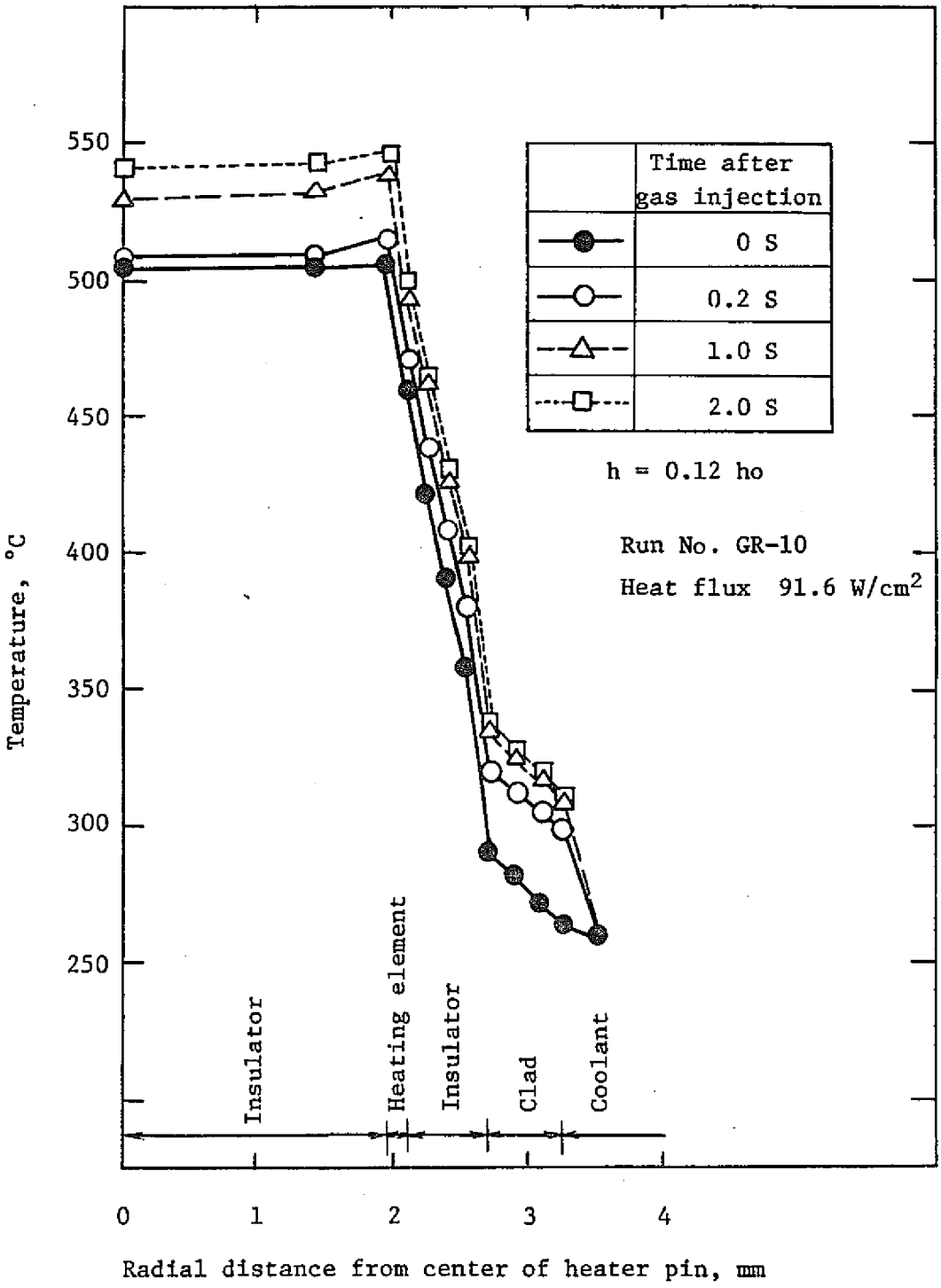

Fig. A-2 Radial temperature distribution in impinged pin calculated by the SURFACE code

Appendix B Heat transfer coefficient of sonic argon gas jet impinged surface

In the following calculation, the argon temperature is taken at 250°C and the gas impinged surface pressure at 2 bars. Let Vs represent sonic velocity, γ specific heat ratio, R gas constant, and T absolute temperature,

$$Vs = \sqrt{\gamma RT} = \sqrt{1.66 \times 208.2 \times (250 + 273)}$$

$$= 425 m/s$$

Let De represent the equivalent pin diameter, μ viscosity coefficient, and ρ density,

$$Re = \frac{VsDe}{\mu/\rho} = \frac{425\ (m/s) \times 0.0065\ (m/s)}{\frac{3.44 \times 10^{-5}\ (kg/ms)}{1.86\ (kg/m^3)}}$$

$$= 149000$$

Let C_p represent isobaric specific heat and λ thermal conductivity,

$$Pr = \frac{Cp\mu}{\lambda} = \frac{0.528 \times 10^3\ (J/kg°C) \times 3.44 \times 10^{-5}\ (kg/ms)}{2.18 \times 10^{-5}\ (KW/m°C) \times 10^3\ (J/KWs)}$$

$$= 0.833$$

The heat transfer coefficient in the vicinity of the stagnation due to the parallel flow to the cylinder is given by the following equation:[11]

$$Nu = 1.14Re^{0.5}Pr^{0.4}$$

$$= 1.14 \times 149000^{0.5} \times 0.833^{0.4}$$

$$= 409$$

Let h_G represent heat transfer coefficient

$$h_G = \frac{\lambda}{De}Nu = \frac{2.18 \times 10^{-5} \ (KW/m°C)}{0.0065 \ (m)} \times 409 = 1.37 \ (KW/m^2°C)$$

$$= 0.137 \ (W/cm^2°C)$$

Appendix C Relation between gas plenum pressure and expulsion acceleration during transient gas injection

The section T-3 and downstream therefrom can be divided into four regions, the region in which the heater pins are inserted (L_1), the region of test section where is no heater pin (L_2), the tube connecting the test section to the expansion tank (L_3), and the expansion tank (L_4) as seen from the figure at right.

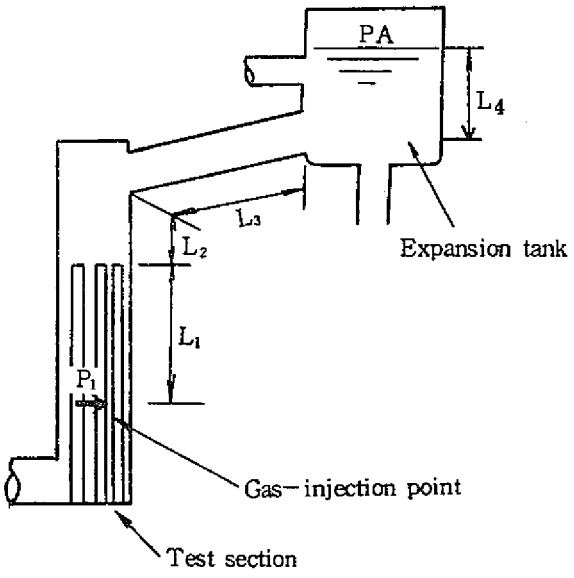

In the one-dimensional model, suppose a pressure difference ΔP ($= P_1 - P_A$) arises between the gas injection plane and the cover gas in the expansion tank due to the transient gas injection, the expulsion acceleration of sodium in the region of the test section in which the heater pins are inserted can be expressed by the following equation.

$$\left[\frac{dV_1}{dt}\right]_{t=0} = \frac{\Delta P}{\rho_N \left(L_1 + L_2 \frac{S_1}{S_2} + L_3 \frac{S_1}{S_3} + L_4 \frac{S_1}{S_4}\right)}$$

$$= \frac{\Delta P}{\rho_N \left(L_1 + L_2 \frac{S_1}{S_2} + L_3 \frac{S_1}{S_3}\right)} \quad \cdots\cdots\cdots\cdots\cdots\cdots \quad (1)$$

$$(S_4 \gg S_1)$$

where S_1, S_2, S_3 and S_4 are the sections of the respective flow channels and ρN is the density of sodium.

If the frictional pressure loss during the flow in the injection nozzle is neglected, the pressure loss due to the contraction and expansion veins in the injection nozzle can be expressed as follows:

$$P_0 - P_1 = (\zeta_1 + \zeta_2) \frac{\rho_G V^2}{2} \quad \text{.....(2)}$$

where Po is gas plenum pressure and P_1 is the pressure of gas after it is injected into the flow channel, and ζ_1 is the coefficient of pressure loss due to the contraction vein during the flow of gas from the plenum into the injection nozzle and $\zeta_1 = 0.41$ when the sectional area ratio is less than 0.1, and ζ_2 is the pressure loss due to the expansion vein during the flow of gas from the injection nozzle to the outside and $\zeta_2 = 1$ when gas flows out into a very wide flow channel. ρ_G is gas density and V is flow velocity. Since the flow is critical in the present, the flow velocity is equal to the sonic velocity.

[Numerical calculation]

Consider the case in which gas is released through the injector nozzle at a temperature of 250°C and a gas plenum pressure of 60 bars. The cover gas pressure is 1.3 bars.

The pressure in the injection nozzle, if assumed to be critical, can be calculated to be 29.28 bars from 0.488 x 60. Since the density of argon is 1.78g/ℓ at 0°C and 1.013 bars,

$$\rho_G = 1.78 \times \frac{273.15}{273.15 + 250} \times \frac{29.28}{1.013} = 26.86 g/\ell$$

$$= 26.86 kg/m^3$$

V is the sonic velocity 425m/s. From equation (2),

$$P_0 - P_1 = (0.41 + 1.0) \times \frac{26.86 \times 425^2}{2}$$

$$= 3420000 \quad N/m^2$$

$$\Delta P = P_0 - (P_0 - P_1) - P_A$$

$$= (60 - 34.2 - 1.3) \times 10^5 \quad N/m^2$$

$$= 24.5 \times 10^5 \quad N/m^2$$

In equation (1),

$$L_1 = 925mm, \quad L_2 = 382mm, \quad L_3 = 9210mm$$

$$S_1 = 924mm^2, \quad S_2 = 2107mm^2, \quad S_3 = 2248mm^2$$

$$\rho_N = 892 kg/m^3 \text{ (Sodium at 250°C)}$$

we obtain

$$\left[\frac{dV_1}{dt}\right]_{t=0} = \frac{24.5 \times 10^5}{892 \times (0.925 + 0.382 \times \frac{924}{2107} + 9.210 \times \frac{924}{2248})}$$

$$= 563 m/s^2$$

Appendix D Continuous gas release test conditions

The test conditions used in the continuous gas release tests carried out in 1975, together with thoses used in the tests for sodium single-phase flow heat transfer before gas injection, are shown below.

Table 2. Experimental conditions of sodium single-phase flow tests and continuous release tests

Symbols used are explained below.

Pg : Gas plenum pressure

Vin: Sodium inlet velocity

q : Heat flux

Tin: Sodium inlet temperature

w : Gas release rate

x : Quality

ΔT : Temperature rise T-Tin (gas impingement area 185mm downstream from starting point of heated section and inlet)

ΔT^*: Temperature rise T-Tin (gas impingement area 225mm downstream from starting point of heated section and inlet)

(a) Date : June 4, 1975
Nozzle diameter : 0.3mm, Number of heated pins 7

Run No.	Pg (bar)	Vin (m/s)	q (W/cm^2)	Tin (°C)	w (g/s)	X	ΔT* (°C)
37H-201	-	0.45	8.0	271.8	-	-	18.5
37H-204	-	1.92	7.9	280.3	-	-	4.6
37H-204-3	-	1.97	38.9	278.9	-	-	29.8
37H-214	-	4.94	38.9	288.8	-	-	14.9
37H-217	-	4.85	63.8	277.2	-	-	25.6
37H-219	-	4.88	77.3	273.5	-	-	31.5
G-2101	13	0.47	8.1	284.4	0.08	2.1×10^{-4}	24.0
G-2102	13	1.09	8.0	285.2	0.08	$9.\times10^{-5}$	13.5
G-2104	13	1.91	8.1	285.1	0.08	5.3×10^{-5}	8.3
G-2104-2	13	1.90	24.0	278.9	0.08	5.3×10^{-5}	25.6
G-2104-3	13	1.90	40.3	271.0	0.08	5.3×10^{-5}	41.6
G-2110	13	2.92	40.1	268.5	0.08	3.4×10^{-5}	35.4
G-2112	13	3.86	40.1	259.0	0.11	3.4×10^{-5}	26.7
G-2114	11	5.03	39.9	263.2	0.09	2.1×10^{-5}	24.2
G-2117	12	4.93	62.8	270.3	0.09	2.1×10^{-5}	36.3
G-2119	12	4.91	77.3	271.3	0.09	2.1×10^{-5}	44.5
G-2301	33	0.50	7.9	280.8	0.23	5.7×10^{-4}	15.0
G-2302	33	0.93	7.9	279.9	0.23	3.1×10^{-4}	11.3
G-2304	33	1.91	7.8	284.6	0.23	1.5×10^{-4}	9.7
G-2304-2	33	1.95	23.3	286.0	0.23	1.5×10^{-4}	34.1
G-2304-3	33	1.95	39.2	284.0	0.23	1.5×10^{-4}	47.3
G-2310	33	2.93	38.9	289.2	0.23	9.7×10^{-5}	33.7
G-2312	33	3.96	38.9	291.7	0.23	5.8×10^{-5}	25.6
G-2314	33	4.90	39.2	289.9	0.23	5.9×10^{-5}	21.8
G-2317	33	4.87	62.4	280.6	0.23	5.9×10^{-5}	34.6
G-2319	33	4.88	77.0	275.3	0.23	5.8×10^{-5}	45.7
G-2601	61	0.49	8.2	280.1	0.24	6.0×10^{-4}	23.7
G-2602	61	0.93	8.13	280.3	0.24	3.0×10^{-4}	15.8
G-2604	61	1.83	8.13	279.4	0.24	1.5×10^{-4}	10.9
G-2604-2	61	1.89	23.8	273.5	0.24	1.5×10^{-4}	27.4
G-2604-3	61	1.91	38.5	268.5	0.24	1.5×10^{-4}	42.5
G-2610	61	2.85	31.2	267.8	0.24	1.0×10^{-4}	39.7

Run No.	Pg (bar)	Vin (m/s)	q (W/cm^2)	Tin (°C)	w (g/s)	X	ΔT (°C)
G-2612	61	3.90	39.3	271.2	0.24	7.5×10^{-5}	25.0
G-2614	61	4.89	39.2	273.5	0.24	6.0×10^{-5}	17.8
G-2617	61	4.87	62.3	271.9	0.24	6.0×10^{-5}	31.0
G-2619	61	4.90	77.9	274.4	0.24	6.0×10^{-5}	41.5

(b) Date : June 25, 1975
Nozzle diameter : 0.3mm, Number of heated pins 7

Run No.	Pg (bar)	Vin (m/s)	q (W/cm^2)	Tin (°C)	w (g/s)	X	ΔT (°C)
37H-3619	-	4.85	78.5	276.0	-	-	24.2
G-3601	65	0.46	7.8	260.1	0.06	1.5×10^{-4}	16.6
G-3602	65	0.91	7.8	269.3	0.06	7.5×10^{-5}	6.2
G-3604	65	1.93	7.9	274.5	0.06	3.8×10^{-5}	6.0
G-3604-2	65	1.94	23.6	277.4	0.06	3.8×10^{-5}	15.0
G-3604-3	65	1.95	37.4	289.9	0.06	3.8×10^{-5}	31.8
G-3610	65	2.90	38.0	276.2	0.06	2.5×10^{-5}	30.9
G-3612	65	3.85	37.6	267.1	0.06	1.9×10^{-5}	27.9
G-3614	65	4.88	38.1	272.7	0.06	1.5×10^{-5}	35.4
G-3617	65	4.84	61.9	275.7	0.06	1.5×10^{-5}	47.2
G-3619	65	4.89	79.1	275.3	0.06	1.5×10^{-5}	63

(c) Date : July 11, 1975
Nozzle diameter : 0.5mm, Number of heated pins 7

Run No.	Pg (bar)	Vin (m/s)	q (W/cm^2)	Tin (°C)	w (g/s)	X	ΔT (°C)
37H-401	-	0.46	7.9	276.4	-	-	16.4
37H-4043	-	4.82	78.5	291.4	-	-	23.1
37H-419	-	4.82	78.5	264.7	-	-	24.8
G-4101	11	0.48	7.9	274.5	0.23	5.8×10^{-4}	17.7
G-4102	11	0.95	7.9	272.4	0.23	2.9×10^{-4}	9.6
G-4104	11	1.86	8.0	271.2	0.23	1.4×10^{-4}	8.9
G-4104-2	11	1.86	23.3	279.6	0.23	1.4×10^{-4}	29.5
G-4104-3	11	1.89	40.4	256.7	0.18	1.1×10^{-4}	55.7
G-4110	11	2.87	40.0	263.8	0.18	7.5×10^{-5}	32.4
G-4112	11	3.82	39.9	269.8	0.18	5.6×10^{-5}	37.5
G-4114	11	4.86	39.3	278.9	0.18	7.0×10^{-5}	41.1

Run No.	Pg (bar)	Vin (m/s)	q (W/cm^2)	Tin (°C)	w (g/s)	X	ΔT (°C)
G-4117	11	4.92	62.7	283.2	0.18	7.0×10^{-5}	57.8
G-4119	11	4.89	79.1	280.7	0.18	7.0×10^{-5}	43.0
G-4301	32	0.49	8.0	269.5	0.68	1.7×10^{-3}	18.6
G-4302	32	0.92	8.0	266.7	0.68	8.5×10^{-4}	11.9
G-4304	32	1.95	8.0	263.6	0.76	4.8×10^{-4}	10.1
G-4304-2	32	1.93	23.4	255.4	0.76	4.8×10^{-4}	28.0
G-4304-3	32	1.90	39.3	238.7	0.76	4.8×10^{-4}	44.6
G-4310	32	2.90	38.8	249.1	0.89	3.6×10^{-4}	44.3
G-4312	32	3.91	38.6	254.9	0.89	2.7×10^{-4}	35.6
G-4314	32	4.71	38.6	264.3	0.89	2.2×10^{-4}	42.2
G-4317	32	4.75	59.2	270.9	0.87	2.1×10^{-4}	65.5
G-4319	32	4.71	78.0	270.4	0.87	2.1×10^{-4}	83.2
G-4601	63	0.49	7.9	281.3	1.49	3.6×10^{-3}	12.3
G-4602	63	0.91	7.9	282.4	1.49	1.8×10^{-3}	7.2
G-4604	63	1.89	7.9	285.8	1.49	9.1×10^{-4}	6.3
G-4604-2	63	1.91	23.1	286.7	1.57	9.8×10^{-4}	19.7
G-4604-3	63	1.85	39.3	280.5	1.77	1.1×10^{-3}	31.6
G-4610	63	2.94	37.8	280.5	1.79	7.2×10^{-4}	28.0
G-4612	63	3.87	38.5	280.8	1.73	5.2×10^{-4}	29.8
G-4614	63	4.75	38.0	281.4	1.73	4.2×10^{-4}	29.3
G-4617	63	4.73	62.7	271.5	1.94	4.7×10^{-4}	44.5
G-4619	63	4.73	78.3	271.9	2.38	5.8×10^{-4}	55.5

(d) Date : July 24, 1975
Nozzle diameter : 0.5mm, Number of heated pins 7

Run No.	Pg (bar)	Vin (m/s)	q (W/cm^2)	Tin (°C)	w (g/s)	X	ΔT* (°C)
37H-519	-	4.92	78.4	236.2	-	-	29.0
G-5019	8	4.98	78.8	247.2	0.26	6.3×10^{-5}	22.8
G-5119	12	4.97	78.8	249.4	0.22	5.4×10^{-5}	22.6
G-5219	21	4.92	78.8	252.2	0.45	1.1×10^{-4}	37.9
G-5319	31	4.98	79.1	253.8	0.72	1.8×10^{-4}	37.2
G-5419	43	4.93	80.5	256.1	1.02	2.5×10^{-4}	36.6
G-5519	63	4.92	79.5	257.8	1.01	2.5×10^{-4}	31.3
G-5619	60	4.90	79.6	258.3	1.70	4.1×10^{-4}	36.5

(e) Date : September 10, 1975
Nozzle diameter : 0.5mm, Number of heated pins 6

Run No.	Pg (bar)	Vin (m/s)	q (W/cm^2)	Tin (°C)	w (g/s)	X	ΔT (°C)
37H-619	-	4.94	91.1	221.3	-	-	25.1
G-6019	6	4.99	90.1	240.4	0.15	3.7×10^{-5}	46.5
G-6119	9	5.02	90.7	244.1	0.25	6.1×10^{-5}	40.7
G-6219	18	5.02	90.8	245.7	0.50	1.2×10^{-4}	36.1
G-6319	30	5.00	91.5	247.3	0.80	2.0×10^{-4}	31.0
G-6419	41	4.92	90.7	249.2	1.10	2.7×10^{-4}	31.8
G-6519	52	4.89	91.0	250.0	1.40	3.4×10^{-4}	29.6
G-6619	61	4.89	91.4	251.2	1.70	4.1×10^{-4}	29.0

(f) Date : September 23, 1975
Nozzle diameter : 0.5mm, Number of heated pins 6

Run No.	Pg (bar)	Vin (m/s)	q (W/cm^2)	Tin (°C)	w (g/s)	X	ΔT (°C)
37H-804	-	1.91	36.1	232.7	-	-	31.0
37H-819	-	4.92	91.2	232.5	-	-	26.6
G-8004	6	1.92	37.1	252.6	0.07	4.3×10^{-5}	54.0
G-8104	14	1.87	37.0	257.3	0.45	2.8×10^{-4}	33.1
G-8204	23	1.84	36.8	260.2	0.60	3.8×10^{-4}	43.5
G-8304	34	1.78	36.0	262.8	0.91	5.6×10^{-4}	30.1
G-8404	44	1.76	36.5	266.7	1.25	7.8×10^{-4}	33.6
G-8504	55	1.76	37.6	268.7	1.66	1.0×10^{-3}	33.7
G-8604	59	1.73	36.8	271.0	2.04	1.3×10^{-3}	30.8

(g) Date : September 30, 1975
Nozzle diameter : 0.8mm, Number of heated pins 6

Run No.	Pg (bar)	Vin (m/s)	q (W/cm^2)	Tin (°C)	w (g/s)	X	ΔT (°C)
37H-904	-	1.89	35.9	235.0	-	-	21.3
37H-919	-	4.95	91.6	237.3	-	-	27.9
G-90804	8	1.89	35.3	243.3	0.36	2.3×10^{-4}	27.4
G-91204	13	1.86	35.7	251.1	0.72	4.5×10^{-4}	39.9
G-91604	19	1.83	36.0	255.7	1.13	7.0×10^{-4}	36.4
G-92004	23	1.82	36.8	259.4	1.36	8.5×10^{-4}	33.7
G-92504	29	1.92	36.0	268.4	1.68	1.1×10^{-3}	29.5

Run No.	Pg (bar)	Vin (m/s)	q (W/cm^2)	Tin (°C)	w (g/s)	X	ΔT (°C)
G-92704	27	1.93	35.9	278.4	1.76	1.1×10^{-3}	29.0
G-93004	31	1.90	35.7	274.4	1.81	1.1×10^{-3}	29.5

(h) Date : October 7, 1975
Nozzle diameter : 0.5mm, Number of heated pins 6

Run No.	Pg (bar)	Vin (m/s)	q (W/cm^2)	Tin (°C)	w (g/s)	X	ΔT (°C)
37H-1001	-	0.47	9.0	220.4	-	-	16.6
37H-1002	-	0.97	18.1	225.6	-	-	18.4
37H-1004	-	1.95	74.4	228.2	-	-	21.4
G-100701	7	0.43	8.8	239.0	0.11	2.8×10^{-4}	16.2
G-101001	11	0.48	8.8	242.0	0.20	5.0×10^{-4}	16.3
G-102001	19	0.50	8.9	237.5	0.45	1.1×10^{-3}	16.3
G-103001	34	0.52	8.9	239.4	0.56	1.4×10^{-3}	23.3
G-104001	42	0.52	8.9	240.2	1.01	2.5×10^{-3}	16.7
G-105001	48	0.52	8.9	240.1	0.89	2.2×10^{-3}	17.4
G-106001	64	0.54	8.9	240.0	1.52	3.8×10^{-3}	19.0

(i) Date : October 23, 1975
Nozzle diameter : 0.5mm, Number of heated pins 6

Run No.	Pg (bar)	Vin (m/s)	q (W/cm^2)	Tin (°C)	w (g/s)	X	ΔT (°C)
37H-1112	-	0.97	18.2	246.7	-	-	17.4
37H-1119	-	4.80	90.7	245.3	-	-	25.8
G-11002	6	0.90	18.2	262.7	0.13	1.6×10^{-4}	18.9
G-11602	63	0.85	20.0	263.6	0.13	1.6×10^{-4}	15.6

(j) Date : October 28, 1975
Nozzle diameter : 0.5mm, Number of heated pins 6

Run No.	Pg (bar)	Vin (m/s)	q (W/cm^2)	Tin (°C)	w (g/s)	X	ΔT (°C)
37H-1202	-	0.87	18.5	230.6	-	-	20.8
37H-1219	-	5.03	90.3	235.3	-	-	24.8
G-12152	18	0.93	18.1	259.6	0.30	3.8×10^{-4}	17.8
G-12202	23	0.92	18.1	256.4	0.36	4.5×10^{-4}	18.6
G-12302	30	0.94	18.1	254.0	0.61	7.6×10^{-4}	20.5

Run No.	Pg (bar)	Vin (m/s)	q (W/cm^2)	Tin (°C)	w (g/s)	X	ΔT (°C)
G-12159	15	5.07	49.7	243.2	0.40	9.8×10^{-5}	44.1
G-12259	27	5.06	50.0	245.1	0.51	1.2×10^{-4}	61.7
G-12309	30	5.05	49.8	248.3	0.56	1.4×10^{-5}	60.2

(k) Date : November 18, 1975
Nozzle diameter : 0.8mm, Number of heated pins 6

Run No.	Pg (bar)	Vin (m/s)	q (W/cm^2)	Tin (°C)	w (g/s)	X	ΔT (°C)
37H-1504	-	1.85	36.5	236.5	-	-	20.2
37H-1509	-	4.84	90.9	236.2	-	-	25.5
G-15104	11	1.94	36.2	245.6	0.56	3.5×10^{-4}	20.2
G-15304	29	1.92	36.2	245.8	1.08	6.8×10^{-4}	19.4
G-15604	61	1.92	36.5	245.6	3.14	2.0×10^{-3}	23.9
G-15079	9	4.83	91.7	239.1	0.11	2.7×10^{-5}	30.9
G-15109	15	4.84	91.7	299.8	0.63	1.5×10^{-4}	25.3
G-15209	24	4.81	92.0	241.0	1.22	3.0×10^{-4}	30.9
G-15309	31	4.82	92.3	241.8	1.49	3.6×10^{-4}	32.6
G-15409	42	4.83	91.3	242.8	2.17	5.3×10^{-4}	57.1
G-15509	55	4.79	92.2	243.2	2.75	6.7×10^{-4}	28.7
G-15609	61	4.64	91.3	242.5	3.44	8.4×10^{-4}	32.4

Appendix E Sodium-gas two-phase heat transfer flow test conditions

Table 3 Experimental conditions of two-phase heat transfer tests

Symbols used are explained below.

Vin: Sodium inlet velocity

q : Heat flux

Tin: Sodium inlet temperature

w : Gas release rate

X : Quality

ΔT : Temperature rise T-Tin (265mm downstream from starting point of heated section and inlet)

Date : November 11-12, 1975
Nozzle diameter : 0.5mm, Number of nozzles 4
Number of heated pins 6

Run No.	Vin (m/s)	q (W/cm^2)	Tin (°C)	w (g/s)	X	ΔT (°C)
37H-001	0.40	9.3	227.5	-	-	26.4
37H-002	0.84	18.0	220.8	-	-	30.8
37H-004	1.81	36.1	242.2	-	-	33.4
37H-009	4.50	90.3	233.6	-	-	42.6
GS-059	4.93	91.1	237.5	0.29	7.1×10^{-5}	43.4
GS-079	4.90	91.8	238.0	0.50	1.2×10^{-4}	42.7
GS-109	4.92	91.9	239.0	0.67	1.7×10^{-4}	44.0
GS-139	4.93	92.3	240.7	0.69	1.7×10^{-4}	43.8
GS-169	4.92	93.8	241.2	0.76	1.9×10^{-4}	44.4
GS-199	4.89	92.4	241.8	0.90	2.2×10^{-4}	45.4
GS-229	4.92	93.8	242.0	1.39	3.4×10^{-4}	44.9
GS-259	4.83	92.1	242.4	1.67	4.2×10^{-4}	48.4
GS-064	1.93	35.7	252.1	0.34	2.1×10^{-4}	36.2
GS-084	1.91	35.9	249.9	0.49	3.1×10^{-4}	36.9
GS-114	1.92	35.9	247.0	0.71	4.5×10^{-4}	36.0
GS-144	1.95	35.7	245.3	0.77	4.8×10^{-4}	35.7
GS-174	1.94	35.3	243.8	1.00	6.2×10^{-4}	38.3
GS-204	1.91	36.5	242.5	1.15	7.3×10^{-4}	39.4'
GS-244	1.91	35.4	241.4	1.40	8.9×10^{-4}	39.5
GS-042	1.00	18.0	277.7	0.24	2.4×10^{-4}	28.6
GS-062	0.99	18.0	273.6	0.28	3.5×10^{-4}	29.0
GS-082	0.98	18.0	269.4	0.49	6.1×10^{-4}	29.2'
GS-102	0.99	18.3	266.8	0.56	6.9×10^{-4}	31.0
GS-132	0.99	18.0	264.5	0.70	8.6×10^{-4}	30.4
GS-162	0.99	18.2	262.6	0.93	1.1×10^{-4}	31.2
GS-212	1.00	18.0	258.9	1.18	1.4×10^{-3}	32.0
GS-252	1.00	18.0	257.1	1.54	1.9×10^{-3}	32.2
GS-051	0.50	9.2	270.2	0.24	5.8×10^{-4}	22.5
GS-081	0.51	9.4	272.7	0.37	9.0×10^{-4}	22.5
GS-091	0.51	9.5	277.0	0.47	1.1×10^{-3}	22.2
GS-181	0.52	9.7	278.4	1.15	2.7×10^{-3}	24.9
GS-121	0.51	9.4	278.1	0.62	1.5×10^{-3}	23.1
GS-141	0.50	9.5	279.0	0.81	2.0×10^{-3}	24.1

Run No.	Vin (m/s)	q (W/cm^2)	Tin (°C)	w (g/s)	X	ΔT (°C)
GS-181	0.52	9.7	278.4	1.15	2.7×10^{-3}	24.9
GS-201	0.50	9.4	278.2	1.15	2.8×10^{-3}	24.8
GS-261	0.52	9.1	277.7	1.63	3.8×10^{-3}	23.9
GS-291	0.56	9.1	236.4	1.71	3.7×10^{-3}	24.3
GS-351	0.55	9.1	234.9	2.05	4.5×10^{-3}	25.3

Appendix F Relation between Two-Phase and Liquid Single-Phase Heat Transfer Coefficient Ratio and Void Fraction

Assuming the sodium-gas two-phase thermal conductivity conforms to Maxwell's equation, Hori and Friedland[24] deduced the relation between two-phase and liquid single-phase heat transfer transfer coefficient ratio (h_{TP}/ho) and void fraction (α). On the basis of this model, the relation between h_{TP}/ho and α is derived as follows, using Subbotin's equation for the liquid single-phase heat transfer coefficient.

$$Nu = 5 + 0.025Pe^{0.8} \quad \cdots\cdots (1)$$

and

$$Nu = \frac{hDe}{\lambda} \qquad h = \frac{\lambda}{De} \cdot Nu \quad \cdots\cdots (2)$$

$$Re = \frac{\rho VDe}{\mu}$$

$$Pr = \frac{\mu C_p}{\lambda}$$

$$Pe = RePr = \frac{\rho VCpDe}{\lambda} \quad \cdots\cdots (3)$$

where

Cp: isobaric specific heat

De: flow force equivalent diameter

Nu: Nusselt number

Pe: Peclet number

Pr: Prandtle number

Re: Reynolds number

V:: velocity

h : heat transfer coefficient

λ : thermal conductivity

μ : viscosity coefficient

ρ : density

In the case of single-phase flow (indicated by subscript "0")

$$ho = \frac{\lambda_0}{De}(5 + 0.025Pe_0^{0.8}) \quad \cdots\cdots\cdots\cdots\cdots\cdots (4)$$

In the case of two-phase flow (indicated by subscript "TP") Flow velocity, density, specific heat and thermal conductivity are considered as follows.

$$V_{TP} = \frac{V_0}{1 - \alpha} \cdots\cdots\cdots (5), \quad \rho_{TP} = \rho_0 (1 - \alpha) \cdots\cdots\cdots (6)$$

$$Cp_{TP} = Cp_0 (1 - \alpha) \cdots (7), \quad \lambda_{TP} = \lambda_0 \frac{1 - \alpha}{1 + 0.5\alpha} \cdots\cdots (8)$$

(5), (6), (7), (8) are substituted into (3)

$$Pe_{TP} = \frac{1 + 0.5\alpha}{(1 - \alpha)\lambda_0} \cdot \rho_0 (1 - \alpha) \cdot \frac{V_0}{1 - \alpha} \cdot Cp_0 (1 - \alpha) De$$

$$= (1 + 0.5\alpha) \frac{\rho_0 V_0 Cp_0 De}{\lambda_0}$$

$$Pe_{TP} = (1 + 0.5\alpha) Pe_0$$

Hence

$$h_{TP} = \frac{1 - \alpha}{1 + 0.5\alpha} \lambda_0 \cdot \frac{1}{De} (5 + 0.025 Pe_{TP}^{0.8})$$

$$h_{TP} = \frac{1 - \alpha}{1 + 0.5\alpha} \cdot \frac{\lambda_0}{De} (5 + 0.025 \{(1 + 0.5\alpha) Pe_0\}^{0.8}) \quad .. \quad (9)$$

From (9) ÷ (4)

$$\frac{h_{TP}}{h_0} = \frac{1 - \alpha}{1 + 0.5\alpha} \cdot \frac{5 + 0.025 \{Pe_0 (1 + 0.5\alpha)\}^{0.8}}{5 + 0.025 Pe_0^{0.8}}$$